AN EXPERIMENTAL STUDY OF THE AERODYNAMIC SHROUD IN AXIAL VENTILATION FAN SYSTEMS

By

Douglas R. Neal

A THESIS

Submitted to

Michigan State University

in partial fulfillment of the requirements

for the degree of

MASTER OF SCIENCE

Department of Mechanical Engineering

2002

ABSTRACT

AN EXPERIMENTAL STUDY OF THE AERODYNAMIC SHROUD IN AXIAL VENTILATION FAN SYSTEMS

By

Douglas R. Neal

An experimental investigation was performed on a building ventilation fan with an installed aerodynamic shroud. The fan system used for this study was characterized by its high volume flow rate, low pressure rise and downstream conical diffuser. A new definition of efficiency is presented that differs than the currently accepted industry standard. Arguments are presented to support this definition, and its use not only in this type of fan, but also other turbomachinery applications. An energy balance is derived that includes this definition of efficiency and the specific loss mechanisms of turbomachinery. This formulation clearly shows how the efficiency can be increased by reducing these loss mechanisms.

Integral measurements of pressure rise vs. flow rate and efficiency are presented for a number of different configurations, blade designs, diffusers and aerodynamic shroud conditions. These data show that the aerodynamic shroud is able to increase the flow rate by over 35% while simultaneously increasing the efficiency by over 15%. Furthermore, it is shown that the choice of blade design is critical to these improvements and that a larger diffuser cone can be used. Particle Image Velocimetry (PIV) measurements are presented to show how the aerodynamic shroud affects the flow field downstream of the fan. These data show that the aerodynamic shroud is able to reduce specific loss mechanisms that were identified in the energy balance and also create a more uniform exit profile at the exit of the diffuser cone. Finally, a new fan system is proposed that incorporates the modifications that were made and proven successful in this study.

ACKNOWLEDGEMENTS

I would like to thank Dr. John Foss, my advisor, friend and much more of the past several years. His guidance, persistence and dedication to his students is tremendous. The quality of this manuscript is largely due to his careful review. Additionally, I would like to thank the efforts of Dr. Ahmed Naguib, Dr. Charles Petty and Dr. Tom Shih for their thoughtful comments during the review process. The engineering faculty at MSU create a solid academic research environment.

I would also like to thank my colleagues in the Turbulent Shear Flows Laboratory (TSFL): Richard Prevost, Scott Treat, Kyle Bade and Al Lawrenz. Without Al Lawrenz, I often wonder how the laboratory would continue to function. A special thanks to Scott Morris, who I shared an office in the TSFL with for several years. Scott provided hours of engaging conversation that have really stimulated my interest in scientific research, and he knows the value of strong black coffee in the success of research. Thanks for making thousands of pots of coffee. I look forward to continued interactions down the road.

Finally, I want to thank members of my family, including my fellow MSU alumnus and uncle, James T. Neal (M.S. 1959). I will enjoy having a publication that shares a space in the MSU library alongside his thesis. Lastly, my mother and father, who have always encouraged me and taught me the valuable lesson that the most important things in life are not bought and sold, but earned and maintained. They continue to support my academic (and other life) endeavors.

TABLE OF CONTENTS

LIST OF FIGURES

LIST OF TABLES

TABLE 4. A Comparison of the Salient Features of the Tested Diffuser Cones (see Figure 6.5 for a description of the variables: a, b, and L) 61

NOMENCLATURE

Roman:

A	Area
C_d	Discharge coefficient
E	DC Voltage (VDC)
Q	Volumetric flow rate
$\dot{Q}$	Heat transfer rate
p	Pressure
$\wp$	Power (Watts)
Re	Reynolds number
$\dot{m}$	Mass flow rate
$\vec{V}$	Velocity vector
V	Velocity magnitude
U	Spatially averaged velocity
g	Gap height for aerodynamic shroud
i	Alternating current (AC)
e	AC voltage (VAC)
q	Volume flow rate in cfm (ft^3/min)
t	Time
r	Radial direction
x′	Horizontal coordinate for PIV measurements in diffuser wall interior region
y′	Vertical coordinate for PIV measurements in diffuser wall interior region
z	axial direction

Greek:

α	Kinetic energy flux correction factor
η^*	System efficiency
η	Static efficiency
η_a	Efficiency definition currently used in the agricultural ventilation fan industry
ν	Kinematic viscosity

ρ	Density of air
r	Radial component
z	Axial component

Subscripts:

A	Auxiliary flow
I	Instantaneous
N	North side metering nozzle
S	South side metering nozzle
ci	Calibration inlet
i	Inlet to control volume of Figure 2.1 on page 10.
e	Exit to control volume of Figure 2.1 on page 10.
p	Primary (fan flow)

1.0 Introduction

1.1 Problem Statement and Background Information

The exchange of fresh air and proper distribution of ventilating air within greenhouses profoundly affects the health of the plants that are raised in these environments. Heat, dust and other pollutants must be routinely removed from the air inside the greenhouse. Excess heat is generated through a process of trapped thermal energy that is commonly known as the greenhouse effect, see Hanan (1998). In this process, shortwave radiation in the form of visible light is transmitted into the greenhouse through the walls, which are typically made of glass, acrylic panels or plastic films. This sunlight will contact the interior surfaces, such as the foliage or internal structures and it heats these surfaces. Much of this absorbed energy is in turn re-radiated as longwave infrared radiation. Since materials such as glass, acrylic or plastic are opaque to longwave radiation, this energy remains trapped inside the greenhouse. Solar energy can quickly elevate a closed greenhouse to temperatures that are well in excess of the optimum for plant health. Most commercial greenhouses rely on ventilation fans to discharge this warm air and replace it with cool, outside air. Additionally, proper circulation of air in commercial greenhouses is critical to preventing mold and mildew, which can destroy crops. Most mechanically ventilated greenhouses use an exhaust, or negative pressure system (Wheeler and Both, 2002). The ventilation fans are mounted on an exterior wall to exhaust air from the greenhouse, as shown in Figures 1.1 and 1.2.

Fresh air ventilation and air circulation within livestock production buildings also affects the health and growth rate of confined animals. This is especially true during periods of high ambient temperatures when thermal stress resulting from the elevated temperatures within a livestock enclosure negatively alters the rates of production, growth, conception and survival for almost all livestock species (Mangold, et al., (1967); Fuquay, (1981); Nienaber, et al., (1985) and (1987)). These effects are especially pronounced in the production of swine and poultry where the animals are confined at relatively high density. In the case of dairy cattle, declines in feed intake and milk production are common indicators of heat stress, especially in high producing cows (Johnson, (1965); Yousef and Johnson, (1966)).

Increased air velocity over the body surface of a dairy cow and the resultant increased convective heat and mass transfer can offset some of the negative effects of hot weather (Brody, et al., (1954). Traditionally this has been accomplished by maximizing the open area in sidewalls in naturally-ventilated barns. This technique is widely recommended to increase summer air exchange and to improve convective and evaporative cooling (Bickert, (1988)). However, with the high levels of milk production possible today with improved breeding, feeding, management and facilities, the cows' need to dissipate metabolic heat is substantially increased (Tyrrell, et al. (1988); Tillotson and Bickert, (1994)). Using fans to increase air velocity in the vicinity of the cow during hot weather has been found to be an important asset (Chastain, (1991)).

It has been quantitatively shown that a form of "tunnel ventilation," in which an axial velocity of order 5.5 km/hr (1.5 m/s) of evaporatively cooled air passing over the chickens in a poultry enclosure will significantly enhance their egg production (layers) and weight gain (broilers). This cooling airflow is induced by placing a bank of exhaust fans at the end of a (typically) 122 m long building, as shown in Figure 1.3; see Overhults and Gates.

(1993). The importance of ventilation in swine buildings has been documented by Mangold, et al. (1967) and Nienaber, et al. (1987). However, implementing a tunnel ventilation system will substantially increase the producer's costs. Overhults and Gates (1997) reported the following regarding the energy requirements for operating tunnel ventilated broiler houses:

- "Electrical energy in this study was only about one-fourth of the total energy requirement but was about one-half of the total energy cost. Thus, the decision to tunnel ventilate (or perhaps even to mechanically ventilate) the broiler house will noticeably increase the grower's cost."

Previously, Overhults and Gates (1993) noted the following:

- "Summer flocks required 2 times as much electricity as winter flocks, reflecting increased use of the tunnel ventilation system for cooling."
- Note: Summer flocks refers to broilers raised to market age (41-49 days) during summer months, winter flocks are raised to market age during winter months.
- Electricity use during winter months averaged 112 kWh/1000 birds. During summer months the usage was 222 kWh/1000 birds.

The documented evidence, cited above, clearly states the importance of adequate ventilation and air circulation in the operation of greenhouse and livestock buildings. This evidence also indicates the high costs associated with operating such ventilation systems. Developments to ventilation systems that would reduce the operating costs associated with greenhouse and livestock facilities would be of great benefit to U.S. producers. However, during the last decade, improvements to agricultural fans have been limited to passive devices such as better inlet shrouds and the addition of exit flow diffusers. Although current fans provide adequate airflow, they fail to achieve the maximum performance and efficiency that can be achieved by active control techniques. Given the narrow profit margins in agriculture and significant cost of electricity to operate ventilation fans, it is appropriate to consider active techniques to improve efficiency and to obtain lower operating costs.

1.2 The Aerodynamic Shroud Concept - Previous Work

The aerodynamic shroud, see Figure 1.4, was originally developed for automotive cooling fans where the relative motion of the engine with respect to the shroud requires a large gap between the fan tip and the outer shroud. This tip clearance region is characterized by energy dissipation effects (i.e., losses) that are associated with the pressure-to-suction surface flows of the propeller blade. These "tip losses" can be a dramatic detriment to the performance and efficiency of an axial fan, and they are estimated to be 20-40% of the total losses, as reported by Lakshminarayana (1996) and Bleier (1998) amongst others.

Morris (1997) conducted the initial study of the aerodynamic shroud application on the engine cooling fan for a light-duty truck. This fan had a diameter of 457.0 mm, and the tip clearance was 25.0 mm. Because of the high system resistance[1] for this configuration, which includes the grill, air conditioning condenser, radiator, and downstream blockage elements such as the engine, the pressure rise of this fan was relatively high (250 - 1000 Pa). The flow rates were moderate, ranging between 0.1 m^3/s and 0.9 m^3/s. Morris found that the aerodynamic shroud was able to enhance the performance at lower flow rates, but that it degraded the performance at higher flow rates. Similarly, he showed that a large system resistance would cause the aerodynamic shroud to lessen the efficiency; however, a small system resistance would allow the aerodynamic shroud to improve the system efficiency. Since the larger system resistance values involved a radial outflow from the fan, it

1. The operating point is the intersection of the performance curve with a parabola that defines the system resistance.

was realized that a contoured, and not a sudden expansion outlet passage, could take advantage of the aerodynamic shroud contribution. The performance benefits of these downstream geometry adjustments are documented in [26].

Morris (1997) also conducted a brief study which showed that a fan with a larger tip clearance, when used in conjunction with the aerodynamic shroud, could produce better performance results than the same fan with a near zero tip clearance. Again, these results show that both performance and efficiency are enhanced at higher flow rates, and degraded at lower flow rates. These data indicate that fan applications where a small tip clearance is allowed could benefit from a larger tip clearance with the aerodynamic shroud.

The latter observation of Morris (1997) created the primary motivation for the work presented here, since agricultural building ventilation fans have high volume flow rates (1.0-3.5 m^3/s) and modest pressure rise (0.0-75.0 Pa) conditions. This idea was initially investigated by Neal and Foss (1999), and it is examined in further detail in the present thesis.

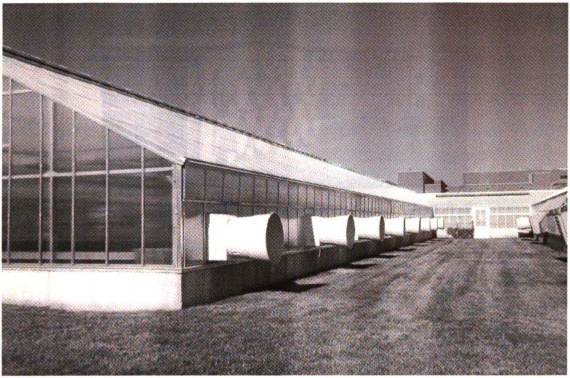

FIGURE 1.1 Greenhouse Ventilation Fan Systems

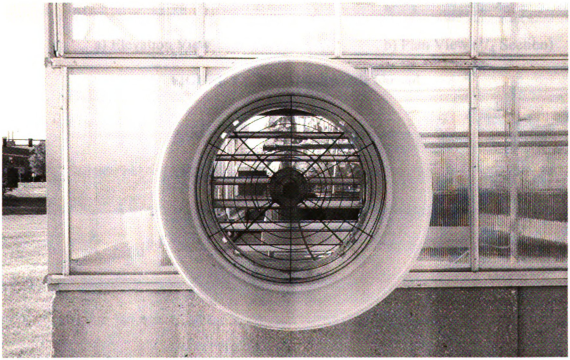

FIGURE 1.2 Close-up View of a Greenhouse Ventilation Fan

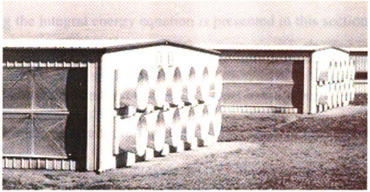

FIGURE 1.3 Livestock Houses with Tunnel Ventilation

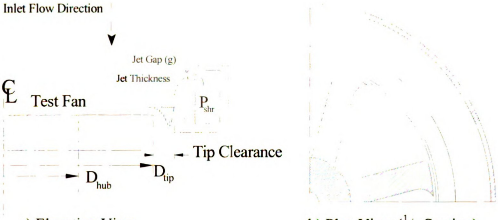

a) Elevation View

b) Plan View ($^1/_4$ Section)

FIGURE 1.4 The Aerodynamic Shroud

2.0 Fan Analysis

An analysis using the integral energy equation is presented in this section in order to provide a complete statement of the loss mechanisms in turbomachinery. Although numerous discussions on loss mechanisms and efficiencies exist in the present literature, detailed analyses using an energy balance are few. Lakshminarayana (1996) derived an integral energy balance for a centrifugal compressor. His result, shown in equation 2.1 is valid for viscous, compressible flows and includes all losses associated with viscous flow over the blades.

$$\frac{P_{shaft}}{\dot{m}} = h_{o1} - h_{o2} \tag{2.1}$$

This equation, while useful, does not provide insight into the specific loss mechanisms associated with turbomachinery, nor does it account for a possible net kinetic energy flux. Another formulation of the energy equation is thus proposed that will provide a better understanding of these losses. The present derivation will begin with the generalized integral energy equation as proposed by Potter and Foss (1982):

$$\dot{Q} - \dot{W}_S - \dot{W}_{shear} - \dot{W}_I = \frac{d}{dt}\int_{cv}\left(\frac{V_I^2}{2} + gz + \tilde{u}\right)\rho dV + \int_{cs}\left(\frac{V_I^2}{2} + gz + \tilde{u} + \frac{p}{\rho}\right)\rho V \cdot \hat{n} dA \tag{2.2}$$

Equation 2.2 describes the instantaneous balance of the terms in this control volume equation. If the equation were integrated over an integer number of cycles (T) of the fan and if each term was then divided by T, the unsteady term would be zero. The remaining terms would describe each quantity averaged over T cycles. The losses in the above equation will be defined as the sum of all the terms representing unusable forms of energy and can be written as:

$$losses = -\dot{Q} + \int_{cv} \tilde{u}\rho V \cdot \hat{n} dA \qquad (2.3)$$

Applying equation 2.2 to the control volume shown in Figure 2.1, the following observations can be made. First, the control volume is stationary and there is no shear work exerted on the surface of the control volume. Also, the velocity at the inlet to the control volume can be assumed to be zero; this would represent the interior domain of a greenhouse or livestock facility. Equation 2.2 then reduces to:

$$\frac{\dot{W}_S}{\dot{m}} = \frac{p_e - p_i}{\rho} + \alpha\frac{\langle V_e \rangle^2}{2} + \sum g h_L \qquad (2.4)$$

In equation 2.4, the term $<V_e>$ is the spatially-averaged exit velocity. The α term in front of this term accounts for the non-uniform velocity profile and allows use of this spatially averaged velocity. The value of α is greater than or equal to unity, with the latter case being for a uniform velocity distribution. The pressure term could also have a coefficient if there were a correlation between the local velocity V(r,θ) and p, such that:

$$\int p\vec{V} \cdot \hat{n} = \gamma\langle V \rangle \langle p \rangle \qquad (2.5)$$

This formulation will assume that this situation does not occur and the pressure across the inlet and outlet will be considered to be uniform. The $\dot{W}_S$ term represents the available shaft work that is delivered to the rotor; it is related to the input power (the true energy cost) by the motor efficiency:

$$\eta_m = \frac{\dot{W}_S}{\wp} \qquad (2.6)$$

The losses described in equation 2.3 are now re-written into the product of gravity and various head losses. These losses can be further defined by their contributing mechanisms. Denoting the losses by their loss coefficient, k, as defined by

$$gh_L = k\frac{V^2}{2} \tag{2.7}$$

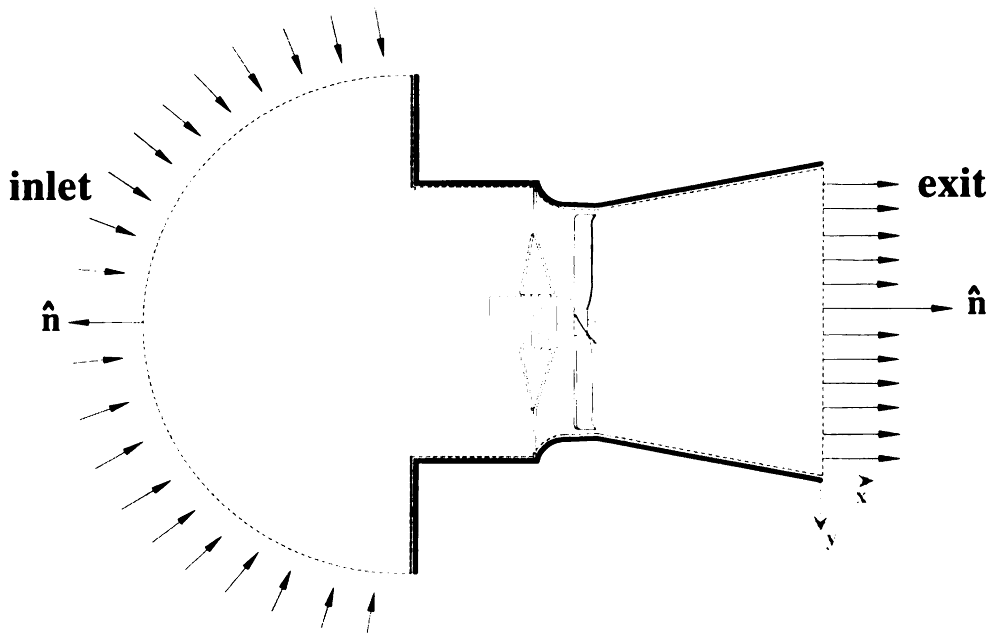

FIGURE 2.1 Control Volume for a Typical Axial Fan

allows for a convenient formulation by which the various losses can be defined with respect to their contribution to the energy budget. A detailed description of these contributing losses is described in the following paragraphs. Only the losses that are relevant to low-speed ventilation fans and their flow fields (i.e. incompressible, no shock waves, etc.) will be considered here. More general information on turbomachinery losses can be found in Lakshminarayana (1996) or Wallis (1983).

The losses that are relevant to the control volume shown in Figure 2.1 are:

1. *Blade profile loss.* These viscous losses are primarily caused by the development of blade boundary layers across the entire span of the rotor and the corresponding wakes behind the passing blade. These losses would also include separated flow on the suction side of the blade, which occurs primarily at high pressure rise (low flow rate) conditions.

2. *Shroud and other passage loss.* These losses result from the boundary layers that form in the shroud and upstream housing regions, as well as the downstream diffuser cone. Separated flow in the diffuser cone will provide an additional loss; therefore, diffuser cones are typically limited to 7 degrees or less. This number is based on empirical data by the manufacturers and is also confirmed in studies discussed by Wallis (1983). A well designed fan housing will typically have very little separated flow in the upstream and downstream region and flow separation is a small contributor to the overall losses.

3. *Tip clearance losses.* The spacing between the rotating blade section and the stationary outer shroud varies significantly from application to application, but this is a source of significant loss in all turbomachinery applications. This type of loss results from the need to have a finite distance between the outermost tip of the blade and the surrounding shroud. The pressure (downstream) side of the blade will interact with the suction side (upstream) of the blade and cause a leakage flow to occur in the axial gap region. Since the leakage flow and main flow in the axial gap region are often at different angles, the mixing of these two dissimilar flows creates further losses as a result of the strong shearing in this region. Additionally, a "tip vortex" can also occur in this region. This resulting vortex can create substantial losses by viscous dissipation of the associated turbulent motions, along with the losses associated with interactions of the tip vortex with the main flow (e.g. entrainment of the main flow by this tip vortex). The magnitude of these losses varies widely depending on the application, but Lakshminarayana (1996) estimates that clearance losses account for 20-35% of the total losses.

4. *Secondary flow losses.* Losses from secondary flows are the result of the mixing and dissipation of energy in the fan system. The loss mechanisms are similar to those

described under tip clearance losses. These losses are often lumped together with the shroud and other passage losses (annulus and hub-wall) boundary layer losses and described as "endwall losses". They are described here separately since significant secondary flow losses occur away from the shroud and passage losses and these effects can be addressed.

Additional losses in a more general discussion would include those from the formation of shock waves for gas flows and cavitation bubbles for liquid flows. These types of losses (blade profile, shroud, tip clearance and secondary flow) will be referenced in the energy equation analysis of 2.4 and 2.5 as k_{bl}, k_{sh}, k_{tc} and k_{sec}, respectively. Their usage in the energy equation analysis requires that the associated velocities be identified. The blade profile losses scale with the velocity of the fan blade, therefore the fan tip speed,

$$U_{tip} = \frac{\Omega D}{2} \tag{2.8}$$

is used. The losses in the tip clearance region, while distinctly different than those in from the blade profile, also scale with the fan tip speed. The losses in fan shroud and other flow passages would scale with the average velocity throughout the fan. This can be calculated by taking the total flow rate through the fan and dividing it by a representative area in the shroud or other internal flow passages. An approximate average area can be used for this calculation and the resulting velocity is termed V_{sh}. The secondary flow losses, including those in the hub-wall, would also scale with V_{sh}. This is supported by the fact that secondary flow losses are often categorized with shroud and passage losses. By incorporating these "itemized" k values, the energy equation is written:

$$\frac{\dot{W}_S}{\dot{m}} = \frac{p_e - p_i}{\rho} + \alpha\frac{\langle V_e\rangle^2}{2} + k_{bl}\frac{U_{tip}^2}{2} + k_{sh}\frac{V_{sh}^2}{2} + k_{tc}\frac{U_{tip}^2}{2} + k_{sec}\frac{V_{sh}^2}{2} \tag{2.9}$$

The introduction of two well-established (Osborne (1966)) non-dimensional ratios can provide useful information. The flow coefficient, ϕ, is a parameter that represents the effect of the mass flow and the blade speed. It is written as:

$$\phi = \frac{V_{sh}}{U_{tip}} \qquad (2.10)$$

The second non-dimensional number is the pressure rise coefficient, ψ_p, which establishes the pressure rise capability of a particular fan geometry at a particular operating speed. It is written as:

$$\psi_p = \frac{\Delta p}{\frac{1}{2}\rho U_{tip}^2} \qquad (2.11)$$

The energy balance can be written as:

$$\frac{\dot{W}_S}{Q} = (p_e - p_i) + \alpha\frac{\rho\langle V_e\rangle^2}{2} + k_{bl}\frac{\rho U_{tip}^2}{2} + k_{sh}\frac{\rho V_{sh}^2}{2} + k_{tc}\frac{\rho U_{tip}^2}{2} + k_{sec}\frac{\rho V_{sh}^2}{2} \qquad (2.12)$$

Since 2.12 has the units of pressure, the entire expression can be made non-dimensional by dividing each term by the product of the density and the square of the tip velocity:

$$\frac{\dot{W}_S}{Q\left(\frac{1}{2}\rho U_{tip}^2\right)} = \psi_p + \alpha\left[\frac{\langle V_e\rangle^2}{U_{tip}^2}\right] + k_{bl} + k_{sh}\phi^2 + k_{tc} + k_{sec}\phi^2 \qquad (2.13)$$

Another choice for non-dimensionalization could have been the pressure rise across the fan, $\Delta p = p_e - p_i$. This is a rational choice for many turbomachinery applications; however, for this specific application, there are complications with using this. This idea is further explained by examining the conventional definition of static efficiency in turbomachinery:

$$\eta_s = \frac{Q \cdot \Delta p}{\wp} \tag{2.14}$$

This definition of efficiency describes the non-dimensional ratio of desired quantities, flow rate and pressure rise, versus the input cost of obtaining these, which is the input power. While this definition is commonly used in many turbomachinery applications, it is not particularly instructive for other applications, such as the agricultural ventilation fan industry. This is because the pressure rise values for these applications are very low and the exit plane kinetic energy (that is not represented in 2.14) is a desired output since it is related to the flow rate. It should be evident from equation 2.14 that if the pressure rise were nominally zero, then it would correspond to an efficiency of zero. Clearly this is problematic for fan systems with very low restrictions, or for fan systems with exceedingly high restrictions, since it is either solely the flow rate or the pressure rise that is required. The former situation is the case with the application studied here.

In general, the term "efficiency" is used to refer to the ratio of desired output over required input, i.e. the benefits over the costs. Typically this is expressed in dimensionless form and the efficiency expressed in this form will be between 0 and 1. Since the definition described in 2.14 does not accurately describe the ratio of the desired output over the required input for a ventilation fan, the agricultural fan industry has created their own definition of efficiency which is described by:

$$\eta_a = \frac{Q}{\wp} \tag{2.15}$$

This ratio is not dimensionless, but instead has the units of volumetric flow rate over power, which is commonly expressed as cfm/watt, or cubic feet per minute per watt, see Ford et al. (1999). In the interest of making this communication applicable to the intended community, the usefulness of this is noted; however this definition of efficiency will not be used to present the results in this thesis.

Another definition of efficiency, which will be developed for discussion purposes here, but not actively used as the definition in this thesis, is the total efficiency. This is denoted as:

$$\eta_T = \frac{Q \cdot \Delta p_T}{\wp} \tag{2.16}$$

This definition attempts to additionally credit the fan with its ability to add kinetic energy to the air, and as Bleier (1998) notes, represents the real fan efficiency. The difficulty with this definition is that it is more difficult to calculate, since the total pressure requires that the velocity contribution of the total pressure be known explicitly.

A definition of efficiency that incorporates the kinetic energy imparted by the blade, along with the flow rate and the pressure rise capabilities of the fan is:

$$\eta^* = \frac{Q \cdot \left(\frac{1}{2}\rho U_{tip}^2\right)}{\wp} \tag{2.17}$$

This equation better describes the relationship between the desired output of the fan and the required input to the fan, and gives credit for the kinetic energy imparted by the blade. Incorporating this definition into equation 2.13 yields the following equation:

$$\eta^* = \frac{1}{\psi_p + \phi^2\left[\alpha_e\left(\frac{A_{sh}}{A_e}\right)^2 + k_{sh} + k_{sec}\right] + k_{bl} + k_{tc}} \tag{2.18}$$

Taking the definition for the system load curve, which is a parabola, as:

$$\psi_p = \lambda_{system}\phi^2 \qquad (2.19)$$

In this definition, λ_{system} is dimensionless but it represents the sum total of all the restrictions through the fan system. For an agricultural ventilation fan this could include upstream shutters, motor supports and downstream safety guards. These individual losses would be added in either a series or a parallel arrangement, as described by Potter and Foss (1982), amongst others. A fan system, where $\lambda_{system} = 0$ represents a fan operating in open air, between identical upstream and downstream pressures, such as an internal circulator fan within a greenhouse. This is commonly referred to as "free delivery". These fans have high volume flow rates, but they generate essentially no pressure rise. A fan system, where $\lambda_{system} = \infty$ would be indicative of a fan operating at what is commonly known as "shut-off" pressure, or more specifically, a fan that is pressurizing the air in an enclosed box.

Using the definition for the system load curve, equation 2.18 becomes:

$$\eta^* = \frac{1}{\phi^2\left[\alpha_e\left(\frac{A_{sh}}{A_e}\right)^2 + k_{sh} + k_{sec} + \lambda_{system}\right] + k_{bl} + k_{tc}} \qquad (2.20)$$

The objective of any attempt at fan optimization can now be focused on the task of minimizing the denominator of equation 2.20. All the losses associated with the fan system, including those encountered by adding necessary safety mechanisms are included. This communication will explain how the aerodynamic shroud, when incorporated into a well-designed system, can successfully obtain a minimal denominator in equation 2.20.

3.0 Equipment and Facility Calibrations

3.1 The Axial Fan Research and Development (AFRD) Facility

The AFRD was originally designed and built through the primary efforts of S.C. Morris in 1994 for the purpose of studying automotive cooling fans. At this time, the facility was referred to as the Automotive Cooling Fan Research and Development (ACFRD) facility. The details of this original design can be found in Morris et al. (1997). When further viable applications were found by Neal and Bardouwalla (1998), the facility was renamed the AFRD, accounting for the wider range of axial fans that can be tested.

3.1.1 Overview

The AFRD facility, shown in Figure 3.1, was used to acquire data for all of the fan tests. The fan assembly, including diffuser cone, was placed on the top surface of the facility (A). The shaft (L), which is used for driving automotive fans, was used as a mounting base for the centerbody. This feature will be discussed in detail later. The pressure rise across the fan was monitored by a pressure transducer (0 - 134 Pa) that measured the differential pressure from the atmosphere to the upper receiver using a pressure tap located at (B). Air is moved from the lab into the upper receiver and then through a set of nozzles (E), where it enters the lower receiver (H) and the flow metering devices (F & G). The prime mover (K, *Chicago Blower Co. SQ-36.5*) draws air from the lower receiver and exhausts it back into the laboratory. The flow rate through the system can be controlled through a throttle plate (J) that is located at the exit of the prime mover.

The AFRD facility was used to acquire integral performance (Δp vs. q) measurements and efficiency (η vs. Δp) of the fan and cone assembly. The AFRD is able to measure mass flow rates induced by the fan by using a set of metering nozzles that are shown in the schematic representation of the AFRD facility (see Figure 3.1) and then in greater detail in Figure 3.2. These metering nozzles are part of a unique flow measurement system that uses a moment-of-momentum flux principle. As the airflow through the facility, the net moment-of-momentum flux increases and the resistive force that is required to support the turning vane is increased. As shown in Figure 3.2, the output is the response of the strain gage assemblies that are attached to the mechanical supports for the turning vanes. There are two nominally identical measurement systems that operate in parallel in the AFRD. This design allows for a symmetric delivery of air from the upper receiver to the lower receiver. Morris, et al. (2001) have shown this to be an effective technique for measuring the total flow rate through the AFRD.

Since the AFRD utilizes this unique moment-of-momentum flux device, it does not require long settling chambers to properly set the upstream boundary conditions for the flow measuring device, as are typically needed in flow measuring nozzles. This allows the AFRD to be vertically positioned into a relatively small area, thus not requiring the large floor space usually required by similar fan testing facilities. It should be noted that an additional strength of this facility (and similarly the flow measurement system) is the capability to measure a wide range of fans, from very small diameter fans that operate at very high pressure rises to large diameter fans that operate at a very small pressure rise condition. This flexibility requires that the moment-of-momentum flux device can be accurately calibrated against a reliable flow rate. This calibration is described in detail in Sections 3.2.1 and 3.2.2.

The AFRD facility also has the unique capability to allow for the collection detailed measurements downstream of a fan though the use of the traverse system, as shown by (C) in Figure 3.1. This traverse can be maneuvered in each of three dimensions, r, θ, z, which define a polar coordinate system. These directions correspond to the radial, tangential and axial components of velocity that are typically used in fan literature. The traverse was used in this study to make the hot-wire measurements for the C_d study that are described in Section 3.2.1.

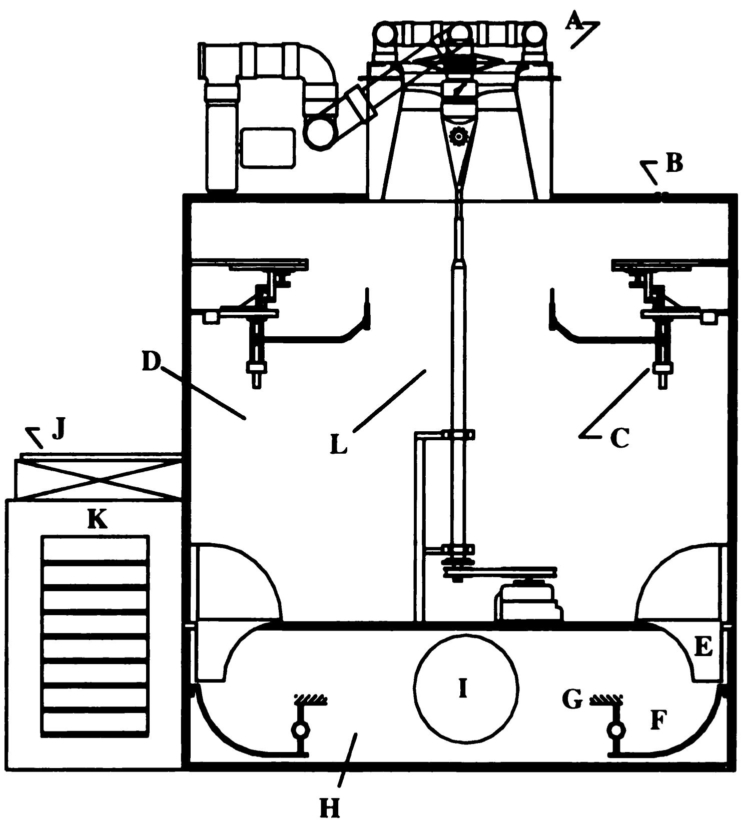

A	**TEST FAN ASSEMBLY**	**G**	**FORCE TRANSDUCER**
B	**PRESSURE TAP**	**H**	**LOWER RECEIVER**
C	**TRAVERSE**	**I**	**INLET TO PRIME MOVER**
D	**UPPER RECEIVER**	**J**	**THROTTLE PLATE**
E	**NOZZLE**	**K**	**PRIME MOVER**
F	**TURNING VANE**	**L**	**SHAFT**

FIGURE 3.1 AFRD Facility with Test Fan Assembly

3.1.2 Flow Rate Measurement System

An integral measurement technique was implemented using a large turning passage to redirect the air through a 90° angle. Figure 3.2 shows a detailed view of one metering device. Details of the apparatus noted in the figure will be identified parenthetically by a capital letter. The mass air flow through the system creates a net moment-of-momentum flux about the pivot support (R).

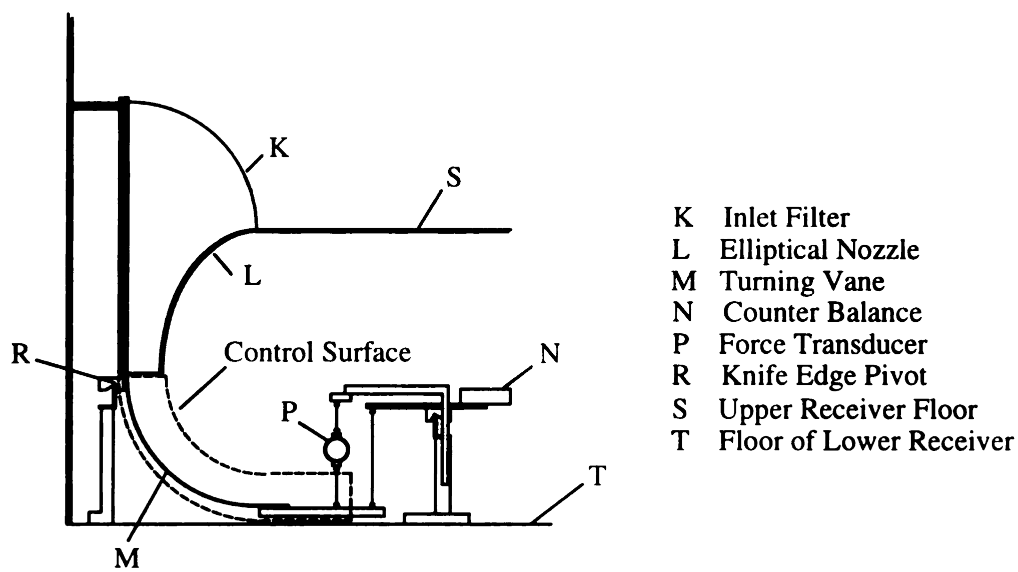

FIGURE 3.2 Schematic Representation of Flow Rate Metering Device

This was balanced by the moment from the force transducer (P). Taking the sum of the moments about (R) (counter-clockwise is positive):

$$\sum M_R = (\vec{r}_F \times \vec{F}_P) + \int_{CS} \rho[\vec{r} \times \vec{V}](\vec{V} \cdot \vec{n})dA = 0 \qquad (3.1)$$

where the control surface (CS) spans the nozzle exit to the exit of the turning passage (see Figure 3.2). The vector $\vec{r}$ represents the radius from the pivot point (R) to the location on the control surface. The derivation of equation 3.1 can be found in Potter and Foss (1982) and Munson et. al (1996). The inflow to the control surface (CS) contributes to the counter-clockwise moment-of-momentum flux (since $\vec{V} \cdot \vec{n} < 0$ and $\vec{r} \times \vec{V}$ is clockwise). The exit flow also contributes to the net counter-clockwise moment-of-momentum flux (since $\vec{V} \cdot \vec{n} > 0$ and $\vec{r} \times \vec{V}$ is counter clockwise).

The integral can be made dimensionless using a characteristic length (L) and velocity (U):

$$(\vec{r}_F \times \vec{F}_P) = -\rho L^3 U^2 \int_{CS} \left[\frac{\vec{r}}{L} \times \frac{\vec{V}}{U}\right]\left(\frac{\vec{V}}{U} \cdot \vec{n}\right)\frac{dA}{L^2} \tag{3.2}$$

The density (ρ) is considered to be constant; this is compatible with the low speed (Mach no.<0.2) flow through the entire system. The integral can be replaced by a constant (c_1) if the dimensionless integral of equation 3.2 is not a function of the flow rate through the system (i.e., the Reynolds number) nor the upstream velocity profile. The magnitude of the force measurement can be written in terms of the mass flux ($\dot{m} \sim \rho L^2 U$) or $\dot{m} = c_2 \rho L^2 U$ where c_2 depends upon the selection of U and L. Also, the quantity $(\vec{r}_F \times \vec{F}_P)$ can be expressed as ($£ \cdot F_p$) with the result that

$$F_P = \left[\frac{c_1}{\rho c_2^2 L £}\right]\dot{m}^2 = k\dot{m}^2 \tag{3.3}$$

In equation 3.3, the coefficient k has dimensions (length/mass) and $\dot{m}$ represents the desired mass air flow rate. Once calibrated, the $\dot{m}$ value can be obtained given the measured force F_p and the coefficient 'k'. An evaluation of k will be discussed in Section 3.2.2.

As noted, the relationship in equation 3.3 is dependent on the insensitivity of the coefficient 'k' to changes to the velocity profile. This specific design has several attributes which cause this condition to be met. First, the acceleration of the fluid due to the streamline curvature from the inlet of the control surface to the exit caused a greater momentum flux at the exit. The accelerated exit profile is relatively insensitive to the upstream conditions. This, along with the larger radius of the exit flow to the pivot point, makes the exit flow the dominant contribution to the integral of equation 3.2.

The force, shown above in equation 3.3, is measured as the output response of the strain gage assemblies that are attached to the mechanical support for the turning vanes. These strain gage assemblies are shown in greater detail in Figure 3.3. Further details on the performance and accuracy of this technique can be found in Morris, Neal, Foss, and Cloud (2001).

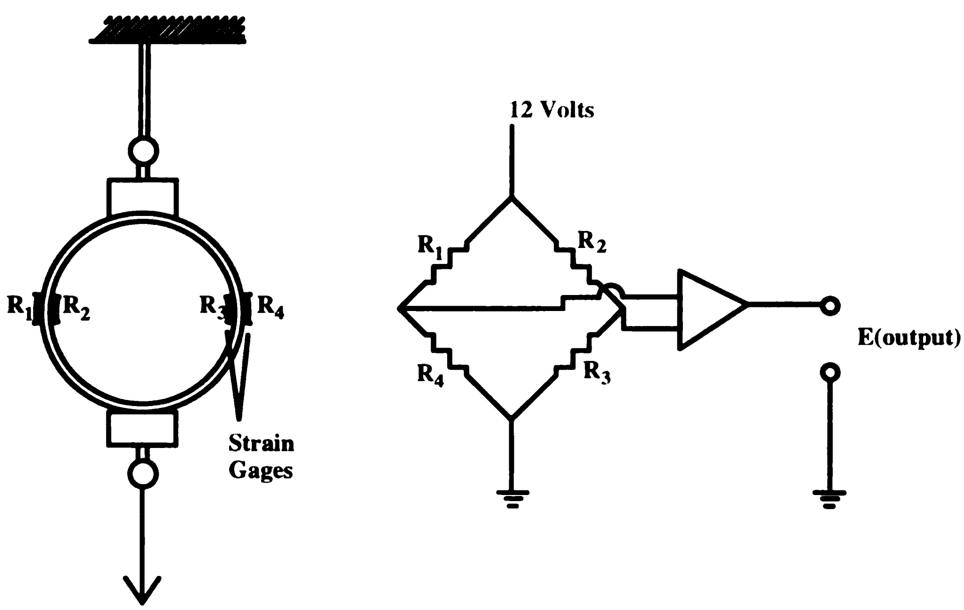

FIGURE 3.3 Details of the "Proving Ring" Force Transducer and Bridge Circuitry

3.2 Calibrations

3.2.1 Calculation of the Discharge Coefficient for the AFRD Calibration Nozzle

The metering nozzles were calibrated using an elliptical shaped contraction with a 3/2 axis ratio. This inlet nozzle provided a 6.3/1 contraction ratio in flow area. The discharge coefficient, C_d, for this device was determined using two separate methods. This section describes the procedure by which the calibration inlet, itself, was calibrated.

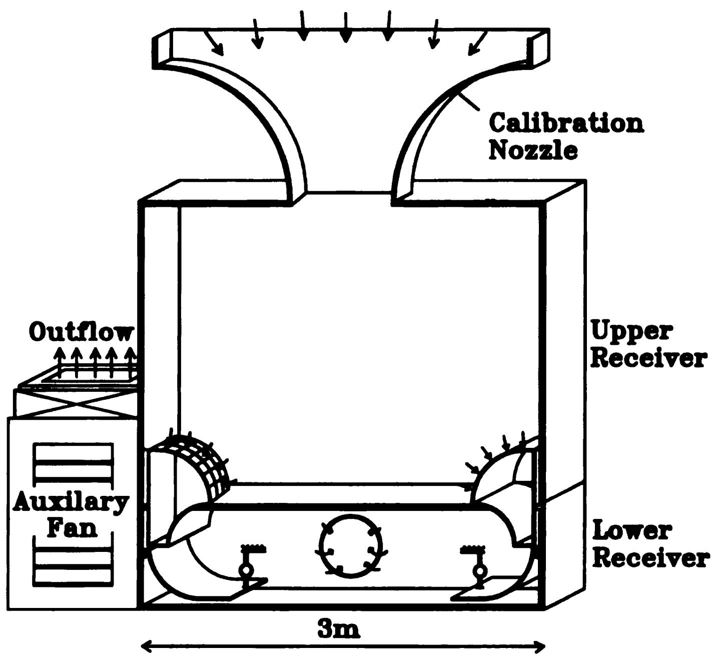

FIGURE 3.4 Schematic Representation of the AFRD Facility with Calibration Nozzle

Given that the mass flow rate through the calibration nozzle $\dot{m}_{ci}$ is equal to the sum of the flow rates through the two metering nozzles: $\dot{m}_m|_N$ and $\dot{m}_m|_S$, a knowledge of $\dot{m}_{ci}$ permits the calibration of the metering nozzles. The mass flow rate through the calibration inlet can be described as

$$\dot{m} = \rho A_{ci} C_d \sqrt{\frac{2}{\rho}(P_{atm} - P_{receiver})} \tag{3.4}$$

Each of the parameters on the right-hand side of equation 3.4 are easily measured except the discharge coefficient, C_d. Since accurate assessment of C_d is important for accurate measurements of flow rate, two methods were used to determine the C_d value for the planar contraction. These are described in the following sections.

3.2.1.1 3/16 Scale Model Study

One method for determining the C_d value was to build a 3/16 scale model of the AFRD facility. The salient features of the AFRD were utilized in the model; namely, the calibration inlet, the outer surface of the AFRD and the interior of the upper receiver were accurately recreated as 3/16 scale. Since the C_d value is only a function of the boundary conditions and the Reynolds number:

$$Re = \frac{U_{ci}\, d_H}{\nu}, \tag{3.5}$$

the prototype C_d value can be determined for the Reynolds number values of the model study.

A Testek model 11359 sonic nozzle test stand was used to generate a known mass flow rate for the model study. The sonic test stand provides a known mass flow rate that ranges from 3.5 kg/hr to 800 kg/hr. The desired flow rate is established by opening and closing an array of nine nozzles. The nozzle areas define a binary progression, as described in equation 3.6.

$$A_n = A_o 2^n \text{ where } A_o = \frac{3.5 kg/hr}{\rho \langle V \rangle} \text{ at STP} \tag{3.6}$$

The open/closed condition for each nozzle is established by a solenoid activated valve. The chamber directly downstream of the nozzles is evacuated to a pressure sufficiently low enough to impose a sonic (M=1) at the throat of the open nozzles. The 3/16 AFRD model was placed onto the sonic nozzle test stand such that test stand removed air from the lower receiver of the model. Therefore, the sonic nozzle test stand acted as the prime mover for the 3/16 AFRD model. This configuration is shown in Figure 3.5.

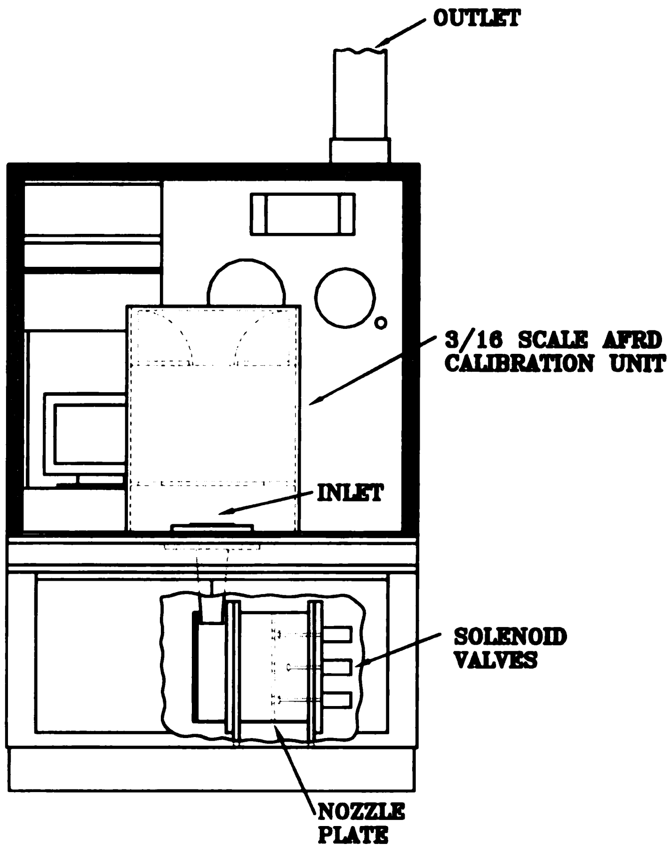

FIGURE 3.5 3/16 Scale Model of the AFRD on the Sonic Nozzle Test Stand

The discharge coefficient was calculated from the known mass flow rate of the model study and the other terms on the right hand side of equation 3.4. A plot of the calculated C_d values vs. Reynolds number is shown in Figure 3.6. This figure shows the C_d value increasing monotonically with Reynolds number before levelling out at a value near 0.980. The high values, which are quite near the ideal value of 1.0, can be attributed to the well-designed contraction. This contraction minimizes frictional losses by thinning the approach boundary layers through flow acceleration.

3.2.1.2 Hot-Wire Study

After completing the study with the 3/16 scale model of the AFRD, an additional study was conducted on the full-scale contraction. These additional measurements confirmed the measurements made with the 3/16 scale model and provided further information for accurate C_d values at higher Reynolds numbers. For this study, hot-wire measurements were made in the near wall region of the exit of the planar contraction for both the length (L) and width (w) sections. These data provided estimates of the displacement thickness, δ^*, associated with each wall's boundary layer. The discharge coefficient can then be estimated as:

$$C_d \cdot wL = wL - 2\delta_L^* L - 2\delta_w^* w \tag{3.7}$$

or

$$C_d = 1 - \frac{2\delta_L^*}{w} - \frac{2\delta_w^*}{L} \tag{3.8}$$

Figure 3.6 shows a composite plot of the model study and the hot-wire study. The range of flow rates that were needed for this study correspond to Reynolds numbers that range from ~150,000 to ~550,000. Figure 3.7 shows a close-up view of the overlapping region between the 3/16 model study and the hot-wire study. The agreement between these two regions further reinforces the accuracy of the C_d values, particularly since different approaches were used in each study. From these data, a C_d value of 0.980 was confirmed for the present study, which required flow rate calibrations that ranged from 1.50 - 4.75 kg/s. This flow rate requirement corresponded to Reynolds numbers that ranged from ~150,000 to ~550,000 for the calibration inlet. Over this range of Reynolds numbers, the C_d values varied no more than 0.5%, as shown in Figure 3.6. Therefore, a constant of value of 0.980 was used in equation 3.4.

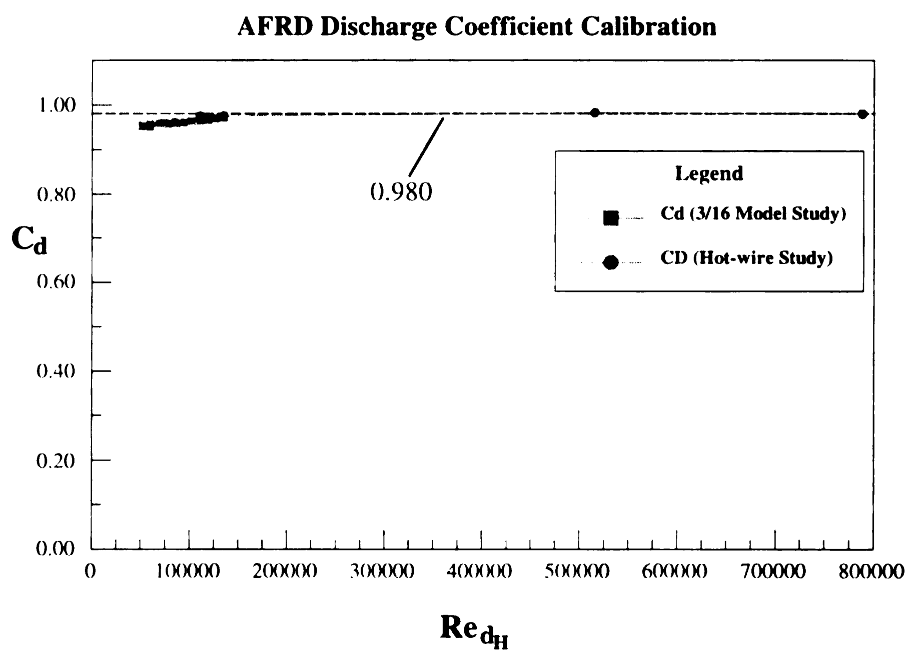

FIGURE 3.6 Discharge Coefficient Values for the 3/16 Scale Model and Hot-wire Study on the Full-Scale Calibration Nozzle

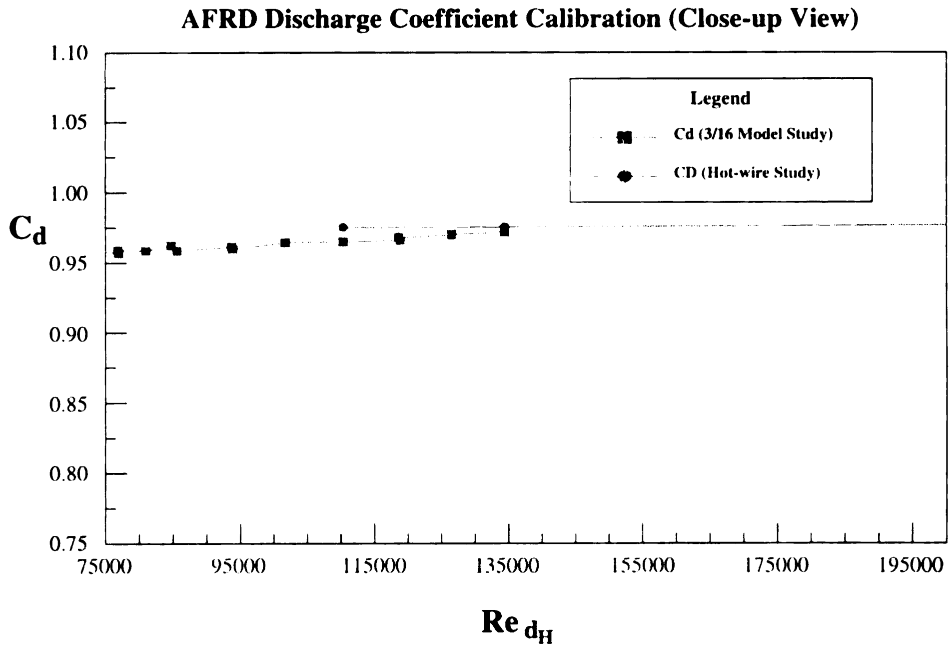

FIGURE 3.7 Close-up View Showing Agreement Between the Model Study and Hot-Wire Study

3.2.2 Calibration of the Flow Rate Measurement System

The metering nozzle calibration was accomplished by the addition of a planar contraction on the top of the AFRD normally occupied by the test fan. The auxiliary fan, shown in Figure 3.4, established an air flow that moved air from the laboratory, through this calibration inlet and into the upper receiver - plenum. From the upper receiver, the air moves through the metering nozzles and into a lower receiver. The air is then returned to the laboratory through the centrifugal fan. A throttle plate at the exit of the auxiliary fan was used to control the flow rates. A range of known flow rates was generated (Section 3.1) and the resulting voltage outputs from the strain gages were recorded for the calibration process.

The rectangular opening (outlet dimensions were 0.75 m x 0.25 m) made it possible to directly test the insensitivity of the metering nozzle to the upstream flow distribution. This was specifically tested by rotating the nozzle 90 degrees around its center axis (from the position shown in Figure 3.4). No systematic change in the k value was observed for these distinctly different inflow conditions to the metering nozzles.

Equation (3.3) can be written explicitly in terms of the mass flow rate give the linear relationship of the measured voltage (E) with the applied force:

$$\dot{m} = k''\sqrt{E-b} \tag{3.9}$$

The coefficients b and k" were empirically determined using a linear ordinary least squares fit of the calibration data. The resulting transfer function for the two flow meters were:

$$\dot{m}_N = 3.5348\sqrt{E_N - 0.490}\ \ (kg/s) \tag{3.10}$$

and

$$\dot{m}_S = 4.3506\sqrt{E_S - 0.507}\ \ (kg/s) \tag{3.11}$$

where E_S and E_N represent the time mean voltages measured from the transducers on the north and south sides of the facility, respectively. These curves show a linear fit between the square root of the measured strain gage voltage and the resulting flow rate. These data confirm the insensitivity of the net moment-of-momentum flux to the inflow condition since calibration data for each of the two orientations were combined to generate the final curve fit. This result was expected since the inlet screens/filters distributed the flow and since an integral effect was inherent in the measurement. The calibration data and the curve fit of these data are shown in Figures 3.8 and 3.9.

The final values for total mass flow rate were determined by taking the average of the two measured values from the two metering nozzles. Total mass flow rate ($\dot{m}$) was then divided by the representative density, yielding a volume flow rate that is reported in the performance curves of Section 6.0 and in the definition of η^*, as described in equation 2.17. This practice is also consistent with the current standards of the ventilation fan industry. Using these devices, flow rates that range from 1.20 - 4.50 m^3/s can be reliably measured. This range of flow rates is well-suited for 24 inch livestock ventilation fans, which typically have flow rates between 1.20 - 3.10 m^3/s, as detailed in Ford et al. (1999). This limited range allows for good resolution in the flow rate measurements.

The quality of the data fit was determined using the standard deviation of the difference between the calibration data and equations 3.10 and 3.11:

$$\sigma_{error} = \sqrt{\frac{1}{N-1}\sum(\dot{m}_{predicted} - \dot{m}_{actual})^2} \qquad (3.12)$$

where the summation is taken from all the calibration data. The deviation for the 'north' metering system was 0.023 kg/sec, or 0.5% of the measurement range. The deviation for the 'south' metering system was 0.019 kg/sec, or 0.4% of the measurement range. These numbers support the replacement of the integral appearing in equation 3.2 with the constant of equation 3.3. They also indicate the relative insensitivity of the technique to the 90 degree rotation of the rectangular calibration nozzle.

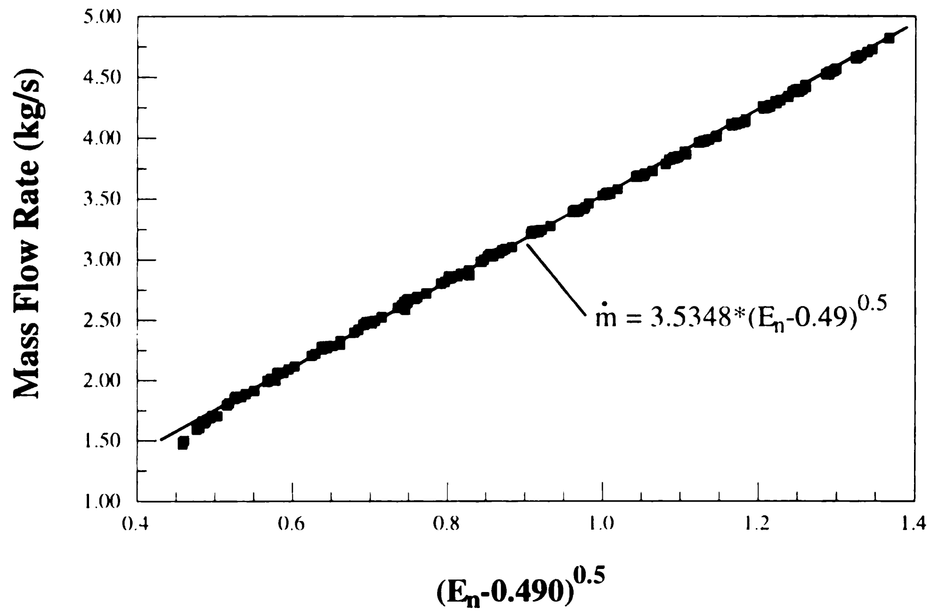

FIGURE 3.8 Calibration Data and Fit for the North Metering System

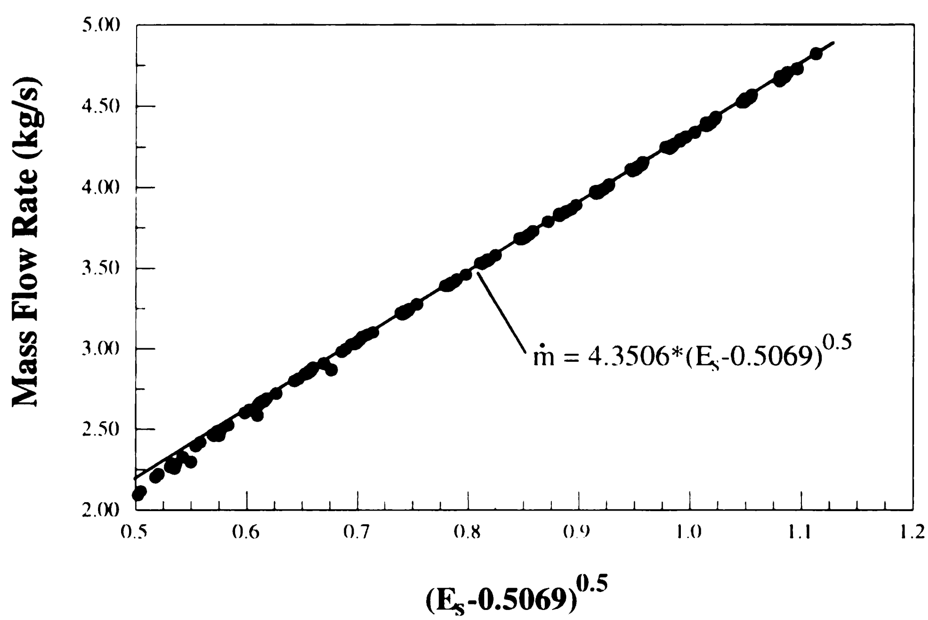

FIGURE 3.9 Calibration Data and Fit for the South Metering System

3.2.3 Shroud Flow Rate - Elbow Meter System

The mass air flow through the aerodynamic shroud Coanda nozzle was determined by an "elbow meter". A calibration of the elbow meter was executed using the Ford Haus facility as shown in Figure 3.11. A calibrated venturi nozzle was used to measure the flow rate through the system. A PC based A/D system and two Validyne pressure transducers were used to measure the pressure differences of both the venturi nozzles and the elbow meter. As shown in Figure 3.11, the elbow meter reading is based upon the outside/inside pressure difference: (P_{out}-P_{in}), which -- from the Euler - "n" equation

$$\frac{\partial p}{\partial n} = \frac{\rho V^2}{R} \qquad (3.13)$$

is expected to be proportional to the mass flow rate squared. For a known density, this becomes $q_a = f(z)$, where $z = \{\rho_{air} \cdot \textit{voltage of the pressure transducer}\}$. The expression

$$q_a = 2 \cdot (-4.57 - 1.98z + 125.39z^{1/2} - 182.60z^{1/3} + 124.17z^{1/4}) \qquad (3.14)$$

provides an acceptable fit to these data. Note the factor of 2 used in equation 3.14. This is used because the elbow meter is located downstream of a split in the delivery system, as shown in Figure 3.12. The equality of the flow in the two branches was checked using a method similar to that used by Morris (11).

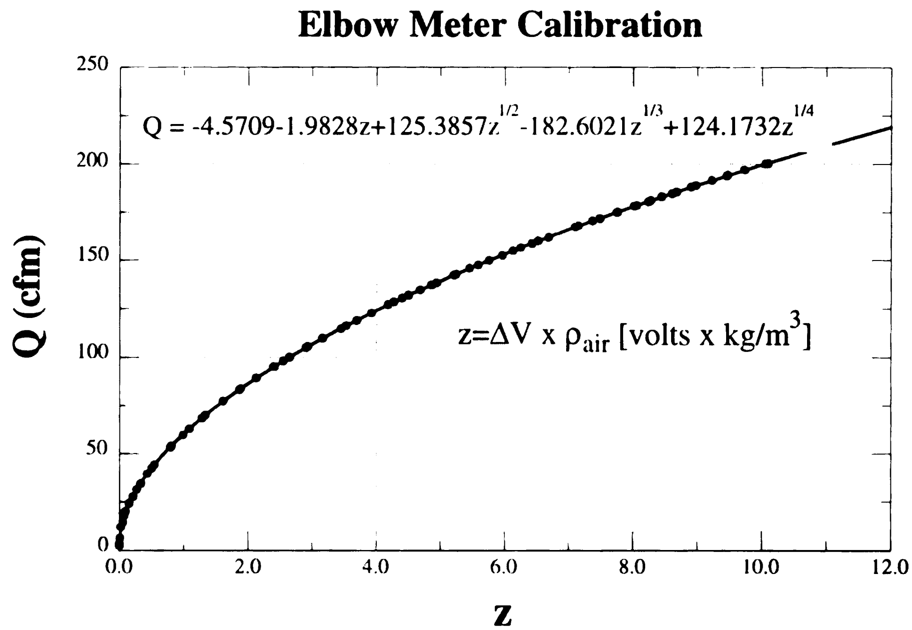

FIGURE 3.10 Data Fit for the Shroud Elbow Meter Calibration

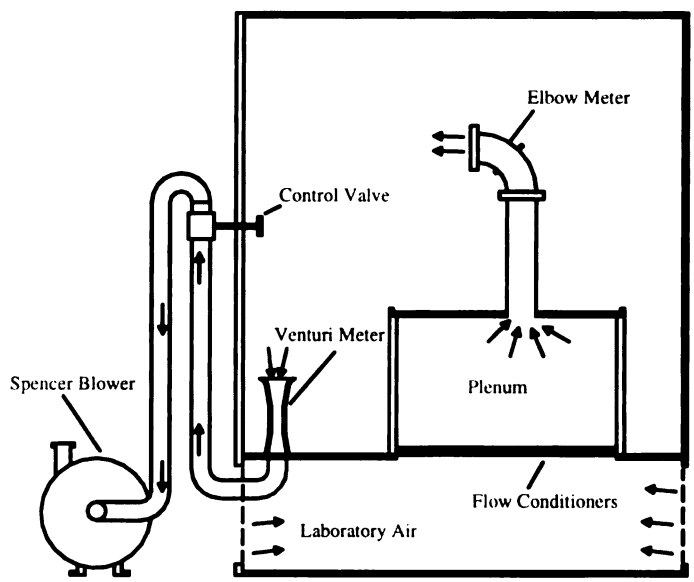

FIGURE 3.11 Calibration of the Elbow Flow Meter Using the Ford Haus Facility

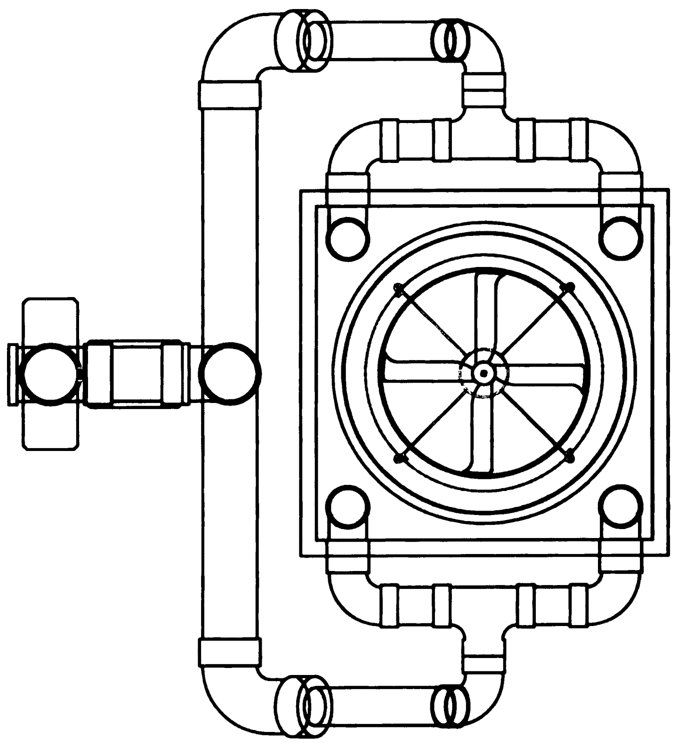

FIGURE 3.12 Overview of the Shroud Delivery with Elbow Flow Meter

3.2.4 Power Meter Calibration

Calculating the efficiency of a ventilation fan requires an accurate measurement of the power consumed by the fan's motor. This was accomplished by measuring the instantaneous voltage across the motor (e_l) and the instantaneous current (i_l) delivered to the motor. The average power defined by equation 3.15 is calculated in its discretized from through the relationship (3.16).

$$\wp = \frac{1}{T_2 - T_1} \int_{T_1}^{T_2} (i(t) \cdot e(t))dt \qquad (3.15)$$

$$\wp = \frac{1}{N}\left(\sum_{j=1}^{N} (i_l \cdot e_l)\right) \qquad (3.16)$$

or

$$\wp = \tilde{i} \cdot \tilde{e} \cdot \cos\phi \tag{3.17}$$

Since the instantaneous voltage and current (and not the RMS values of the right hand side of equation 3.17) are measured, the phase relationship ϕ is not required for the evaluation of $\wp$. The value of N and the increment in j of (3.16) are selected to ensure that an even number of cycles are represented in the summation. The instantaneous voltage and current were measured by using a voltage divider and a current sensor, respectively. Each of these devices output a voltage that was measured using Analog-to-Digital (A/D) hardware. A detailed schematic of this custom circuit is shown in a model CLN-25 closed loop Hall effect current sensor from F.W. Bell Technologies was used for these measurements. This sensor is capable of measuring either AC or DC currents on a continuous time basis and provides electrical isolation between the current carrying conductor and the output of the sensor. The manufacturer's specifications indicate that the sensor's output is linear to better than ±0.2% with a response time of under 1μs. For calibration, the current sensor and voltage divider were calibrated against a reliable source, the Hewlett-Packard 6632A system DC power supply. Using this reference, the following transfer functions were established.

$$\textit{System Amperage} = 2.5228(E_{CS}) - 0.004 \tag{3.18}$$

$$\textit{System Voltage} = 20.063(E_{VD}) + 0.0021 \tag{3.19}$$

Where E_{CS} represents the voltage output of the current sensor and E_{VD} represents the voltage output of the voltage divider.

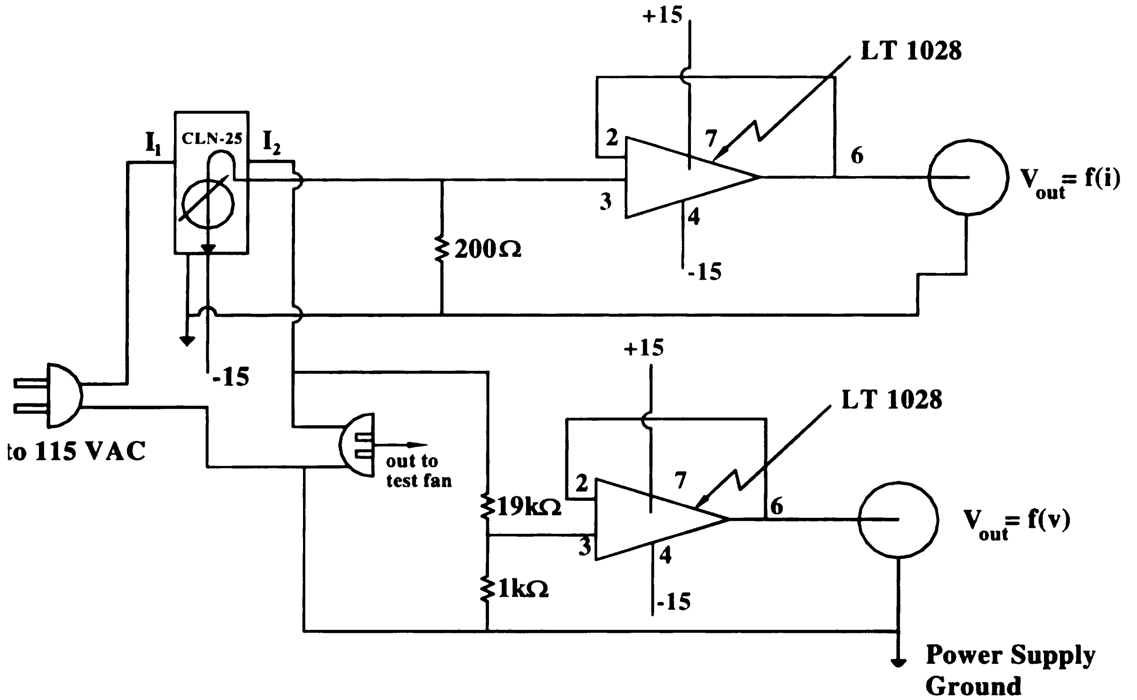

FIGURE 3.13 Schematic of the Current and Voltage Circuit Used to Measure Fan Power

3.3 Data Acquisition and Processing System

The integral data and hot-wire measurements were acquired using an Analogic Fast-16 A/D (Analog-to-Digital) board that was placed in an Intel x86 computer. Measurements that needed to be sampled simultaneously were collected using an 8 channel "sample and hold" card that "instantaneously" stores data from 8 channels before writing to the storage, without a channel-to-channel delay in scanning. The boards were run in a differential mode, with a range of ±10 volts. This range resulted in a least significant bit (LSB) of ~0.3 mv. This value was confirmed by connecting a short circuit to the channel inputs and noting the "bit flipping" around E = 0.

Collected raw data were transferred to a DEC Alpha αXP-150 computer. Custom FORTRAN programs, which were written in part by the author, were used to process the data. Post-processing programs that were used include Matlab, Excel, PSI-Plot and TecPlot.

3.4 Pressure Transducers

Several different types of differential pressure transducers were used, depending on the required range of the measurement. For the ΔP_{fan}, an MKS Baratron model 310CD-0001 head unit and an MKS Baratron 170M-6C signal conditioner were used. The 310CD-0001 has a range of 0-134 Pa. For the ΔP_{shroud}, an MKS Baratron 398HD-00010 head unit with an MKS Baratron type 270B signal conditioner was used. This unit has a range of 0-1340 Pa. Finally, the pressure drop across the elbow meter that monitored the shroud flow rate was measured using a Validyne DP15-20 head unit with a CD15 carrier demodulator. The reported accuracy of the DP15-20 is ±0.25%, which includes effects from non-linearity, hysteresis, and non-repeatability.

3.5 Optical Encoder

The rotational speed of the fan was measured using a custom designed and built optical encoder circuit. The schematic of this circuit is shown in Figure 3.14. Infrared light is generated from a diode device that sends light directed towards the hub of the fan (labeled A-K in Figure 3.14). A small piece of reflective tape was placed on the hub that reflected the light back to the collector-emitter (of the transistor) side of the circuit (labeled C-E in Figure 3.14). The output signal of this device is 0 - 5 volt square wave that was measured by the A/D board. The fan rotational speed was calculated from this signal. Using the measured average rotational speed, the fan tip for any particular test can be calculated. The fan tip speed is necessary for the calculation of the system efficiency, h*, as defined in equation 2.17.

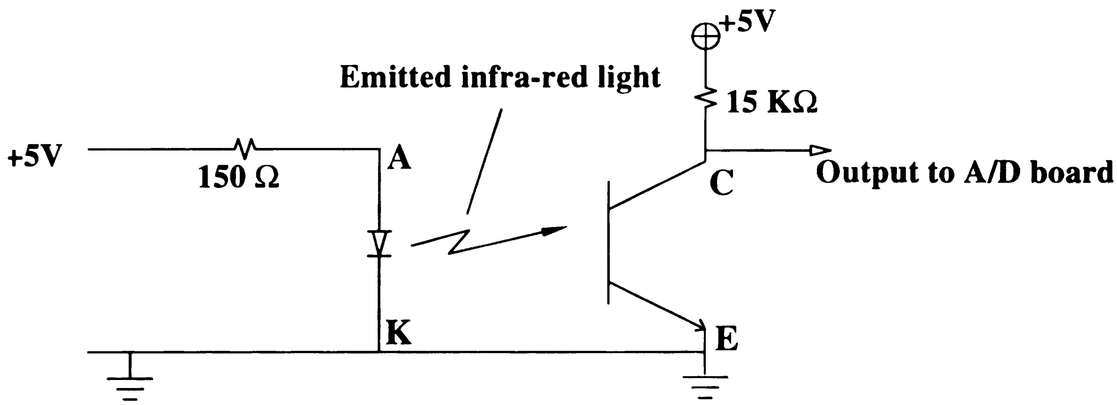

FIGURE 3.14 Circuit Schematic for AFRD Optical Encoder

3.6 Uncertainty Considerations

The reliability of measurements made in the AFRD facility is important for both the relative comparisons made in the laboratory, but also for comparing results generated in the AFRD with those from other facilities. This can be divided into two separate measures of uncertainty: repeatability and accuracy.

3.6.1 Repeatability

The uncertainty of repeated (test-to-test) measurements in the AFRD facility are shown in Figure 6.1 on page 76 for flow rate (performance) measurements and on Figure 6.2 on page 76 for efficiency measurements. References [1] and [9], provide criteria for acceptable tolerances when making comparative measurements. Ford et al. (1999) list that a fan's airflow and efficiency must fall within ± 6% of the listed values to maintain certification. This criteria is established as the basis for individual fan companies to "challenge" the published (Ford et al. (1999)) values of a competitor's fan. AMCA (Air Movement and Control Association, Inc.) provide a slightly different criteria in [3]. They list that the airflow must be within ± 3-4% over the entire range of the performance curve, and within ± 5% for the power efficiency. The four individual tests that are shown in Figures 6.1 and 6.2 were used as a measure of the repeatability of the data collected in the AFRD facility.

TABLE 1. Flow Rate and Efficiency Data from Four Independent Tests

Test #	Interpolated Pressure (Pa)	Q (m^3/s)	η^*
Test 1	25.0	2.79	9.56
Test 2	25.0	2.79	9.73
Test 3	25.0	2.78	9.46
Test 5	25.0	2.76	9.25

TABLE 2. Mean, Standard Deviation and Uncertainty from the Data in Table 1.

Variable	Mean	Standard Dev.	% Uncertainty $(\tilde{x}/\bar{x}) \times 100$
Q (m^3/s)	2.779	0.0144	0.52
η^*	9.500	0.2006	2.11

The data in Table 2 show the repeatability to be 0.52% for volumetric flow rate (Q) measurements and 2.11% for efficiency (η^*) measurements. These values fall within the guidelines established by [1] and [9].

3.6.2 Accuracy

The accuracy of measurements was determined by assessing the individual uncertainties associated with each of the primary variables that were measured. A comparison of measurements collected in the AFRD vs. published literature as found in Ford et al. (1999) will be shown later in Section 6.0. This comparison is not exact, since the configurations are slightly different; however, these differences are noted and estimates of their effect on volumetric flow rate (Q) and efficiency (η^*) are noted in Section 6.0. This section addresses the accuracy of the measurements with respect to the techniques and equipment that were used.

3.6.2.1 Accuracy of Flow Rate Measurements

The accuracy of the volumetric flow rate measurements (Q) depends primarily on the accuracy of the discharge coefficient that is used for the calibration nozzle. Section 3.2.1 details the two separate approaches that were used to determine the discharge coefficient for the planar contraction nozzle. Figures 3.6 and 3.7 show the agreement between the two techniques. The accuracy of the scale model approach can be analytically determined by recalling the following relationship:

$$C_d = \frac{Q}{U_o A} \tag{3.20}$$

The numerator, Q, is measured by the Testek model 11359 sonic nozzle test stand, which has a rated (NIST traceable) accuracy of 0.5% of a mass flow reading, as reported by [20]. The uncertainty of the C_d value can be determined by:

$$\delta C_d = \left\{\left[\left(\frac{\partial C_d}{\partial Q}\right)\delta Q\right]^2 + \left[\left(\frac{\partial C_d}{\partial U_o}\right)\delta U_o\right]^2\right\}^{1/2} \tag{3.21}$$

From this equation, the uncertainty of the measured C_d value as described in Section 3.2.1 was estimated to be ±0.006. This value also agrees well with the stated repeatability for flow rate measurements, as shown in Table 2.

3.6.2.2 Accuracy of the Efficiency Measurements

The accuracy of the efficiency (η^*) measurements depends primarily on the accuracy of the electrical power measurement technique, which is described in Section 3.2.4. The accuracy was evaluated by comparing the output of the current and voltage measuring device (described in Section 3.2.4) with that of a known reference current and voltage. These reference values were measured using a Hewlett-Packard 3457A multi-meter. Using the following relationship for the uncertainty of the power measurements,

$$\delta \wp = \left\{ \left[\left(\frac{\partial \wp}{\partial i} \right) \cdot \delta i \right]^2 + \left[\left(\frac{\partial \wp}{\partial e} \right) \cdot \delta e \right]^2 \right\}^{1/2} \tag{3.22}$$

and then taking the power consumed by a representative operating condition of $\Delta P \approx 25$ Pa, the uncertainty of the power measurement was estimated to be $\approx 0.22\%$. This number, which was calculated without considering the manufacturer's specifications, is slightly higher than the rated uncertainty of the Hall effect current sensor (see Section 3.2.4), indicating that the current measurement is the dominant source of uncertainty in the power measurement.

4.0 Experimental Configuration

Data were collected in the AFRD Facility with the fan and diffuser cone situated as shown in Figure 4.1. This vertical-flow configuration differs from the fan's typical (wall-mounted and horizontal-flow) configuration. This configuration accommodated the AFRD Facility's calibration inlet. Further detail can be seen in Figure 4.1, which shows the schematic layout of the fan and cone combination. The auxiliary air supply that pressurized the shroud was delivered through PVC piping and into the four corners of the aerodynamic shroud's housing.

4.1 Baseline Configuration: A Standard 0.61m Production Assembly

The initial set of measurements were taken with an Aerotech standard four blade fan that had a 7-degree stock diffuser cone. This combination of components is very similar to that found on the Advantage© style fan, which is shown in Figure 4.2. This line of fans is Aerotech's highest-quality, and subsequently, best-performing fan. Figure 4.2 shows that there is a set of inlet shutters upstream of the fan plane and a safety guard downstream of the fan plane. Neither of these accessories were included in the assembly that was tested for this study. It is recognized that these will provide additional system resistances that are not included in the tested assembly; however, there is an additional system resistance from the piping for the shroud delivery system that is included in the tested assembly, for both the "shroud off" and "shroud on" test conditions. It was determined that the pressure rise created from this additional system resistance was comparable to that of the missing components. This point is further discussed and quantitative data are provided to reinforce this assertion in Section 6.1.1.

4.2 Modified Configurations

4.2.1 Different Fan Blade Designs

A new blade design was considered after fully evaluating the baseline configuration in both a "shroud-off" and a "shroud-on" configuration. A flow visualization and subsequent particle image velocimetry study were conducted, both of which provided initial insight into the limitations of the production 4-blade fan. This new blade design incorporated the salient features that were thought to be an improvement from these limitations. The 5-blade version of this newer fan design is shown in Figure 4.4. and the results of this design in both the "shroud off" and "shroud on" are presented in Section 6.4 on page 65.

Further data were collected on fan designs that were similar to that of the 5-blade fan in Figure 4.4. An 8-blade and a 3-blade fan, as shown in Figures 4.5 and 4.6, resp., were tested and these results can be found in Section 6.5 on page 69.

4.2.2 Installed Centerbody Device

The flow visualization study also suggested that a centerbody device, as shown schematically in Figure 4.7, might improve the performance and efficiency of the fan system, particularly when used with the newer blade designs described in Section 4.2.1. The centerbody was a cylindrical section that has a diameter that matched that of the 5-blade fan. Figure 4.8 shows a close-up view of the hub region and top portion of the centerbody. A 2.0 mm gap separated the top edge of the centerbody from the trailing edge of the hub. The results of the centerbody and 5-blade fan can be found in Section 6.6. This configuration was only evaluated with the 11 degree cone.

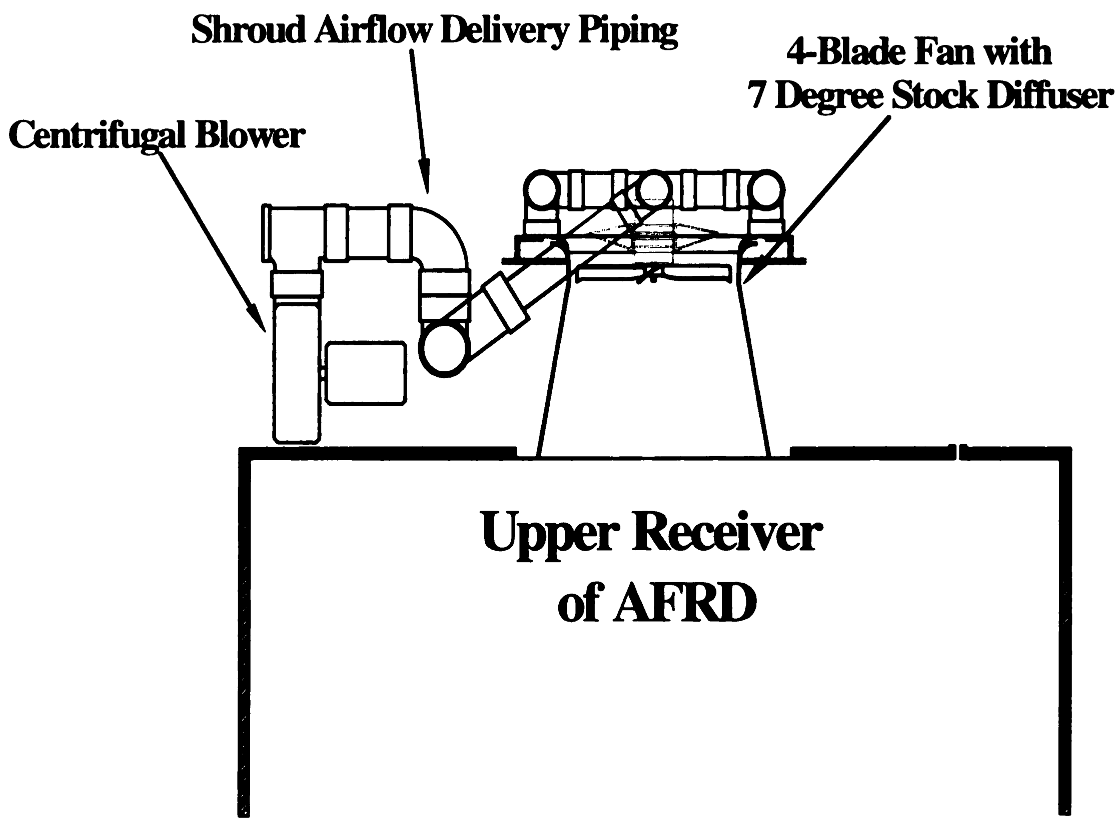

FIGURE 4.1 Schematic View of the Production 0.61m Ventilation Fan and Diffuser Cone

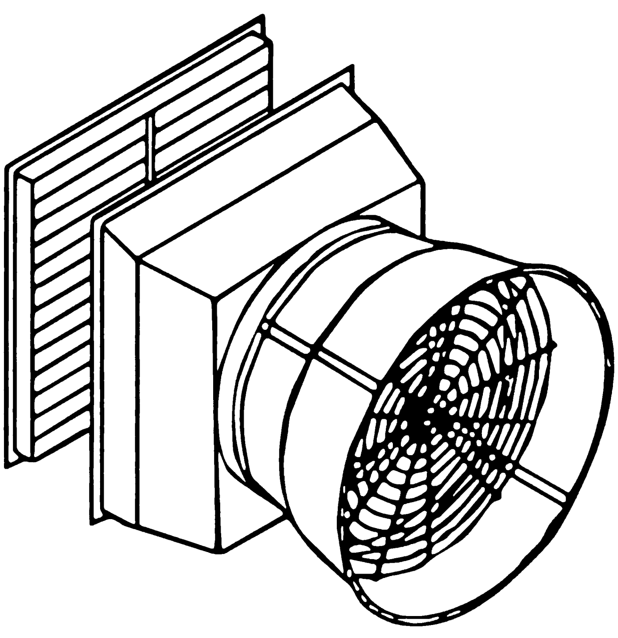

FIGURE 4.2 Schematic of Standard Production Assembly

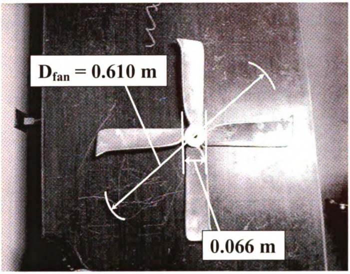

FIGURE 4.3 Production 4-Blade Propeller

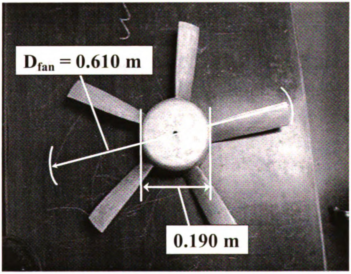

FIGURE 4.4 Prototype 5-Blade Propeller

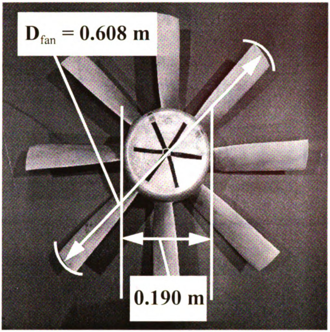

FIGURE 4.5 Prototype 8-Blade Propeller

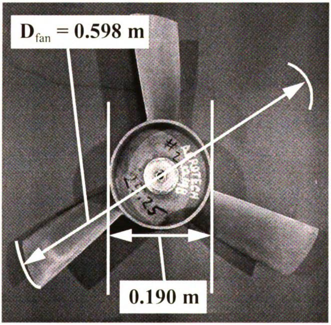

FIGURE 4.6 Prototype 3-Blade Propeller

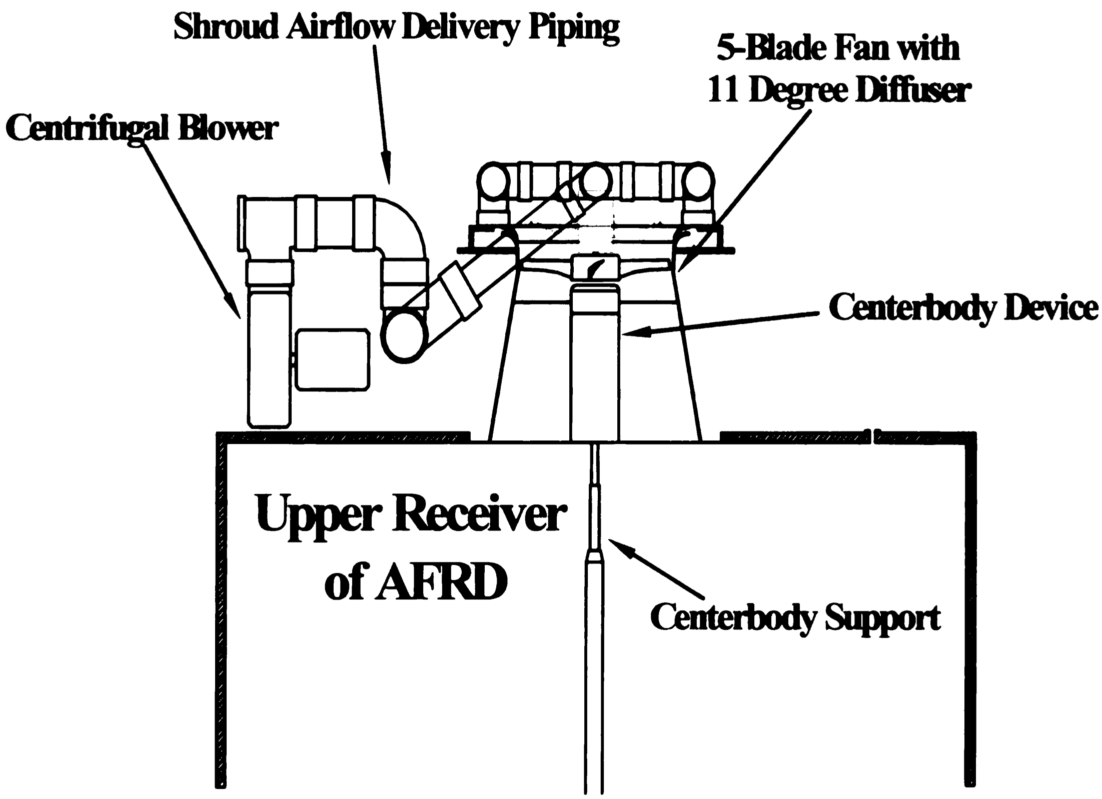

FIGURE 4.7 Schematic View of the Production 0.61m Ventilation Fan and Diffuser Cone with Installed Centerbody

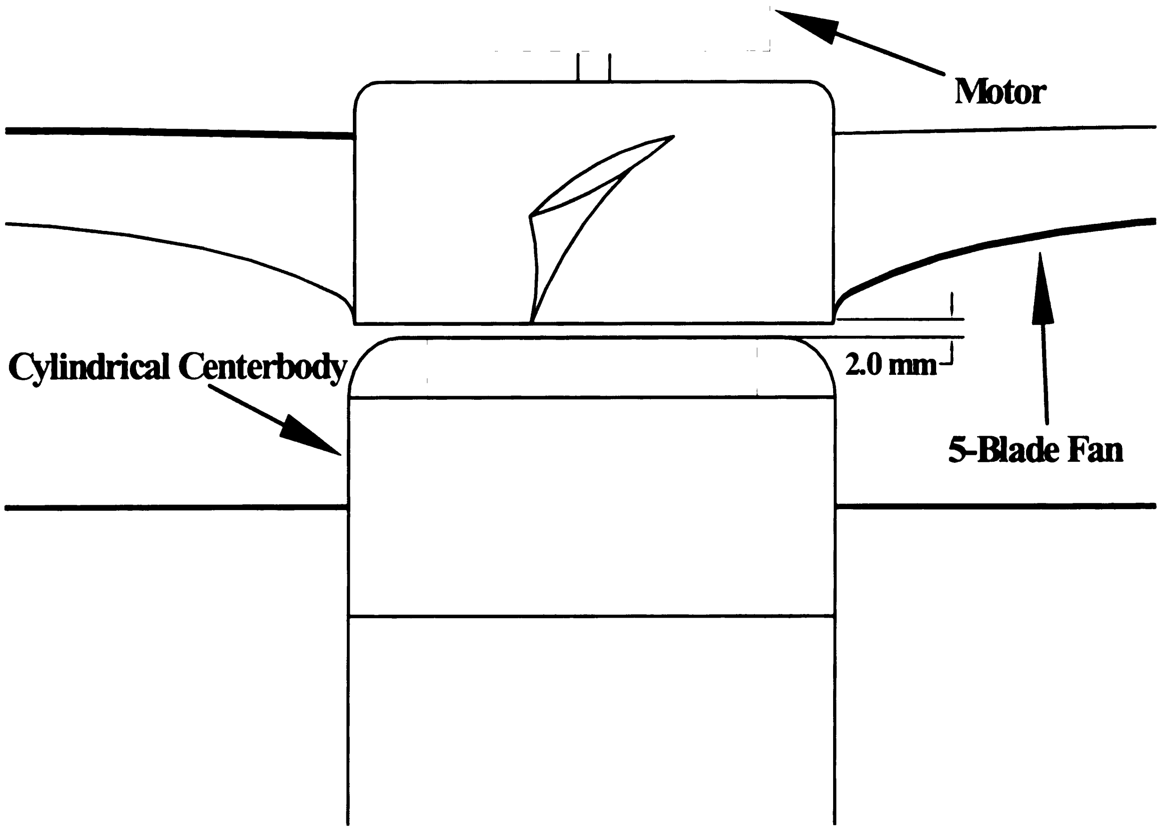

FIGURE 4.8 Close-up View of Centerbody and 5-Blade Hub

5.0 Experimental Techniques

5.1 Integral Measurements

The primary quantities of interest in turbomachinery exist in an integral form. These variables are the volumetric flow rate, Q, expressed in m^3/s, the pressure rise across the fan blades or fan system, which is denoted as Δp, and expressed in Pa, and the system efficiency, η^*, defined as

$$\eta^* = \frac{Q \cdot \left(\frac{1}{2}\rho U_{tip}^2\right)}{\wp} \tag{5.1}$$

The various definitions and interpretations of efficiency are explained in detail in Section 2.0, but the choice of using η^* was made because it was non-dimensional and it also has a solid physical interpretation. It is recognized that the industry standard definition is

$$\eta_a = \frac{Q}{\wp} \tag{5.2}$$

This definition of efficiency, η_a, is found in literature that is standard in the agricultural ventilation industry; see Ref. [1] and [9]. The data found in these references were converted to the definition of efficiency as found in equation 5.1, since all the information can readily be obtained in either Ref. [1] and [9]. These values were then compared with industry accepted standards to ensure the reliability of the measurements. Care was taken to ensure that the measurement procedure was similar to that of BESS and AMCA testing standards. The one omission is the placement of shutters upstream of the fan plane. It is recognized that in practice these are a detriment (albeit necessary for safety issues) to the performance and efficiency of a ventilation fan, but their inclusion was not feasible given the configuration detailed in Figure 4.1. Since the baseline measurements did not incorporate shutters, the relative differences (expressed in percentages) are expected to remain consistent when shutters are included in the final production version.

When the efficiency was evaluated for a fan with the aerodynamic shroud activated, termed the "shroud on" condition, a more specific definition of equation 5.1 was used:

$$\eta^* = \frac{Q_{total} \cdot (\rho U_{tip}^2)}{\wp_{fan} + \Delta P_{shroud} \cdot Q_{shroud} \cdot (1/\eta_{shroud})} \tag{5.3}$$

This definition expands the denominator from equation 5.1 to separate the individual power consumption of the fan, denoted by $\wp_{fan}$, from the power consumed from the added apparatus of the aerodynamic shroud. The term η_{shroud} is the efficiency of the aerodynamic shroud, which is estimated for this work. Since a non-optimized assembly is used to pressurize the shroud, evaluating its efficiency directly is not instructive for this study. Instead, information found in a previous study by Herz (1998) was used to estimate the value $\eta_{shroud} = 0.70$ for all the "shroud on" cases.

The value of $\eta_{shroud} = 0.70$ was chosen based on Herz's conclusions that the efficiency range for centrifugal blowers is between 0.60 and 0.80. An efficiency of 0.80 corresponds to a backward curved centrifugal blower that is optimized for higher flow rates and lower pressure rises. Similarly, an efficiency of 0.60 is representative of a forward curved design that is optimized for lower flow rates and very high pressure rises. Since the aerodynamic shroud would require performance characteristics similar to those provided by a backward curved assembly, the author speculates that this type of blower, and the corresponding efficiency, could be used for the final assembly. Assuming the use of this type of blower, the value of $\eta_{shroud} = 0.70$ is chosen after taking into account losses that will occur in the flow delivery system downstream of the auxiliary blower.

These quantities were measured using techniques and equipment that are defined in Section 3.0, using a standard 16-bit A/D board. Once an operating condition was set (using the throttle on the AFRD as described in Section 3.1.1) the static quantities of flow rate, pressure rise, shroud pressure and shroud flow rate were sampled for 10 secs at 100 Hz. Other quantities, including input voltage, input current, and shaft RPM, were sampled at 10 kHz for 10 secs, using a sample and hold card. This sample and hold card insured that these channels were sampled simultaneously, rather than the small time delay that exists for the baseline A/D board. This requirement was necessary for calculating the power as defined in equation 3.15. The sampling time of 10 secs was determined to be optimal for statistically converged measurements.

Specific operating conditions were targeted for each test, nominally values of $\Delta p = 0$ Pa, 12.5 Pa, 25 Pa, 37.5 Pa, 50 Pa, 62.5 Pa, and 75 Pa. These values were selected since they correspond to the same operating conditions tested in Ford et al. (1999) and direct comparisons could be made with only small interpolations. The plots in Section 6.0 show typically two measured points at each operating condition. These redundant measurements were made to determine the repeatability of each data point, and also to indicate if there were any hysteresis effects. Each test involved first running the fan from the "shut-off" condition to "free-delivery" condition and then reversing the throttle on the auxiliary blower of the AFRD so the fan would move from a "free-delivery" condition back to a "shut-off" condition. There were minimal hysteresis effects in most of the test cases.

5.2 Particle Image Velocimetry (PIV) Measurements

A better understanding of the flow field in the fan system environment was obtained through the use of Particle Image Velocimetry (PIV) measurements. PIV is a measurement technique that provides instantaneous velocity maps of a particular region of interest with two or three components of the velocity being recorded. The two components are in the plane of the light sheet. A two-camera stereo system permits the out-of-plane component to be determined. These instantaneous maps can be ensemble averaged to provide time mean velocity information for a particular region of the flow. A description of the PIV measurement technique, along with specific techniques that were used for this study, will be provided in this section.

PIV measurements require that the fluid motion can be reliably traced by neutrally buoyant seed particles that are added into the flow. When a thin slice of the flow field is illuminated by a light-sheet, the illuminated seeding scatters the light. This reflected light is recorded by a camera that is placed at a right angle to the light sheet. The light sheet is pulsed, very quickly (~5 ns), twice at a precisely known interval (150 - 500 μs for the present study). The first pulse of the laser captures an image of the initial positions of the seeding particles in the light sheet. The camera frame is then advanced and the second frame is exposed to the light scattered by the particles from the second pulse of the laser. For each desired instantaneous velocity map, a pair of images are recorded.

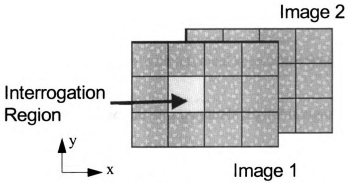

FIGURE 5.1 PIV Interrogation Region

The two images are then processed to find the velocity vector[1] map of the flow field. First each image pair is subdivided into a set of interrogation regions. The displacement of groups of particles between image 1 and image 2 in each interrogation region is measured using cross-correlation techniques, which are implemented using FFT algorithms as described in [8] and [16]. This displacement is termed: $\vec{d}$. Since the time interval (t) between these two images is well-known, the velocity can be easily inferred from the following equation:

$$\vec{V} = M \cdot (\vec{d}/t), \tag{5.4}$$

where M is the magnification factor between the camera's CCD chip and the measurement area.

A single-camera digital PIV system[2] was used to acquire the velocity data in the wake of the test fan. A Rosco brand theatrical fog machine was used at the fan inlet to produce a relatively uniform seeding density at the measurement locations. Two ND-Yag pulsed

1. The present technique obtains the projection of the 3-D velocity vector onto the image plane. The image obtained is a vector: $\vec{V} = iu + jv$.
2. A Dantec PIV2000 processor and PC based data acquisition system are subcomponents of the Multi-Phase Flow Facility (MFF) of the College of Engineering at MSU.

532nm lasers and a Kodak Megaplus ES1.0 CCD camera was used. These ND-Yag lasers illuminated the region of interest (nominally 20x20cm) with a 1 mm thick laser sheet. The two lasers were triggered sequentially with a typical separation time of 0.3 msec.

The digital camera was used to acquire two grayscale digital images. The measurement region was divided into 32x32 pixel interrogation regions to calculate the individual vector displacements. The calculation used a Gaussian window function and a 2-D Fourier transform of the image data to correlate the two images. The individual interrogation regions were overlapped by 25% (8 pixels) for increased resolution. This resulted in 1722 measured velocities for each set of images acquired.

The configuration described above provided accurate results given that the seeding was distributed in a nominally uniform manner in each image. However, at some locations high shear or poor seeding would cause poor signal to noise ratios that would lead to vector maps with many "bad" or "spurious" vectors. These were post processed using several validation techniques to ensure the integrity of the data. First, a "peak validation" was used to ensure that the maximum value of the cross correlation was a minimum of 1.2 times greater than the next highest value. This calculation removed typically 90% the suspect vectors. Second, a range validation was used such that the magnitude of the velocity in the plane of the laser light sheet could not exceed 25m/s, which is 3.2 times the average axial velocity through the fan. Finally, a moving average validation was implemented as a final check. This moving average validation is used to accept or reject velocity magnitude based on a comparison between neighboring values. Continuity of the flow field's behavior is an implicit assumption in the moving-average validation method. Further details on the algorithms used for these validations can be found in references [8], [14] and [16].

A total of 1000 vector maps were recorded and processed for each of the measurement regions described in the following section. The time averaged velocity field was then computed from the validated vectors. Note that phase averaging the data to the rotating fan would have provided more information on the blade dynamics. However, it is the time averaged quantities that lead to the net flow rates of interest, and therefore the latter representations are used in this initial study.

5.2.1 PIV Measurement Locations

As previously stated, there were three distinct regions of interest for the fan/shroud combinations. These locations, shown in Figure 5.2, include: (I) at the exit plane of the discharge cone, (II) the near wall region of the discharge cone, and (III) the region directly downstream of the hub. The selection of these regions was based on the following considerations: Region III was selected after initial observations with wool tufts indicated that the angle of attack of the blade in the near hub region was not sufficient to impart axial momentum into the flow. Region II was measured to determine if the boundary layer along the wall of the 11 degree cone remained attached. Previous studies (Patterson (1938) and Squire (1953)) had indicated that in general, axial fans equipped with discharge cones that were greater 9 degrees would exhibit a separated boundary layer (stall condition) near the wall. This boundary layer separation would result in decreased fan performance. Region I was selected to measure the exit profile of the fan and more specifically, to determine if a reversed flow condition existed near the centerline of the fan. Preliminary observations using wool tufts suggested that the velocities were highest at the outer region of the fan, with much lower velocities near the mid-blade region and near-zero velocities towards the centerline of the fan.

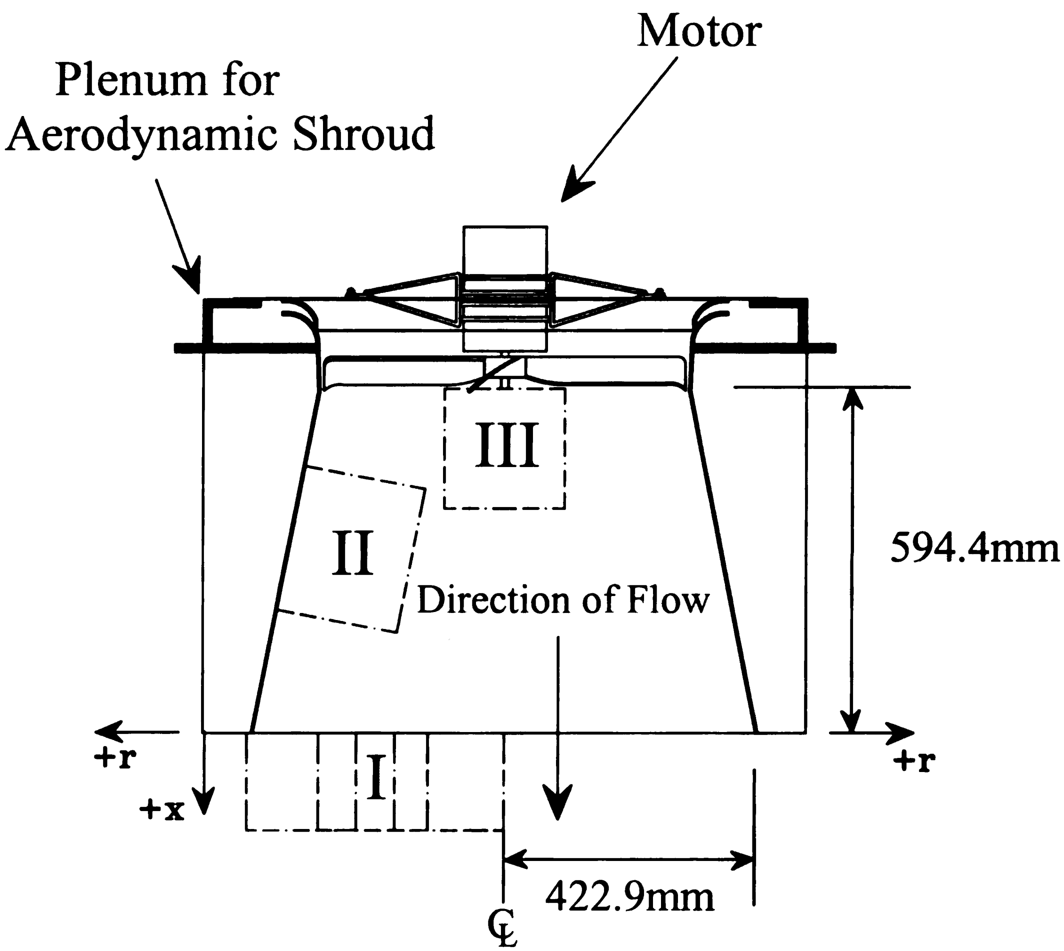

FIGURE 5.2 Location of PIV Measurement Regions

6.0 Results and Discussion - Integral Measurements

6.1 Baseline Measurements - 4-Blade Fan with 7 Deg. Diffuser Cone

6.1.1 Baseline Measurements (Production Assembly) - "Shroud Off" Condition

The repeatability of the measurements was established by taking a series of independent performance (ΔP vs. Q) and efficiency (ΔP vs. η^*) curves before experimenting with various shroud configurations. The results of this study are shown in Figure 6.1 and Figure 6.2. A total of five such data sets were collected and four of these are shown in the figures. Since this configuration is very close to that of the current production assembly, these data will serve as the reference condition to which all future data sets will be compared.

These data were compared to published data for the Aerotech AT24Z, Test: 93086, as found in Ford et al. (1999). This comparison is to ensure that these results were consistent with prior performance measures. A table of these values is shown below.

TABLE 3. Comparison of Results Obtained in the AFRD vs. Published Data

Fan Comparison for ($\Delta P = 0.10$ in H_20)	Published Data (BESS Labs)	AFRD Data	% Difference from Published Data
Volume Flow Rate (m^3/s)	2.71	2.78	+2.58
Efficiency (η^*)	8.59	9.28	+8.03

The Aerotech AT24Z is close to, but not exactly the same as, the fan that was tested in the AFRD. The AT24Z does use the same propeller as was used on the experimental fan, but the two fans have shrouds that are quite different. The AFRD data does show a slightly higher flow rate and efficiency than the published data. This is caused, in part, by the absence of inlet shutters that are on the production fan. Ford et al. (1999) states that the addition of inlet shutters will typically reduce the efficiency and flow rate of a fan by 10 to 25%. The differences indicated in Table 3 are below this range. These differences, which are lower than expected, can be explained by noting the different inlet geometries of the two shrouds. The inlet side of the experimental fan's shroud contains the additional apparatus of the delivery pipes for the aerodynamic shroud (even though these are baseline data, the aerodynamic shroud delivery system was not removed). This piping system creates additional blockage that would not be found in a final, production configuration. Thus the close agreement, as shown in Table 3, between the data for the AFRD-tested configuration and those found in the literature indicates that the blockage of the shroud delivery system is close to the blockage created by the inlet shutters and the safety guards. These data confirm that the baseline data measured in the AFRD are accurate and reliable, and consistent with the analysis that was derived in Section 3.6. Finally, it should be noted that once an optimal configuration is identified, a final production aerodynamic shroud would incorporate a more aerodynamic inlet to minimize the blockages of the prototype.

The data presented in the following section show the entire performance range (i.e. from "shut-off" condition to "free-delivery" condition). However, specific percentage gains or losses will often be noted based on a typical operating condition. This operating condition, chosen to be nominally 25 Pa, is based on information obtained from Ford et al. (1999) where they specifically state that a ventilation building fan will operate at a range around 25 Pa. They note that slight variations can occur if the housing and shutters of the fan system are excessively dirty (thereby increasing the ΔP) or if there is a strong headwind facing the downstream exit plane of the diffuser cone (again increasing the ΔP). Despite these variations, a typical fan system (fan + shroud + inlet shutters) will operate with a pressure rise of ~25 Pa for the majority of its operating life cycle.

6.1.2 Production Assembly - "Shroud On" Condition

Once baseline measurements were established to be accurate and repeatable, the effects of a range of shroud pressures were examined with this experimental configuration. The resulting pressure rise vs. flow rate (ΔP vs. Q) and pressure rise vs. efficiency (ΔP vs. $\eta *$) are shown in Figure 6.3 and Figure 6.4, respectively. From Figure 6.3, there is a clear increase in flow rate as the shroud pressure is increased from the "off" condition, to pressures of 249 Pa, 498 Pa and 996 Pa. These gains are obtained at the cost of by the decreasing values of efficiency that are shown in Figure 6.4. Examining the typical operating condition of $\Delta P \approx 25$ Pa, the flow rate increases from 2.77 m^3/s to 3.15 m^3/s, from the "shroud off" condition to the "shroud on" condition of 996 Pa. This represents a gain of nearly 14% in volume flow rate. This would be a notable increase if a comparison of the efficiencies at the same shroud conditions ("shroud off" condition to $\Delta P_{shroud} = 996$ Pa were not for the accompanying decrease in efficiency, in this case from approximately 9.65 to 7.07, a decrease in 26.7%. From these two figures, the aerodynamic shroud did not provide an unambiguous benefit for this production assembly.

6.2 The 4-Blade Fan with an 11 Deg. Diffuser Cone

After initial measurements with the production assembly did not show appreciable improvements in performance without substantial decreases in efficiency, a larger diffuser cone, 11 degrees, was incorporated into the system. Numerous references, among them Wallis (1983), have stated that diffuser angles for axial fans cannot be larger than 7-9 degrees before the boundary layer that is formed in the sidewall of the cone will separate. This separated flow will result in decreased performance and efficiency, offsetting the static pressure recovery gains that would exist in the inviscid case. Even in the cases noted by Wallis, a diffuser cone of 9 degrees represents the upper limit and is attainable only in carefully controlled laboratory conditions. Flow separation would appear in an actual installed condition for diffuser cone angles higher than nominally 7 degrees. The current production diffuser cone has an approximately 7 degree exit angle. Aerotech, Inc. has tested diffusers with larger angles, but the 7 degree diffuser cone yielded the optimal increases in performance and efficiency of any other devices. It should be noted that they have evaluated numerous cones with both larger and smaller angles.

Although these larger diffuser cone angles (> 7 degrees) have larger geometric exiting areas, the separated flow in the exiting wall boundary layer reduces the effective flow area. A device that would maintain attached flow in the boundary layer could make the use of these larger diffuser angles feasible. Specifically, the wall jet that is produced by the aerodynamic shroud could provide sufficiently high momentum to prevent this separated condition. The current production 7 degree cone has an exit area of 0.46 m^2. A new diffuser cone, with an angle of 11 degrees was fabricated to test this hypothesis. This nominally 11 degree cone had a much larger exit area of 0.56 m^2. The potential increase in static pressure recovery from this larger exit area is notable and was one of the primary motivations for evaluating larger diffuser cones with the aerodynamic shroud.

It should be noted that describing a diffuser by only its exit angle is ambiguous and insufficient, since it does not fully describe the capabilities of the device. The salient features of these diffusers is shown in Table 4 and schematically explained in Figure 6.5. One can quickly see that a 7 degree cone with a much larger length, L, could have an outlet area comparable to that of the 11 degree cone. However, this configuration would also have much larger sidewall losses, designated as k_{sh} and described in Section 2.0, “Fan Analysis,” beginning on page 8. There is also an additional constraint that is less apparent. The use of diffuser cones longer than the current production cone (L = 594.4 mm) is problematic because it will fall off from the weight of snow or heavy winds. Therefore, any new device must remain within the current limits.

TABLE 4. A Comparison of the Salient Features of the Tested Diffuser Cones (see Figure 6.5 for a description of the variables: a, b, and L)

Cone Size	a (mm)	b (mm)	L (mm)	Inlet Area (m^2)	Outlet Area (m^2)
7 Degree	622.3	762.0	594.4	0.3042	0.4560
11 Degree	629.9	845.8	594.4	0.3116	0.5619

6.2.1 The 4-Blade Fan and 11 Deg. Diffuser - "Shroud Off" Condition

The first tests conducted with the 11 degree cone were performed in the "shroud off" condition. These measurements provided a baseline by which further tests could be compared. Surprisingly, these data show a negligible difference in performance between the 7 & 11 degree diffusers, as shown in Figure 6.6. When the efficiencies for these two configurations were compared, the results were very similar. This is evident in Figure 6.7. Further explanation on why this occurred will be discussed in Section 7.0.

6.2.2 The 4-Blade Fan and 11 Deg. Diffuser - "Shroud On" Condition

After establishing baseline performance for the 4-blade fan with an 11 degree diffuser, this configuration was evaluated with the aerodynamic shroud. Two shroud pressures, 249 and 498 Pa, were tested. Figure 6.8 shows the performance curves for the 7 degree and 11 degree diffusers at the lower shroud pressure. For reference, the 7 degree - "shroud off" data are also shown. Each of the two "shroud on" conditions shows enhanced flow rate from the baseline data, but very little difference exists between the 7 degree - "shroud on" and the 11 degree - "shroud on" data. Taking an operating point at 25 Pa, a performance increase of approximately 4.5% occurs at this shroud pressure. Figure 6.9 shows a plot comparing the efficiencies of the same three configurations. From this figure, there is no apparent improvement in efficiency between the baseline data, the 7 degree - "shroud on" and the 11 degree - "shroud on" data.

Next the shroud pressure was increased to 498 Pa and the same configuration was evaluated. Figure 6.10 shows a performance curve that compares the same three test conditions. Here the 11 degree - "shroud on" condition shows appreciable gains in performance. By taking an operating point at 25 Pa, there is approximately an 11.5% improvement compared to the baseline data. However, Figure 6.11 shows that these performance gains are accompanied by a decrease in efficiency. Taking an operating point of 25 Pa, the efficiency decreases over 6%. The gains in performance are accompanied by the strong decrease in efficiency.

6.3 The 4-Blade Fan and 11 Deg. Diffuser Cone at Variable Shroud Gaps

6.3.1 The 4-Blade Fan and 11 Deg. Diffuser at a Medium Shroud Gap (g = 5.0 mm)

After the initial tests with the 4-blade fan in the "shroud on" condition failed to improve the flow rate without having an appreciable decrease in efficiency, the effect of gap height was evaluated. Previous tests had used a gap height of 1.0 - 2.0 mm, but additional tests were taken with a gap height of 5.0 mm. By increasing this height (but maintaining the same shroud pressure), the volume flow rate contributed by the aerodynamic shroud would be greater and the resulting wall jet would be thicker. The idea was that this thicker, higher momentum wall jet might be more effective in preventing separated flow on the sidewall of the cone. Additionally, the entrainment capabilities of the jet might be improved. These ideas were stimulated from the observation that the total flow rate measured was greater than the sum of the "shroud off" condition plus the shroud flow rate.

$$\eta^* = \frac{Q_{total} \cdot (\rho U_{tip}^2)}{\wp_{fan} + \Delta P_{shroud} \cdot Q_{shroud} \cdot (1/\eta_{shroud})} \tag{6.1}$$

As shown in equation , the efficiency, η^*, has the total flow rate in the numerator, and the product of ΔP_{shroud} and Q_{shroud} in the denominator. Therefore, a substantial increase in Q_{total} with respect to a smaller increase in $\Delta P_{shroud} Q_{shroud}$ will result in increased η^* values. It was thought that this could potentially be accomplished through a larger gap height.

Figure 6.12 shows the results of performance data for the medium gap height assembly. Pressures of 125 Pa, 249 Pa and 498 Pa were measured, and for each subsequently higher shroud pressure resulted in a higher system flow rate. At the operating point of 25 Pa, a 16 percent gain in flow rate is shown between the "shroud off" condition and the highest "shroud on" condition, ΔP_{shroud} = 498 Pa. However, at this shroud condition, the efficiency, shown in Figure 6.13, was substantially decreased by 20.7%, which detracts from the improvements in performance. Interestingly, at the lower "shroud-on" condition of ΔP_{shroud} = 125 Pa, the efficiency actually increased from 8.9 to 9.5, which is an improvement of 6.75%, while showing modest improvements in flow rate of 8%. This study proved that with a different gap height, moderate gains in both flow rate and efficiency could be simultaneously obtained. However, if the shroud flow rate is set excessively high, the resulting higher improvements in flow rate are accompanied by drastically lower efficiencies.

6.3.2 The 4-Blade Fan and 11 Deg. Diffuser at a Large Shroud Gap (g = 7.0 mm)

The data collected in Section 6.3.1 (the 4-blade fan with 11 degree diffuser and a medium gap height) represent the first test condition where simultaneous gains in both flow rate and efficiency were obtained for any particular combination of diffuser cone, shroud pressure and shroud gap height. These results, specifically the notion of increasing the shroud flow rate while simultaneously decreasing the shroud pressure, led to the testing of an even larger gap height for the incoming jet of the aerodynamic shroud. This condition, described as the "large" gap height condition resulted in g = 7.00 mm.

Figure 6.14 shows the performance data for the large gap height condition at the baseline "shroud off" condition, and also for shroud pressures of 125 Pa, 249 Pa and 374 Pa. The highest shroud pressure, while lower than the highest condition evaluated in the medium gap height condition, represented the limit of the auxiliary blower that was used to pressurize the shroud. The performance data clearly show a systematic trend of increased total flow rate for each subsequently higher shroud pressure condition. Taking the referenced operating condition of $\Delta P \approx 25$ Pa, the maximum increase of Q is nearly 16% from the "shroud off" condition to the $\Delta P_{shroud} = 374$ Pa condition.

The efficiency data for this test condition is shown in Figure 6.15. Although the shroud pressure of 374 Pa had a substantial increase in flow rate, it was also accompanied by a significant decrease (19.4%) in efficiency. The only shroud condition that did not experience a decrease in efficiency was the $\Delta P_{shroud} = 125$ Pa, which had nominally the same efficiency as the "shroud off" condition. This shroud pressure had small improvement in flow rate at the operating point of 25 Pa, from 2.76 m^3/s to 3.00 m^3/s, a gain of 6.4%.

None of the measured shroud pressures at this gap height were able to increase both the flow rate and the efficiency simultaneously. It was determined that the optimal condition for the 4-blade fan is the medium gap height (g = 5.0 mm) with a $\Delta P_{shroud} = 125$ Pa. This was the one condition for the 4-blade fan that could make simultaneous increases in both Q and η^*.

6.4 Comparison of the 5-Blade and the 4-Blade Fans

Observations made while testing the 4-blade assembly led to an interest in testing another blade design with the aerodynamic shroud configuration. These observations were initially made using simple flow visualization techniques like tufting as described by Morris (1997) and also introducing smoke into the flow. Subsequent PIV measurements confirmed and further characterized these initial flow visualization observations.

A radically different fan propeller, shown in Figure 4.4, was obtained from Aerotech, Inc. This 5-blade propeller had been developed for possible production purposes, but was abandoned when initial tests indicated that it did not provide an enhanced performance (or in some cases, a reduced performance) when compared with the current production propeller. Nevertheless, this fan had specific features which appeared to address observed deficiencies in the 4-blade fan. For example, the flow visualization observations of the 4-blade fan showed that there was a large recirculation region directly downstream of the hub. This recirculation region was approximately the same width as the upstream motor. The 5-blade fan has a large bowl shaped hub that could potentially reduce or effectively eliminate this recirculation. Additionally, the 5-blade fan had thinner, more aerodynamic blade profiles and the angle of attack increased substantially from the tip to the hub. These features, it was reasoned, would have improved lift to drag coefficient ratio (C_L/C_D) and would provide a more uniform velocity profile than that of the current 4-blade fan. These observations provided the motivation to evaluate the 5-blade fan in both the "shroud off" and "shroud on" conditions.

6.4.1 The 4-Blade and 5-Blade Fans - "Shroud-Off" Condition

Initial measurements were collected to verify the previous data of Aerotech that indicated that the 5-blade propeller would not provide higher flow rates and efficiencies than the standard 4-blade propeller when measured in identical configurations. Since the 4-blade fan showed nearly identical performance and efficiency characteristics in both the 7 degree and 11 degree diffuser configurations, the 11 degree cone was chosen as the reference configuration to examine the 4-blade and 5-blade comparisons.

Figure 6.16 shows the performance curves for these two propellers. For pressure rise values below 31 Pa, these data confirm the expected result that the 4-blade provides a higher volume flow rate at each ΔP; however, for pressure rise values higher than 31 Pa, the trend is reversed by roughly the same magnitude as was observed for the lower pressure rise conditions. These magnitudes, approximately 2% for ΔP above and below 31 Pa were considered to be not significant. Thus, the data collected in the AFRD assembly confirmed the previous results; namely that the 4-blade propeller is better-suited to this application than the 5-blade propeller.

A comparison of the efficiency values is shown in Figure 6.17. These data repeat the trend exhibited in the performance data, where again an inflection point exists around $\Delta P \approx 31$ Pa. Similar to the performance curve, the 4-blade fan has a higher efficiency at pressure rise values below 31 Pa and a lower efficiency at pressure rises above 31 Pa. The magnitude of change is slightly larger for the efficiency, averaging approximately 5% over the entire curve (but varying depending on each specific operating point). However, similar to the performance data, the 4-blade propeller would be chosen over the 5-blade propeller, since the operating point for these fans is normally around $\Delta P = 25$ Pa. As shown in both Figure 6.16 and Figure 6.17, the 4-blade propeller out-performs the 5-blade at this projected operating point and its surrounding values.

6.4.2 The 4-Blade and 5-Blade Fan - "Shroud-On" Condition

After verifying the performance of the 5-blade fan in the "shroud-off" condition, this same fan was then tested in the "shroud-on" condition. Considering the "shroud-off" conditions, the 5-blade propeller was a less-desirable choice for a fan system, but it was thought that this fan might perform differently when placed into the "shroud-on" environment. This idea was based on qualitative observations made using the previously mentioned (tufting, etc.) flow visualization techniques performed during the initial testing of the "shroud-off" condition. These observations showed the surprising result that the near wall flow appeared to be separated near the exit of the diffuser cone. Given the large cone angle of 11 degrees, this result is expected; however, one would also then expected the performance and efficiency of the 5-blade fan to be considerably worse than that of the 4-blade fan. As shown by the detailed results of Section 6.4.1, this was not the case. Hence, further experiments were conducted. A gap height of $g \approx 5.0$ mm was selected based on the previous 4-blade studies showing this to be an optimal height for the delivery of the shroud jet.

The results of the 5-blade fan with shroud pressures of 249 Pa and 373 Pa, in addition to the baseline (production) case of the 4-blade fan with a 7 degree diffuser cone, are shown in Figure 6.18. Figure 6.18 shows a substantial increase in volume flow rate for both the "shroud-on" conditions of ΔP_{shroud}= 249 Pa and ΔP_{shroud}= 373 Pa. For these data, the reference operating point ($\Delta P \approx 25$ Pa_ shows performance (flow rate) gains of 20.5% and 32.8%, respectively.

Figure 6.19 shows the efficiency data for the 5-blade fan with the same shroud pressures, 249 Pa and 373 Pa. Examining the reference operating point of $\Delta P \approx 25$ Pa, these two shroud pressures indicate efficiency gains of 10.8% and 7.8%, respectively. These data show substantial improvements in both performance and efficiency simultaneously. This result had not been seen on any of the 4-blade tests except for the medium gap height, but the percentage improvements measured here were significantly higher. These tests were subsequently re-taken several times to ensure the validity of the results, and they were shown to be repeatable to within the uncertainty of the measurements.

6.5 A New Blade Design - Comparisons of 3, 5 and 8-Blade Fans

The success of the new propeller design, shown in the 5-blade tests of Section 6.4.2, led to an investigation of similarly designed fans with slightly different characteristics. These two new propellers, shown in Figures 4.5 and 4.6, are closely related to the 5-blade propeller (larger hub-to-tip ratio, similar angles of attack at various radii, etc.), but they do differ in the number of blades and solidity. A study was conducted to see if maintaining the general salient features of the fan, but changing the number of blades could improve upon either the already significant gains in efficiency and flow rate of the 5-blade fan. Both the "shroud off" and "shroud on" conditions were evaluated in this study.

6.5.1 Comparisons of 3, 5 and 8-Blade Fans - "Shroud Off" Condition

Before evaluating the new propellers with the aerodynamic shroud, a series of baseline data were acquired to determine how each one compares with the existing 4 and 5-blade designs. As previously stated, the new 3 and 8-blade designs were quite similar to that of the 5-blade fan, but the chord lengths were slightly different. The 3-blade fan had a slightly larger chord and the 8-blade fan had a slightly smaller chord. The performance data are shown in Figure 6.20. Previous results had shown that the 4-blade and 5-blade had very similar volume flow rates at the reference operating point of $\Delta P \approx 25$ Pa, with the 4-blade fan having a slightly higher flow rate. Figure 6.20 shows that the 3-blade fan generates a much lower flow than the baseline 4-blade fan (-8.3%). However, the 8-blade fan generates a higher flow rate, showing an increase in volume flow rate of 6.5%. Considering the efficiency, shown in Figure 6.21, it is evident that both the 3-blade and the 8-blade fans have much lower efficiencies at the reference operating point, by -15.0% and -31.2%, respectively.

6.5.2 Comparisons of 3, 5 and 8-Blade Fans - "Shroud On" Condition

The 3-blade and 8-blade fans were then tested in the "shroud on" condition to determine if the aerodynamic shroud could improve upon the initial performance and efficiency results. Based on previous data, the shroud pressure, ΔP_{shroud}, was set to 373 Pa. This shroud pressure had previously provided the optimal trade-off between flow rate increase and efficiency increase. Since the overall fan designs were quite similar, it was reasoned that this would be the best case for the 3 and 8-blade fans. The performance curve results are shown in Figure 6.22. This figure shows that each of the new blade designs (3, 8 and 5-blade) have substantial improvements in flow rate over those of the current production 4-blade fan. The 8-blade fan has the highest performance, producing a volume flow rate of 3.77 m^3/s at the reference operating point of $\Delta P \approx 25$ Pa. The 5-blade fan generates the next highest flow rate at 3.69 m^3/s, and the 3-blade fan is the third highest with 3.52 m^3/s. These data indicate that the 8-blade fan with the aerodynamic shroud would be the choice for maximum ventilation in an agricultural environment.

Figure 6.23 shows the corresponding efficiencies for the data in Figure 6.22. Once again the 4-blade production fan is compared with the more recently designed fans with 3, 5 and 8-blade propellers in the "shroud on" condition. These data show that the 8-blade fan, which had the highest flow rate, has the lowest efficiency, with an η^* value of 9.1. The 4-blade production fan has an η^* value of 9.6. This is somewhat surprising given the substantially different flow rate values between these two fans (the 8-blade had a 36% increase in flow rate). Both the 3 and 5-blade fans had η^* values higher than the production fan, there values were nominally 10.3 and 10.4, respectively.

These data show that the 5-blade fan provides the best compromise between increased flow rate and increased efficiency. This fan was able to generate a volumetric flow rate that was very close to the 8-blade fan, without suffering the significant decreases in efficiency experienced by the 8-blade fan. The 5-blade fan was therefore used as the reference fan for further attempts at refining the overall fan system.

6.6 The 5-Blade Fan with an Installed Centerbody Device

The results of Section 6.5 show that each of the later propeller designs, the 3-blade, 5-blade and 8-blade can simultaneously improve the flow rate and efficiency of a the fan system when they are used in conjunction with the Aerodynamic shroud. However, the 5-blade provided the optimal increase of both flow rate and efficiency. Further flow visualizations made while testing the 5-blade fan suggested that other devices could possibly be used in conjunction with the aerodynamic shroud to reduce losses, as described by equation 2.20. These flow visualizations showed that a large region of reverse flow (i.e. back into the control volume) existed near the center of the downstream exit of the control volume of Figure 2.1. This reversed flow was substantially increased when the fan was operating in the "shroud on" condition. Reversed flow near the exit of the diffuser cone is a detriment to the system performance and efficiency in two distinct ways: (1) It represents lost kinetic energy that detracts from the net system flow rate and, (2) this reversed flow creates a higher value for α, since it creates a highly non-uniform profile at the exit plane. These flow visualizations were later confirmed and quantitatively assessed by the PIV measurements of Section 7.0. Subsequently, a new device, called a "centerbody" was proposed to address these issues and determine if even further improvements could be obtained.

6.6.1 The Cylindrical Centerbody

The first centerbody that was installed was a simple cylindrical shape, which was approximately the same width as the hub on the 5-blade fan. This shape was chosen because it corresponded to the approximate width of the reversed flow region and also because it would block any recirculating flow downstream of the hub of the 5-blade propeller. This straight centerbody also did not appear *a priori* to provide any significant blockage to the primary exiting flow path.

6.6.1.1 The Cylindrical Centerbody - "Shroud Off" Condition

The results of the flow visualization indicated that the straight centerbody device would most likely not benefit the fan in the shroud off condition. This was primarily because there appeared to be very little reversed flow at the exit plane of the diffuser when the 5-blade fan was tested in a "shroud off" configuration. However, there still existed the possibility that the fan could benefit in other ways (i.e. downstream of the hub). Several sets of data were collected to test this idea and also to provide a methodology which was consistent with each previous step ("shroud off" vs. "shroud on"). Figure 6.24 shows the performance curve for the 5-blade fan in the "shroud off" condition with the cylindrical centerbody installed. The previously tested conditions of the baseline production assembly (4-blade, 7 degree cone, and "shroud off") and the 5-blade, 11 degree cone in the "shroud off" condition are shown for reference. From Figure 6.24, the performance is slightly increased throughout the range of potential operating points by adding the centerbody device. This increase is approximately 2.8% for the reference operating point of $\Delta P \approx 25$ Pa.

Figure 6.25 shows a comparison of the efficiencies of the same three configurations that were shown in Figure 6.24. These results show that the efficiency, which was essentially the same for both the baseline production assembly and the 5-blade fan (both in "shroud off") is slightly increased by the addition of the cylindrical centerbody. Again, the 5-blade fan, "shroud off" condition is shown as a reference, along with the baseline 4-blade assembly. Previous results had shown that the 5-blade fan had a decreased efficiency at the higher flow rates, and Figure 6.25 shows that the efficiency is slightly increased at these higher flow rates. This improvement, while minimal, shows that the 5-blade fan, when evaluated with the centerbody device, can deliver a higher flow rate with a nominally equivalent efficiency to that of the baseline production case. Using the reference operating point of $\Delta P \approx 25$ Pa, the efficiency is increased from ≈ 9.7 for the baseline 4-blade assembly to ≈ 9.8 for the 5-blade assembly with cylindrical centerbody. This is also an improvement from the efficiency of the 5-blade without cylindrical centerbody, which had an efficiency of ≈ 9.3. These data indicate that both the flow rate and the efficiency are slightly increased by the addition of the centerbody for the "shroud off" case.

6.6.1.2 The Cylindrical Centerbody - "Shroud On" Condition

The cylindrical centerbody was subsequently evaluated with the aerodynamic shroud in the "Shroud On" condition. The results of Section 6.4 indicated that the optimal shroud pressure for the 5-blade configuration was $\Delta P_{shroud} = 373$ Pa. This information was used as the starting point for the "shroud on" condition, but additional shroud pressures were also evaluated. Figure 6.26 shows the initial performance tests that were conducted at $\Delta P_{shroud} = 373$ Pa for the 5-blade fan with centerbody. The previously shown results for the 5-blade fan at the same shroud pressure without centerbody, as well as the 4-blade baseline fan are also shown. Figure 6.26 indicates that the addition of the centerbody is able to increase the flow further than the same configuration without the centerbody. Referring to the reference operating condition of $\Delta P \approx 25$ Pa, the 4-blade fan has a $Q \approx 2.8$ m^3/s, the 5-blade with centerbody has a $Q \approx 3.7$ m^3/s and the 5-blade with centerbody has a $Q \approx 3.8$ m^3/s. The 5-blade without centerbody configuration increases the flow rate by 32.0% while the 5-blade with centerbody configuration increases the flow rate by 35.7%.

The data in Figure 6.27 show the efficiency curves for these same three configurations. The general trend in this figure is a consistent improvement in efficiency throughout the range of operating conditions. Referencing Figure 6.27 and looking at the target operating point, the 4-blade baseline fan has an efficiency of 9.6, while the 5-blade fan without centerbody has an efficiency of 10.4 and the 5-blade fan with centerbody has an efficiency of 11.1, This is an improvement of 8.3% and 15.6%, respectively. The addition of the centerbody to the 5-blade fan operating with a "shroud on" condition of 373 Pa is able to improve upon the already substantial gains in both flow rate and efficiency.

The effect of shroud pressure when operating with the centerbody was subsequently studied to determine if the optimal shroud pressure would be different than that of the same fan without a centerbody. Figure 6.28 shows the performance curves for this configuration when tested with both the "shroud off" condition, as well as "shroud on" conditions for 249 Pa, 373 Pa and 498 Pa. This figure shows the significant performance gains for each subsequently higher "shroud on" condition. At an operating point of $\Delta P \approx 25$ Pa, the "shroud on" conditions of 249, 373 and 498 Pa show improvements of 23.5%, 34.3% and

38.5%, respectively. Figure 6.29 shows the associated efficiency for each of the three tests. These results show that the efficiency (at $\Delta P \approx 25$ Pa) is increased for each of these three shroud pressures, ΔP_{shroud} = 249 Pa, 373 Pa, and 498 Pa to η^* = 10.9, 11.2, and 10.2 respectively. Comparing these η^* values to those of the 4-blade baseline production case, which has an η^* = 9.8, these shroud pressures represent efficiency improvements of 11.2%, 14.3%, and 4.1%.

These data clearly show that the centerbody, when used in conjunction with the aerodynamic shroud, does improve the performance and efficiency of the 5-blade fan. The maximum increase in flow rate occurs when the ΔP_{shroud} is set to 498 Pa, and this maximum increase in flow rate (38.5%) is accompanied by a 4.1% increase in efficiency. While this is a notable increase in flow rate, it is only a modest improvement in efficiency. However, if the shroud pressure is lowered slightly, to a ΔP_{shroud} = 373 Pa, then the flow rate is increased by 34.3% with an increase in efficiency of 14.3%. This combination would appear to be optimal; however, there may be situations where a maximum flow rate is required and a more modest increase in efficiency could be tolerated. If this were the case, then the shroud pressure of ΔP_{shroud} = 498 Pa might be preferred.

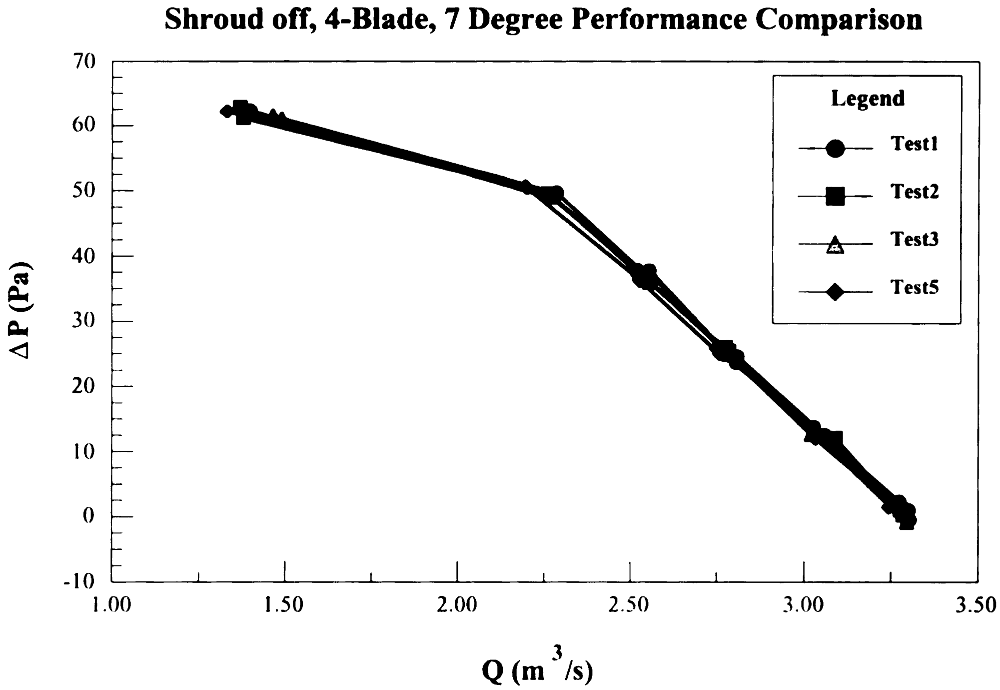

FIGURE 6.1 Baseline (Shroud Off) Performance Measurements for the Production 4-Blade Fan with 7 Degree Diffuser. The Multiple Tests Show the Repeatability of the Measurements

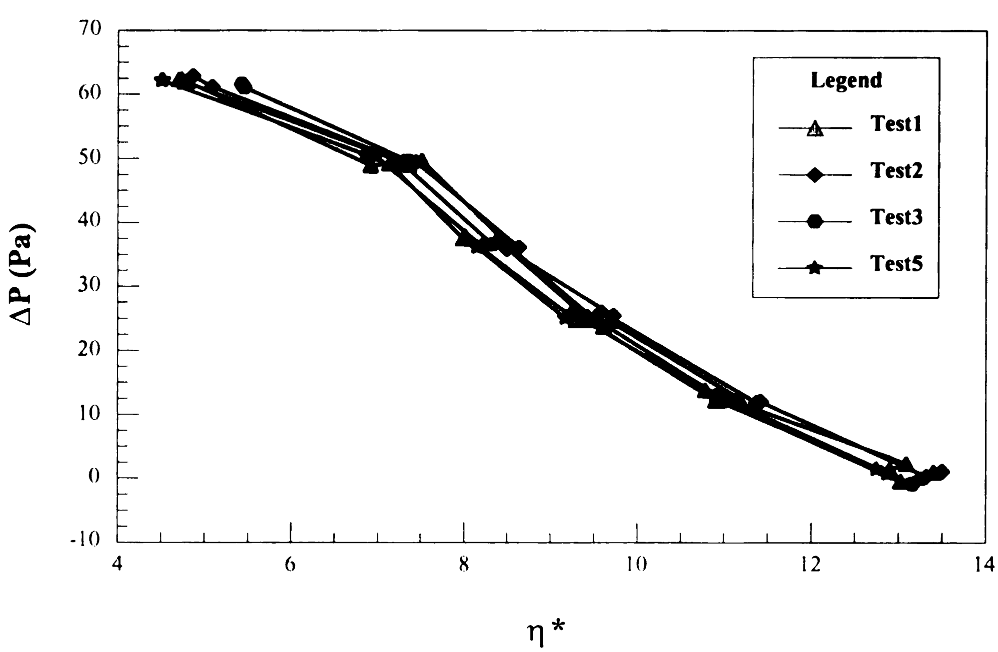

FIGURE 6.2 Baseline (Shroud Off) Efficiency Measurements for the Production 4-Blade Fan with 7 Degree Diffuser. The Multiple Tests Show the Repeatability of the Measurements

Performance Comparison for "Shroud On" Conditions for 4-Blade Fan with 7 Degree Cone

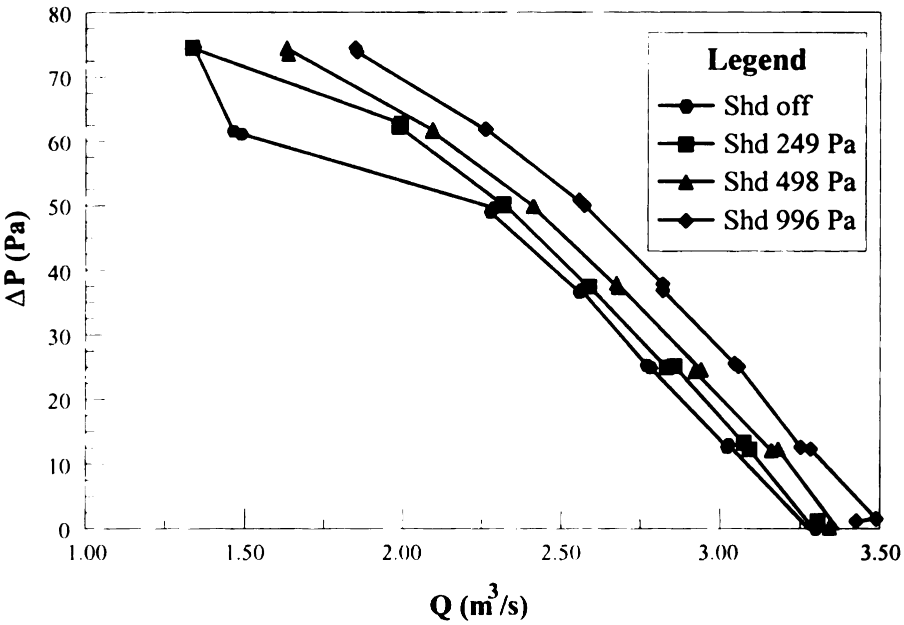

FIGURE 6.3 Performance Data for the 4-Blade Fan with 7 Degree Diffuser at Various Shroud Pressures

Efficiency Comparison for "Shroud On" Conditions for 4-Blade Fan with 7 Degree Cone

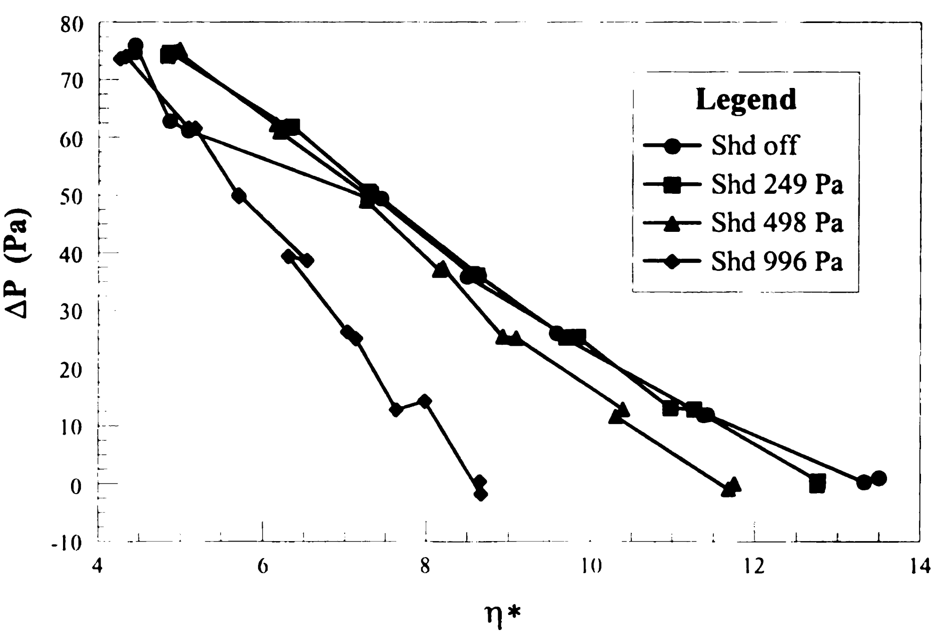

FIGURE 6.4 Efficiency Data for Data for the 4-Blade Fan with 7 Degree Diffuser at Various Shroud Pressures

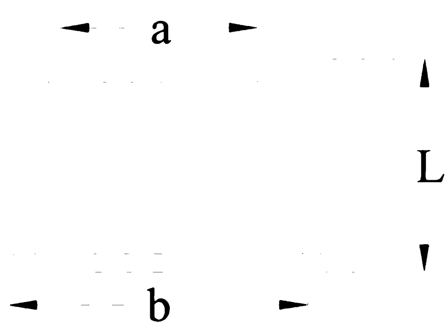

FIGURE 6.5 Geometric Variables for the Diffuser Cone (as described in Table 4)

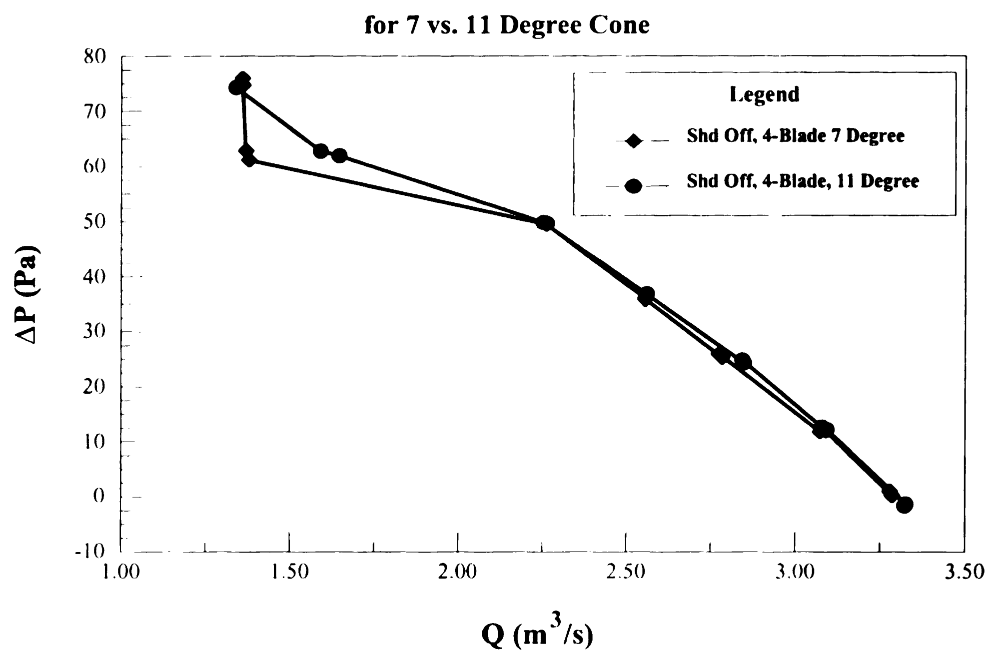

FIGURE 6.6 Performance Curves for the 4-Blade Fan for 7 vs. 11 Degree Diffuser (Shroud Off)

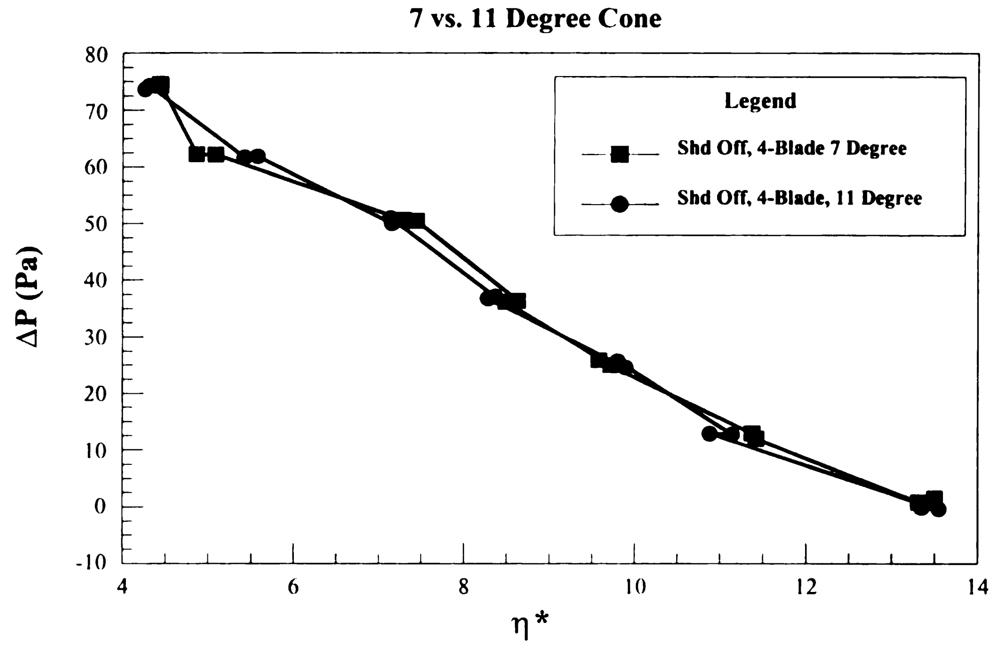

FIGURE 6.7 Efficiency Curves for the 4-Blade Fan for 7 vs. 11 Degree Diffuser (Shroud Off)

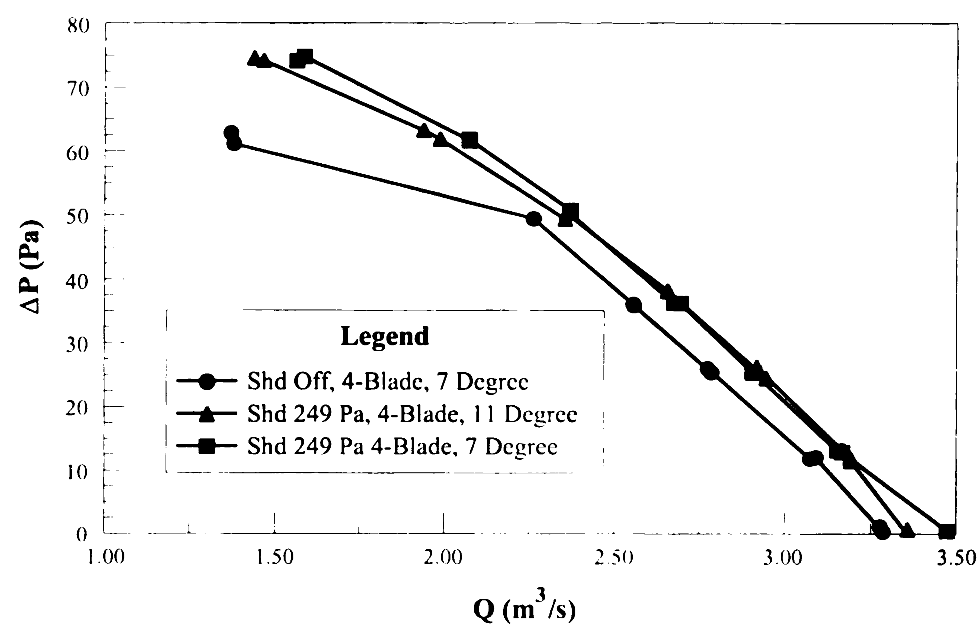

FIGURE 6.8 Performance Data for the 4-Blade Fan with 11 Degree Diffuser - Low Shroud Pressure (ΔP_{shroud} = 249 Pa)

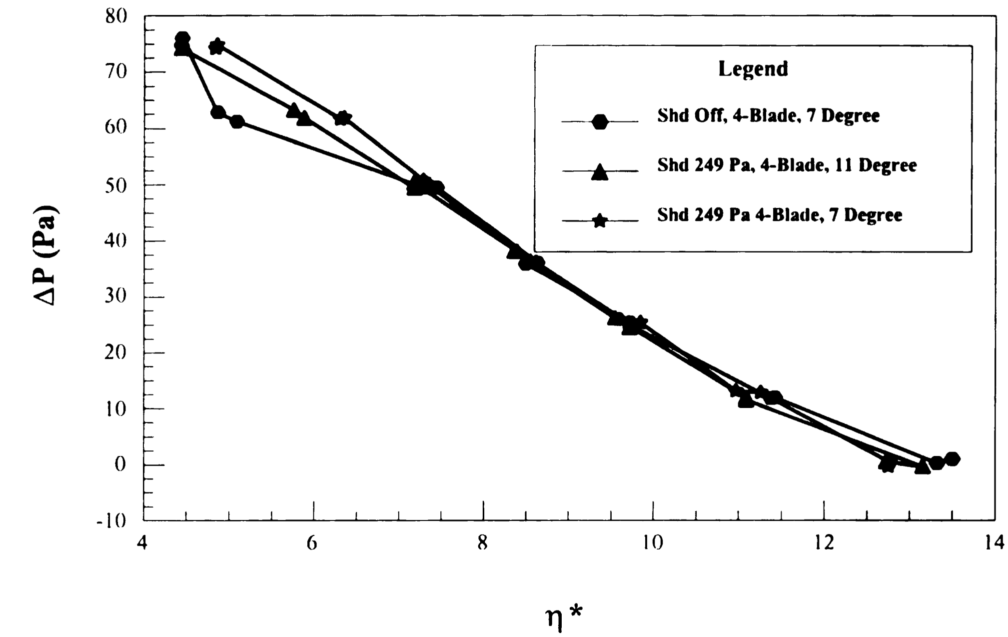

FIGURE 6.9 Efficiency Data for the 4-Blade Fan with 11 Degree Diffuser - Low Shroud Pressure (ΔP_{shroud} = 249 Pa)

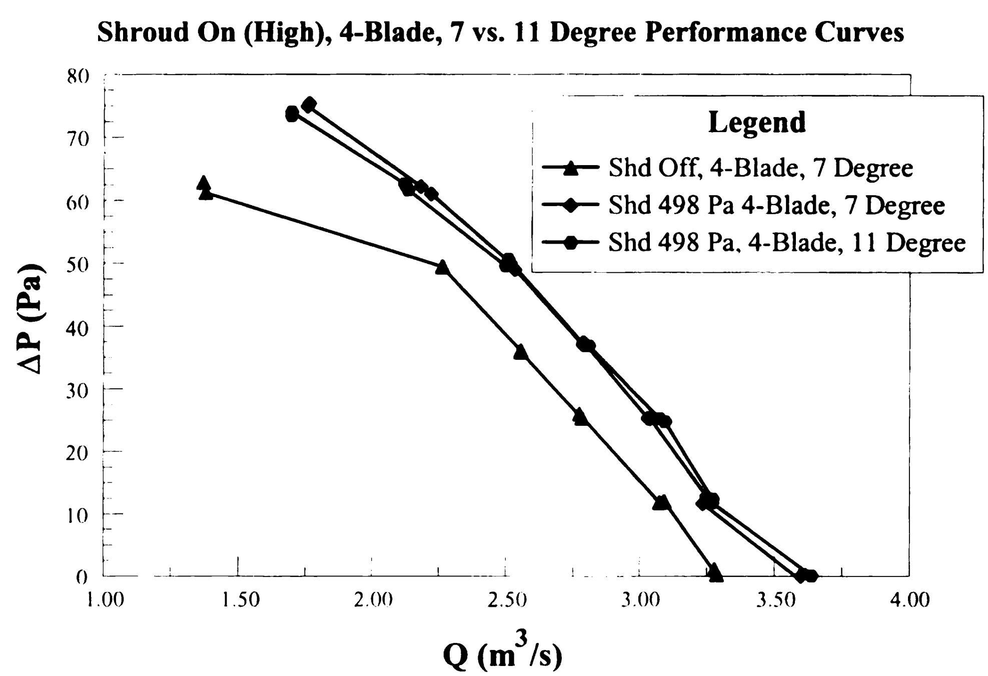

FIGURE 6.10 Performance Data for the 4-Blade Fan with 11 Degree Diffuser at a High Shroud Pressure (ΔP_{shroud} = 498 Pa)

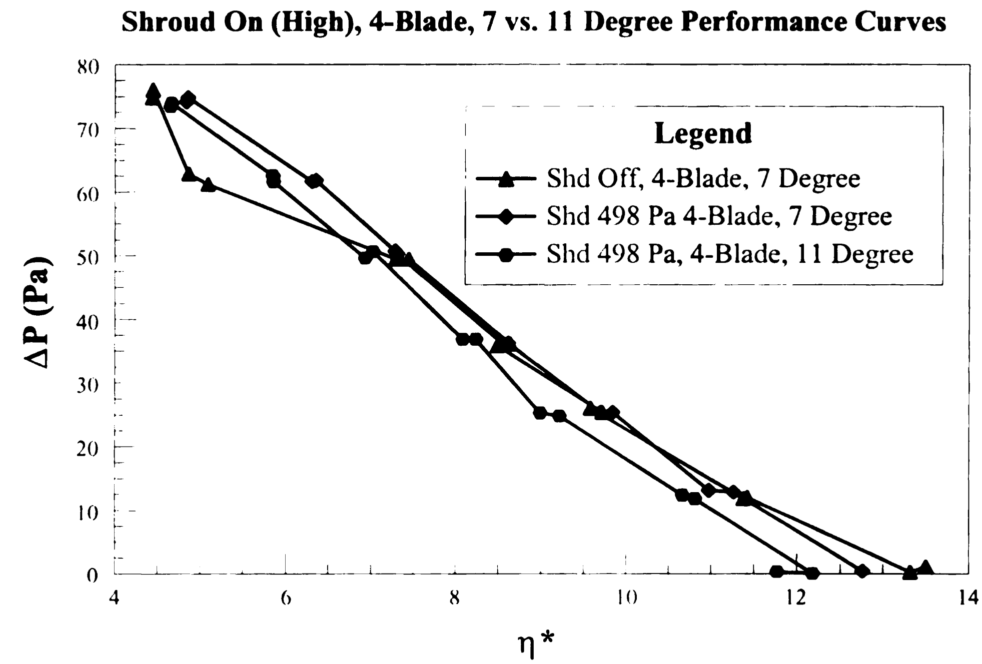

FIGURE 6.11 Efficiency Data for the 4-Blade Fan with 11 Degree Diffuser - High Shroud Pressure ($\Delta P_{shroud} = 498$ Pa)

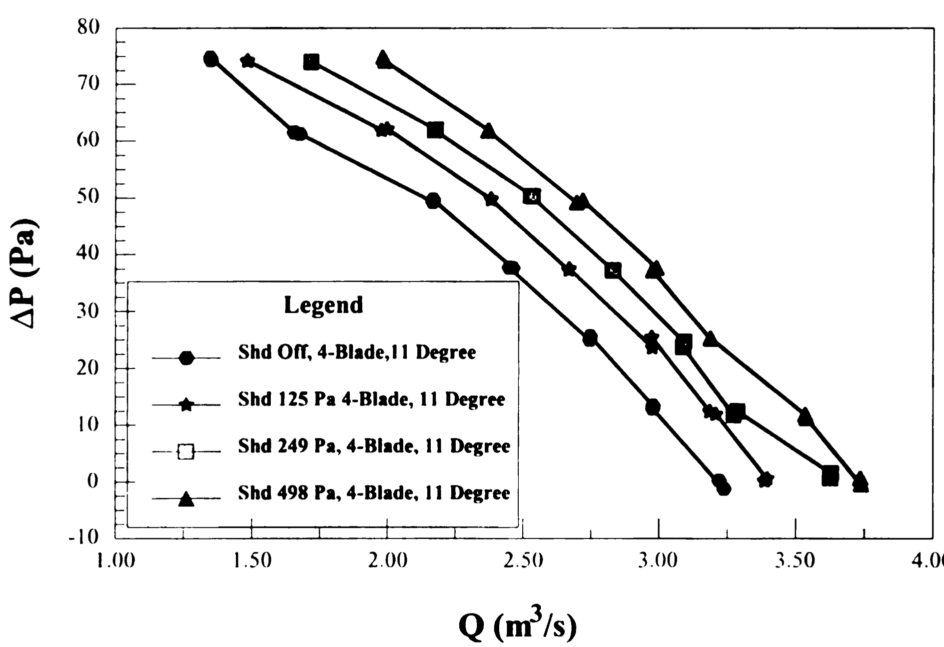

FIGURE 6.12 Performance Data for the 4-Blade Fan with 11 Degree Diffuser - Medium Gap Height (g ≈ 5.0 mm)

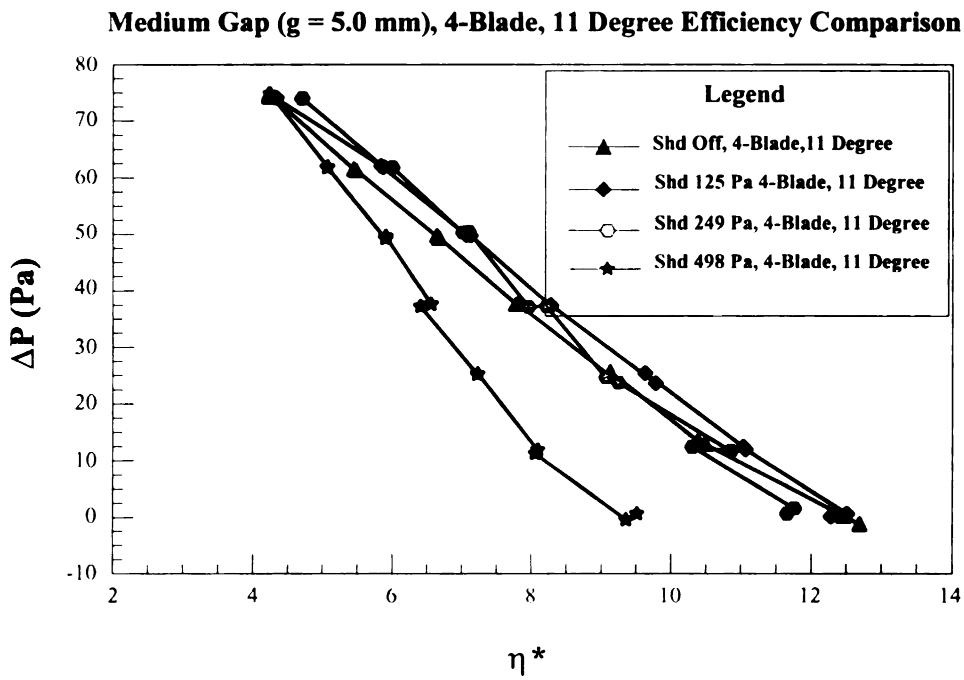

FIGURE 6.13 Efficiency Data for the 4-Blade Fan with 11 Degree Diffuser - Medium Gap Height (g ≈ 5.0 mm)

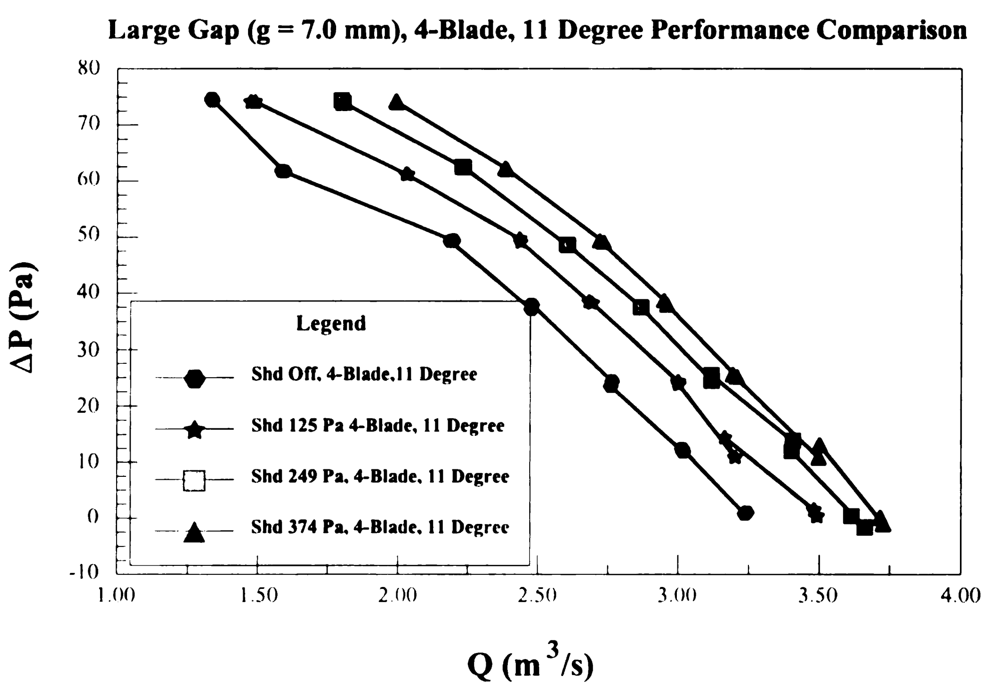

FIGURE 6.14 Performance Data for the 4-Blade Fan with 11 Degree Diffuser - Large Gap Height (g ≈ 7.0 mm)

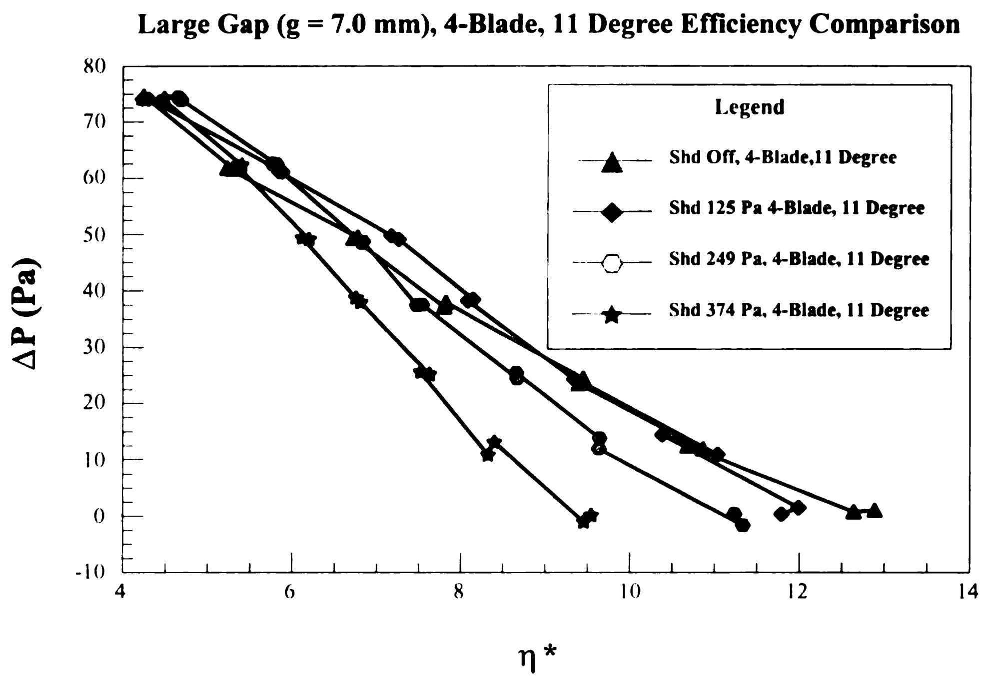

FIGURE 6.15 Efficiency Data for the 4-Blade Fan with 11 Degree Diffuser - Large Gap Height (g ≈ 7.0 mm)

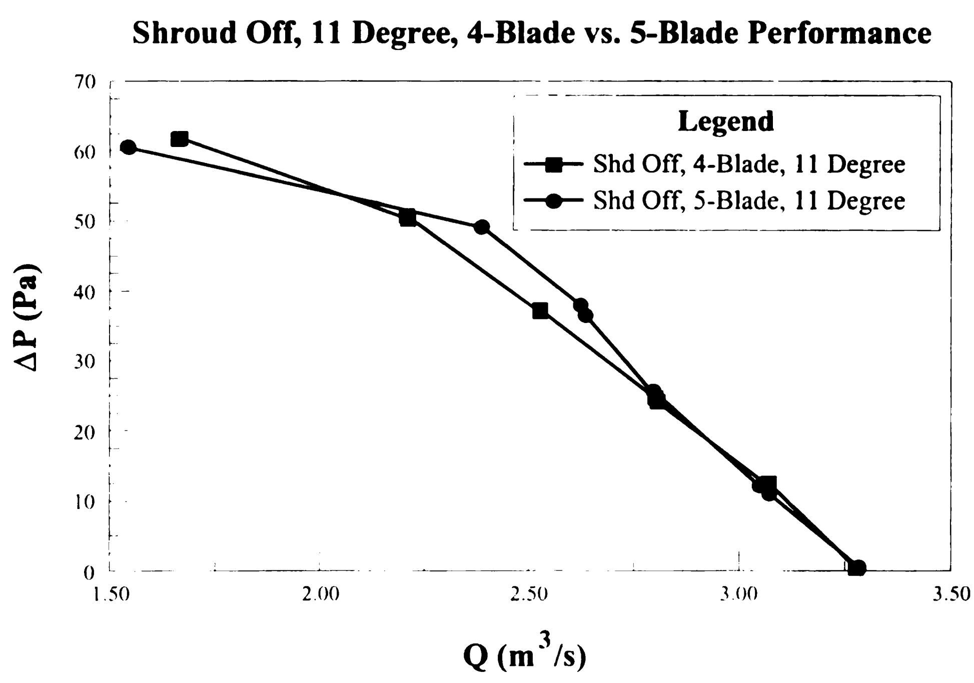

FIGURE 6.16 Performance Data for the 4-Blade and 5-Blade Fans

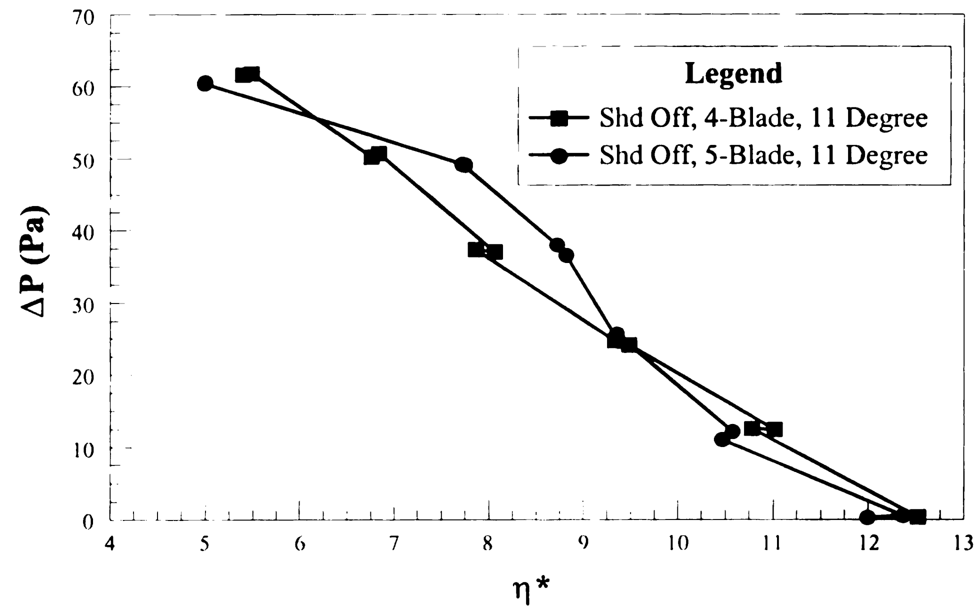

FIGURE 6.17 Efficiency Data for the 4-Blade and 5-Blade Fans

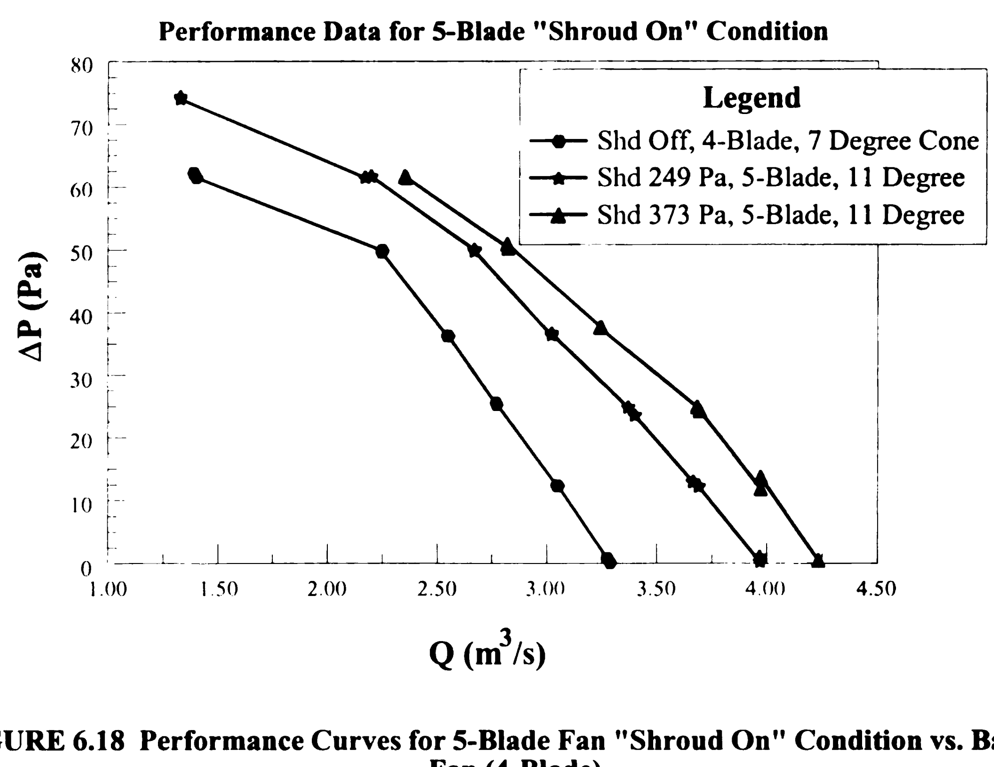

FIGURE 6.18 Performance Curves for 5-Blade Fan "Shroud On" Condition vs. Baseline Fan (4-Blade)

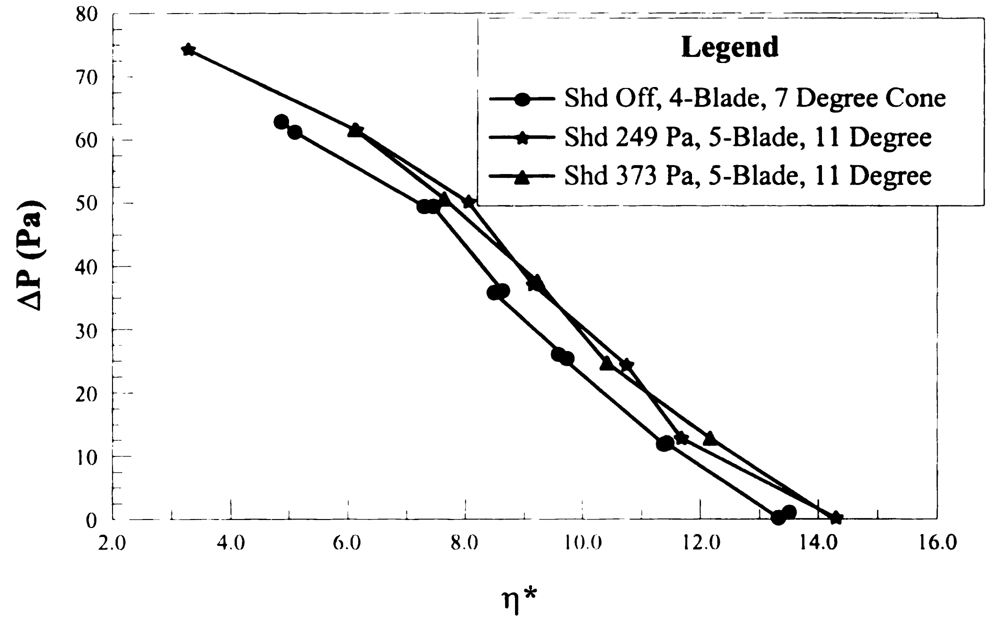

FIGURE 6.19 Efficiency Curves for 5-Blade Fan "Shroud On" Condition vs. Baseline Fan (4-Blade)

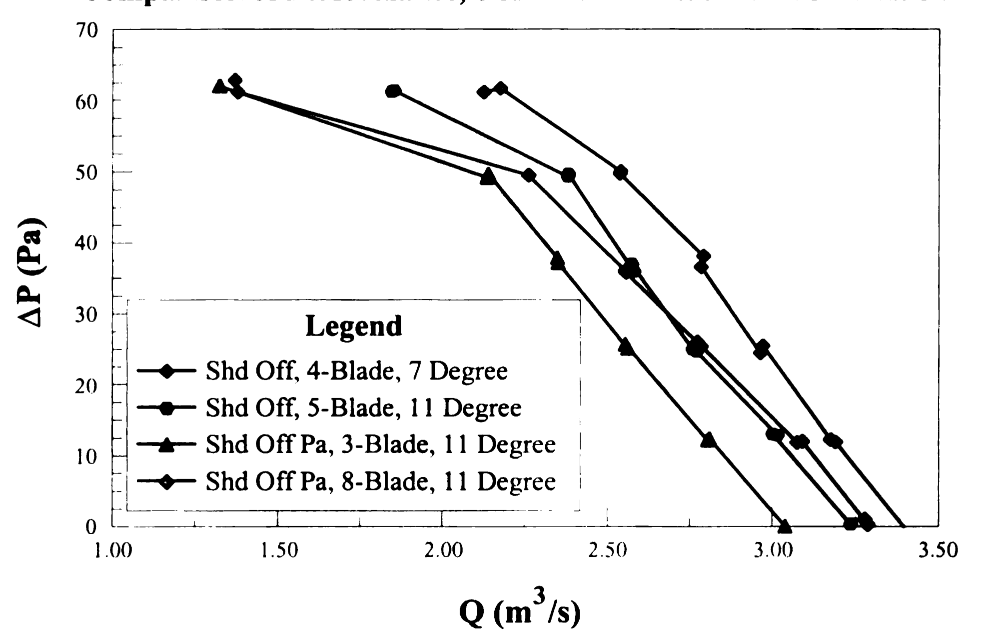

FIGURE 6.20 Performance Curves for 4-Blade fan ("Shroud Off") vs. 5-Blade ("Shroud Off") vs. 3-Blade ("Shroud Off") vs. 8-Blade ("Shroud Off")

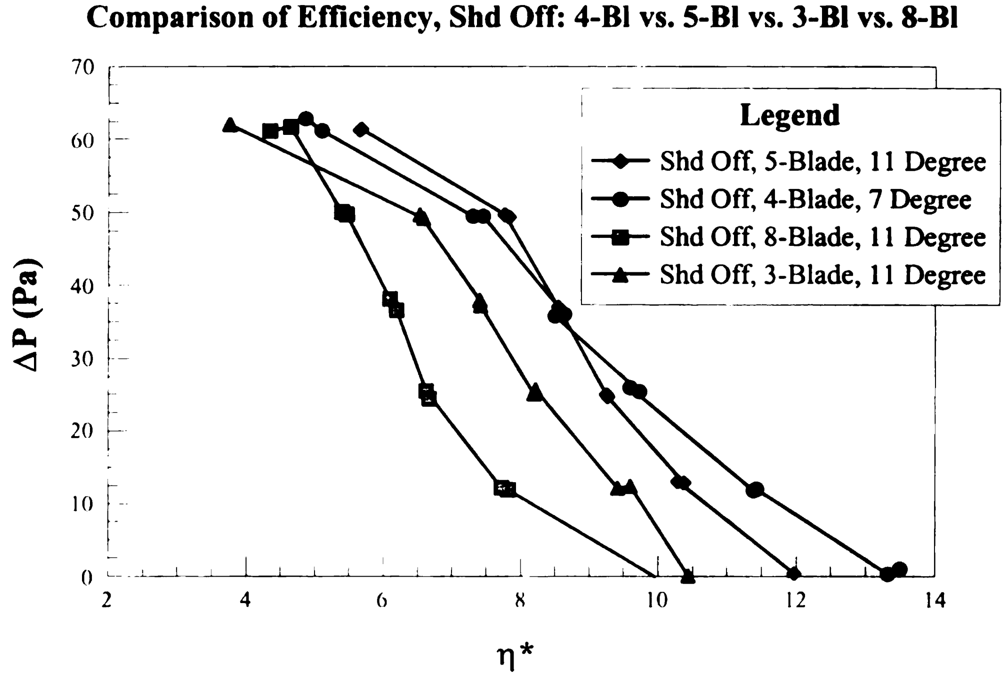

FIGURE 6.21 Efficiency Curves for 4-Blade fan ("Shroud Off") vs. 5-Blade ("Shroud Off") vs. 3-Blade ("Shroud Off") vs. 8-Blade ("Shroud Off")

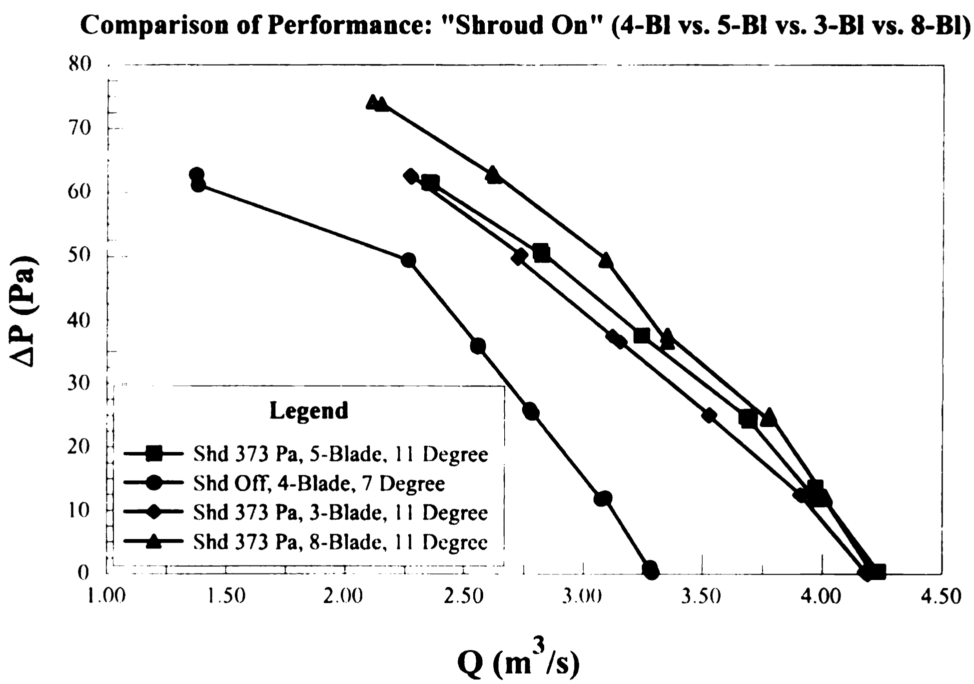

FIGURE 6.22 Performance Curves for 4-Blade fan ("Shroud off") vs. 5-Blade ("Shroud On") vs. 3-Blade ("Shroud On") vs. 8-Blade ("Shroud On")

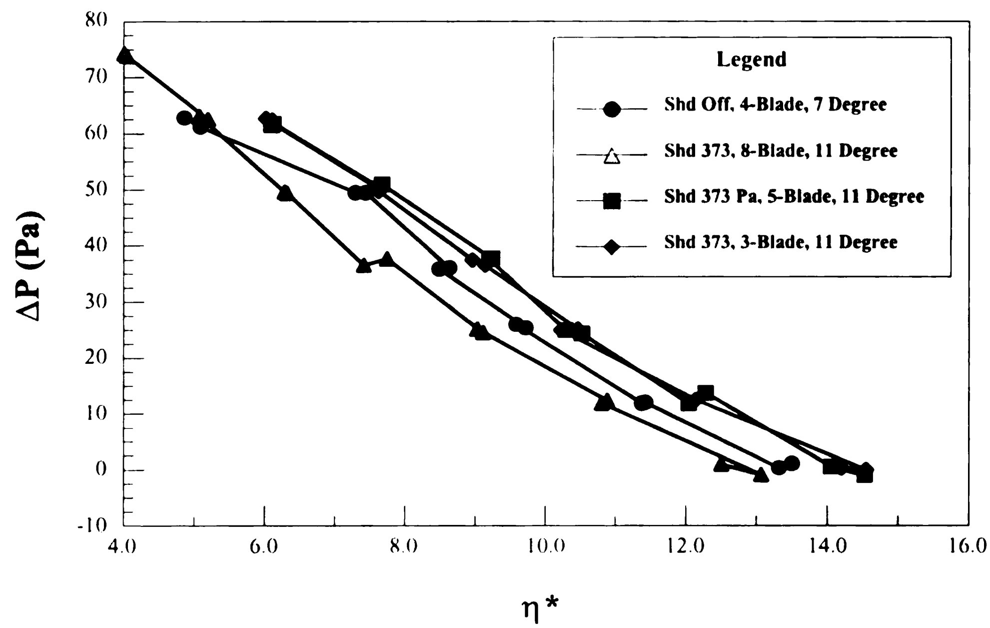

FIGURE 6.23 Efficiency Curves for 4-Blade fan ("Shroud off") vs. 5-Blade ("Shroud On") vs. 3-Blade ("Shroud On") vs. 8-Blade ("Shroud On")

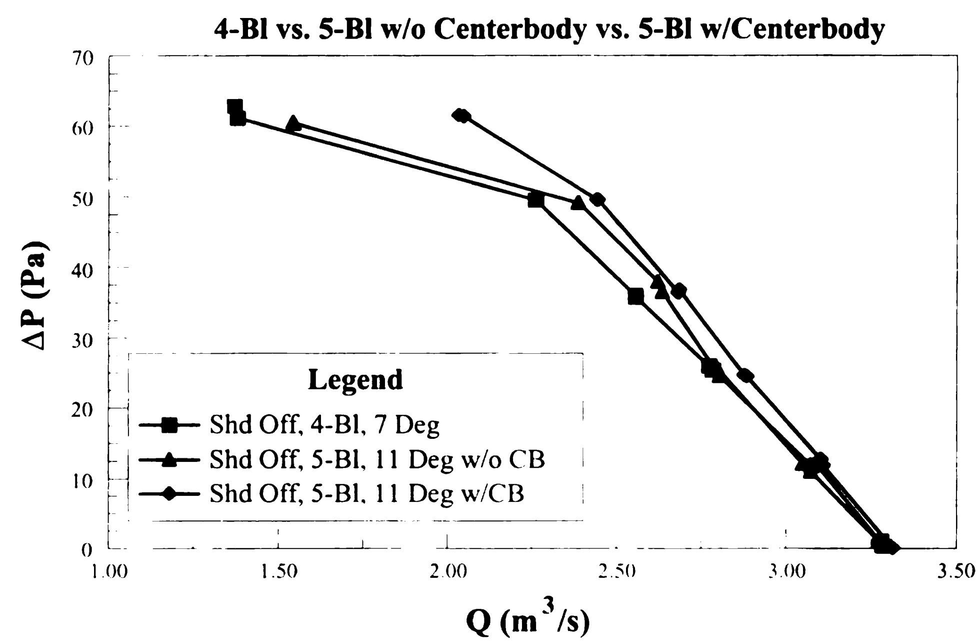

FIGURE 6.24 Comparison of Performance for 5-Blade with and without Installed Centerbody at the "Shroud Off" Condition. The Baseline Production Case (4-Blade, "Shroud Off") is shown as a reference

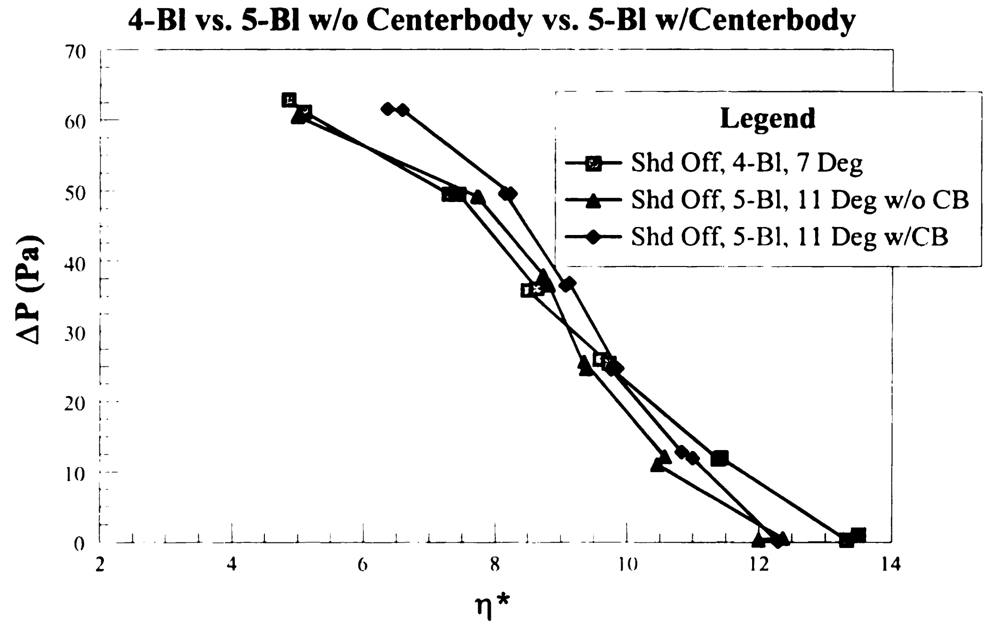

FIGURE 6.25 Comparison of Efficiency for 5-Blade with and without Installed Centerbody at the "Shroud Off" Condition. The Baseline Production Case (4-Blade, "Shroud Off") is shown as a reference

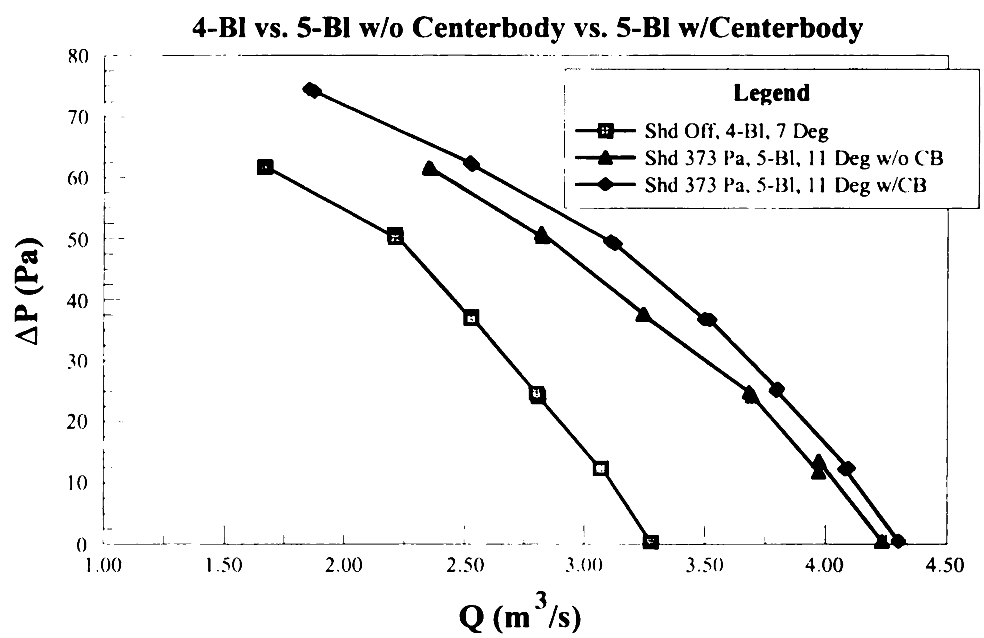

FIGURE 6.26 Comparison of Performance for 5-Blade with and without Installed Centerbody at the "Shroud On" Condition. The Baseline Production Case (4-Blade, "Shroud Off") is shown as a reference

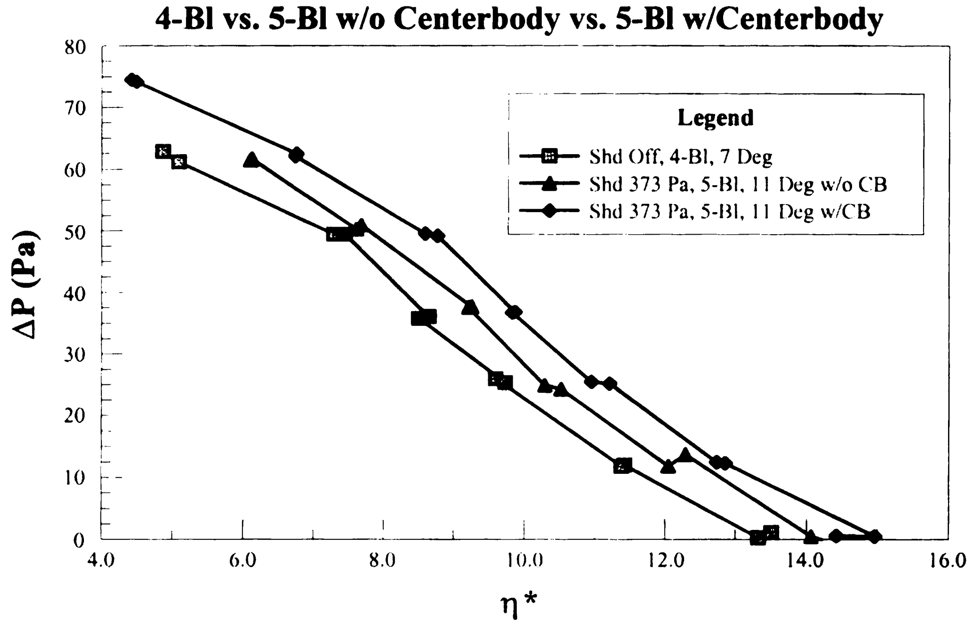

FIGURE 6.27 Comparison of Efficiency for 5-Blade with and without Installed Centerbody at the "Shroud On" Condition. The Baseline Production Case (4-Blade, "Shroud Off") is shown as a reference

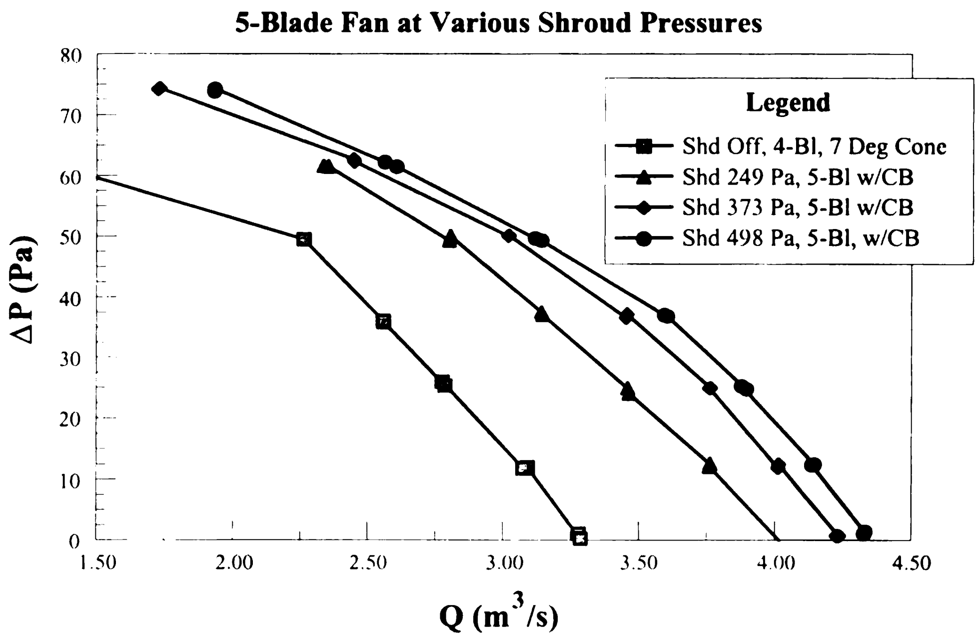

FIGURE 6.28 Performance Data for the 5-Blade Fan with Installed Centerbody at Various Shroud Pressures

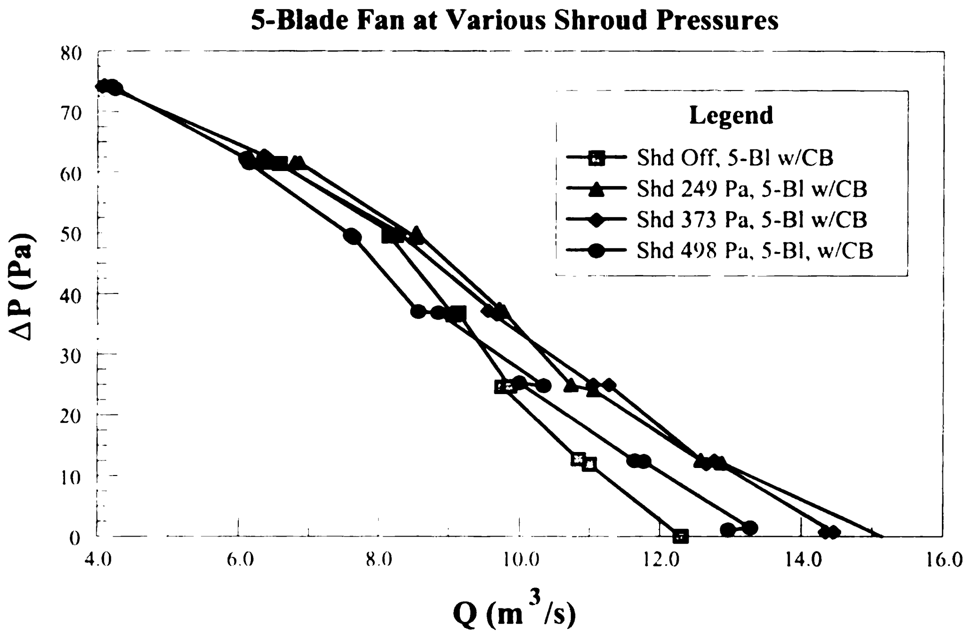

FIGURE 6.29 Efficiency Data for the 5-Blade Fan with Installed Centerbody at Various Shroud Pressures

7.0 Results and Discussion - Velocity Measurements

7.1 PIV Measurements on the Production 4-Blade Fan Configuration

The initial set of PIV measurements was collected on the 4-blade production fan assembly in three separate regions, as previous defined by Figure 5.2. The choice of these three regions was based on observations made using flow visualization techniques such as tufting and smoke visualization. These flow visualization studies were carried out concurrently with the integral measurements and they provide insight on the flow field in this fan system. Referring to Figure 5.2, Region I was selected so the exit velocity profile of the diffuser cone could be evaluated. Data collected in this region provide information about the exit velocity profile (i.e. larger or smaller α_c values in equation 2.20), including the existence of reversed flow. Additionally, these data can yield information about flow separation near the cone wall at the exit plane. Region II was selected to determine if the flow is attached to the sidewall of the diffuser cone at a position upstream of the exit plane. Finally, Region III was selected to measure the effect of the (required) motor assembly. Specifically, in Region III, it was speculated that the interior blade regions of the 4-blade propeller were ineffective at imparting a positive velocity (in the direction of the cone exit plane) because these regions are located in the wake region of the motor. This would indicate that the hub was undersized for this application. The results of each of these three regions are presented in the following sections. These plots are primarily shown as color contours of the z-component of velocity with streamlines added to show the path a particle would follow if the flow field were constant with time. These streamlines[1] are found as the

---

1. Streamlines, as calculated in the PIV data, are defined by the differential equation $v_r dz = v_z dr$

contour curves of the stream function, which is calculated using a predictor-corrector integration algorithm.

7.1.1 Near Hub Region (4-Blade Fan with 11 Degree Diffuser Cone)

Measurements collected in Region III from Figure 5.2 were obtained by cutting a small observation window in the sidewall of the 11 degree diffuser cone for the camera and by shining the laser sheet from the upper receiver of the AFRD, pointing in the upstream direction. The laser was aligned such that it cut the center of the fan's rotation and the corresponding field of view from the camera was approximately 200 mm wide by 200 mm tall. Smoke particles were introduced from an upstream reservoir by using a Rosco Model No. 1600 theatrical fogging machine. The Rosco machine provides particles that range in size from 0.25 μm - 1.0 μm in diameter. The data presented in this section are all presented as time-averaged (i.e. an ensemble of 1000 random blade position images) contour plots.

7.1.1.1 Near Hub Region - "Shroud Off" Condition

Figure 7.2 shows the time-averaged velocity contour plot of Region III. The center of the axis of rotation for this fan is located at (0,-594.4) with z = -594.4 mm representing the downstream edge of the motor shaft. The approximate size and locations of the 4-blade hub and the upstream motor are shown at the top of the figure. These data show that there is a strong recirculating region downstream of the motor, with a reversed flow that has a peak z-component of nearly - 2 m/s. Further downstream, there appears to be a stagnation point at approximately r = 0 mm and z = -480.0 mm. The region adjacent to the recirculating region is characterized by a very low positive velocity, ranging from nearly 0 m/s to a peak of ≈ 1.5 m/s. At larger radii, the velocity continually increases, with a peak velocity of nearly 4.0 m/s for this measurement volume. Figure 7.2 shows that this region of lower speed fluid ($0 < v \leq 1.5$ m/s) that lies just outside of the recirculation area appears to be converging towards the center of the cone in the downstream direction, but the higher speed fluid ($v \geq 2.0$ m/s) appears to be diverging towards the outer edge of the cone. This is most likely a result of entrainment by the higher speed flow as it follows the diverging angle of the diffuser cone. It should be noted that the region of flow in the upper left-hand corner that appears to be moving in the horizontal direction (per the streamlines that are shown in this region) is actually the fan blade that passed through the image plane and correlated on itself. Because of the direction of the blade, this only appeared in the left-hand side.

7.1.1.2 Near Hub Region - Low-Pressure Shroud Condition (ΔP_{shroud} = 498 Pa)

The region directly downstream of the hub was subsequently examined in the low-pressure shroud condition (ΔP_{shroud} = 498 Pa). This is the identical condition to the one that was measured for numerous "shroud on" conditions in Section 6.0. Although the aerodynamic shroud actively controls the outer blade region, it could potentially affect this hub region by altering the radial velocity profile directly downstream of the blade. The contour plot of this shroud condition is shown in Figure 7.3, again with color contours of the z-component and the corresponding streamlines. This figure shows that the downstream hub region is essentially the same as in the "shroud off" condition in both qualitative flow features and magnitudes of velocity.

7.1.1.3 Near Hub Region - High-Pressure Shroud Condition (ΔP_{shroud} = 996 Pa)

A second shroud condition, termed the "high-pressure shroud" condition and corresponding to a $\Delta P_{shroud} = 996$ Pa, was also measured for the near hub region. This represents the highest condition that was tested in the integral measurements of Section 6.0 and also the condition which provide the most significant improvement in flow rate for both the 4-blade and 5-blade propellers. Figure 7.4 shows the contour plot of the z-component of velocity and the corresponding streamlines. These results are similar to those of Figure 7.3 for the low-pressure shroud condition, with nearly identical qualitative flow features and velocity magnitudes. One notable difference is that the low velocity region directly downstream of the recirculation area appears to be biased to the left. This could be a result of the high entrainment rate of the wall jet of the aerodynamic shroud. That is, it is suggested that this region is being "pulled" along. The streamlines are most likely tending to the left because the fan's direction of rotation is counter-clockwise when the viewer is looking in the upstream direction. From the perspective of the camera used for these measurements, the projection of this rotation would point towards the left. It is quite possible that this downstream flow pattern has a slight counter-clockwise swirl component. This 3-D swirl component is being measured as the projection onto the image plane of the CCD camera.

7.1.2 Diffuser Wall Interior Region (4-Blade Fan with 11 Degree Diffuser Cone)

Measurements were made in the interior of the cone for the 4-blade fan with the 11 degree diffuser cone to determine if there was attached flow at a region that was upstream of the exit plane of the diffuser cone. Initial flow visualizations conducted during the integral measurements indicated that for the 4-blade and 11 degree diffuser cone combination, the flow remained attached along the entire length of the cone. However the results of Figures 6.6 and 6.7 clearly show that there is neither an improvement in performance nor in efficiency by adding the 11 degree cone, despite its significantly larger exit area. These PIV measurements were collected with the intent of measuring the flow field along the interior wall of the 11 degree diffuser cone for the "shroud off" condition, along with two different "shroud on" conditions.

Optical access was achieved by placing the camera inside the cone and pointing the laser sheet upwards, as shown in Figure 7.5. This creates an unusual perspective since the laser sheet actually “cuts” through the cone at the perimeter of the images. The results are shown in Figures 7.6, 7.7, and 7.8. These figures are shown with a local coordinate system rather than the global coordinate system used in the PIV measurements previously presented and also the rest of the PIV measurements in this section; the x′ and y′-component values that are shown in the plots are independent of the r, θ, z coordinate system that is used in the remainder of the data. The y-component is aligned with the surface of the cone wall. As a result, the negative y-direction in the these figures is aligned with the streamwise direction of the flow. Similarly, a negative z-component of velocity would represent a flow moving towards the exit plane of the diffuser cone and a positive velocity would represent reversed flow, which would most likely be a result of flow separation. Figure 7.6 shows the "shroud off" condition for the 4-blade fan with the 11 degree cone. At this condition, the peak value for the z-component of velocity, found in the center of the image plane, is approximately -6.00 m/s. This peak velocity decreases in both the positive and negative x-directions as the laser sheet is positioned closer to the surface of the diffuser cone. At the outer most regions, the velocity approaches zero. From Figure 7.6, it is apparent that there is no reversed flow (positive z-component velocity) evident across this section of the cone wall. The region of peak velocity increases from the top of the image to the bottom, which corresponds to the local radius of curvature increasing. Finally, it is notable that the streamlines follow a line that is pointing towards the bottom left of the image. This is evidence of a slight swirl component in the interior wall of the diffuser, which was also observed in the flow visualization measurements.

Figure 7.7 shows the same physical location as in Figure 7.6, only the fan system is operated in the "shroud on" condition, with a $\Delta P_{shroud} = 498$ Pa. This figure shows that the peak velocity, located at the center of the image, has been increased to approximately -7.5 m/s. This is a result of the increased momentum that is imparted by the wall jet from the aerodynamic shroud. Similar to the results of Figure 7.6, this peak velocity decreases in both the positive and negative x-directions, finally resulting in a near zero velocity close to the wall. There also appears to be a slight swirl similar to that observed in Figure 7.6.

The final shroud condition that was evaluated was for $\Delta P_{shroud} = 996$ Pa. These results are shown in Figure 7.8 and, as anticipated, the peak velocity has increased further, to a peak velocity of approximately -8.5 m/s. The overall results of this shroud condition are qualitatively very similar to those of both the "shroud off" and $\Delta P_{shroud} = 498$ Pa conditions.

These results show that there is no evidence of flow separation in the 11 degree diffuser cone when used in conjunction with the 4-blade fan. Given this observation, it is reasonable that there would be an increase in either the performance or the velocity of this configuration compared with the baseline production assembly (4-blade fan with 7 degree diffuser cone). However, the results of Figures 6.6 and 6.7 show that this is not the case. Additionally, it can be seen from these results that the aerodynamic shroud is capable of increasing the momentum flux adjacent to the wall of a diffuser cone. As expected, this momentum flux increased with increasing shroud pressure. Finally there is a swirl component observed in the region adjacent to the wall. Since the initial jet from the aerodynamic shroud has only an axial component, this observation suggests that the wall jet is slightly altered by the swirl component of the fan.

7.1.3 Exit Plane of the Diffuser Cone (7 Degree Cone)

A set of measurements were made near the exit plane of the 7 degree diffuser cone to resolve the exit velocity profile and additional features of the flow field near the exit of the control volume, as described in Figure 2.1. The setup used for these measurements is shown in Figure 7.9. This figure shows that the laser sheet was tilted to a 6° angle to maintain a perpendicular relationship with the CCD camera, which had to be tilted up 6° to gain optical access to the centerline of the cone. The region of interest was from the centerline of the cone, (0,0) in Figure 5.2, to the outer wall of the cone, which is a distance of 381 mm for the 7 degree cone (the 11 degree cone, as described later, has a diameter of 422.9 mm). The experimental configuration, as shown in Figure 7.9, allowed for a field of view that was approximately 185 mm wide; therefore three different radial views were utilized, with a large overlapping region in the middle. This allowed for the entire radial span to be interrogated and the overlapping areas also provided a redundant check on the separate data sets. These three radial measurement regions are referred to as the "center region", "overlap region", and "near wall region", respectively from the center of the cone moving to the outermost radius.

Since the shroud and housing for this fan is axisymmetric, only one azimuthal position was measured. The operating conditions for all data in this section can be described as a pressure rise: $\Delta P = 25$ Pa and three different shroud pressure conditions: i) $\Delta P_{shroud} = 0$ Pa ("shroud off"), ii) $\Delta P_{shroud} = 498$ Pa and iii) 996 Pa. These values represent the range of shroud conditions that were evaluated in the integral measurements of Section 6.0. The time-averaged data are presented as plots that are shown as color contours of the z-component of velocity with added streamlines of the time-averaged flow field. The trailing edge of the diffuser cone is drawn as a solid black line to give the approximate location of the exit plane of the control volume as shown in Figure 2.1.

7.1.3.1 Center Region of the Diffuser Cone Exit Plane (7 Degree Cone)

The center region is shown schematically in Figure 7.10. The field-of-view for this region was approximately 185 mm by 185 mm, and extended from the centerline of the fan exit plane at $r = 0$ outward to a radial position, $r = 185$ mm. The image plane was positioned such that the exit plane of the diffuser cone was at the top of the image, this exit plane corresponds to $z = 0$ mm.

Figure 7.11 shows the center region results for the 4-blade fan with the 7 degree diffuser with the "shroud off" condition. The dark black line across the top of the figure (that lies along the $z = 0$ mm line) designates the location of the exit plane of the diffuser cone. Several interesting observations are evident from this figure. First, there is a region with a negative z-component in the upper right-hand portion of the figure. This region of reversed flow extends from the centerline at $r = 0$ mm and continues out to approximately $r = 60.0$ mm. This is portion is problematic since it reduces the overall flow rate of the system. The second interesting observation is the region of nearly zero velocity just outside the region of reversed flow. This region extends from $r = 60.0$ mm outward to $r = 175.0$

mm. The flow in this region is positive, yet it has a very low velocity (less than 1 m/s). Finally, at the upper left hand corner of the image, a region of higher velocity is shown. The flow in this region has a velocity of approximately 1.5 m/s. Therefore, three distinct regions are shown: an inner region with negative z-component velocities (r = 0 - 60.0 mm), a larger middle region of small (less than 1 m/s) positive z-component velocities (r = 60.0 -175.0 mm) and an outer region of higher (greater than 1 m/s) positive velocity flow.

This center region was then measured in the "shroud on" condition to determine the effects of the aerodynamic shroud on this region of the flow. The center region is quite far from the outer edge of the diffuser cone wall, but it was reasoned that the aerodynamic shroud might alter the velocity across the entire span of the diffuser cone exit plane. The results of the aerodynamic shroud in the low-pressure shroud condition, ΔP_{shroud} = 498 Pa are shown in Figure 7.12. The general features of this region appear to be similar to those of the "shroud off" condition, however the region of reversed flow in the center has increased. At this condition the reversed flow region spans from approximately r = 0 mm out to approximately r = 105 mm. Adjacent to this reversed flow region is a region of small magnitude (less than 1 m/s) positive z-component velocity and a slightly larger outer region of higher magnitude (greater than 1 m/s) positive velocity flow. Overall, the general features of the flow field are similar, but the presence of the "shroud on" condition has widened the region of reversed flow and slightly increased the size of the higher magnitude region.

A second "shroud on" condition was also examined, and the results are shown in Figure 7.13. This second condition had a ΔP_{shroud} = 996 Pa. These results show that there again exists a region of reversed flow that is larger than the shroud off condition. The magnitudes of this region appear to be slightly larger than both the "shroud off" and low-pressure shroud (ΔP_{shroud} = 996 Pa) cases.

7.1.3.2 Near Wall Region of the Diffuser Cone Exit Plane (7 Degree Cone)

The near wall region is defined by the schematic of Figure 7.14. This region had a field of view comparable to that of the center region in Section 7.1.3.1 that measured approximately 185 mm by 185 mm. This region extended just beyond the side wall of the diffuser cone.

Figure 7.15 shows the results for the 4-blade fan with the 7 degree cone when operated in the "shroud off" condition. The location of the exit plane of the diffuser cone, along with the side of the cone wall are shown by the dark black line. Streamlines are placed to show the approximate flow paths. This figure shows that there is a region of high velocity (> 4m/s) near the outer edge of the flow (approximately between r = 280 mm and r = 380 mm), that decreases steadily towards the center of the cone. The peak magnitude in this region is approximately 4.8 m/s. There is no evidence of reversed flow nor any negative z-component flow. The large region of nearly zero velocity that exists near the cone wall is the result of the diffuser cone being visible in the measurement field-of-view. The glare from the laser contacting this surface created a small region adjacent to the solid surface where very few correlations from the PIV image pairs exist. These "washed out" areas are indicated by the ~0 m/s velocity contours.

Next the "shroud on" condition was evaluated with a ΔP_{shroud} = 498 Pa and these results are shown in Figure 7.16. This figure shows the aerodynamic shroud is able to increase the velocity in this region; the aforementioned high velocity region of the "shroud off" condition has increased and the peak z-component velocity in this region now exceeds 5.0 m/s. A second "shroud on" condition of ΔP_{shroud} = 496 Pa was measured and the results are in Figure 7.17. This figure shows that the high velocity region is further increased at this higher shroud pressure. For this case the high velocity region is increased to well over 6.0 m/s. Both of these "shroud on" conditions show that the aerodynamic shroud is capable of increasing the velocity in the near wall region of the diffuser cone.

7.1.3.3 Overlap Region of the Diffuser Cone Exit Plane (7 Degree Cone)

Limitations in the field-of-view of the CCD camera resulted in a measurement region that was approximately 185 m^2. Therefore three measurement regions were required in order to measure the entire exit plane of the diffuser cone from the center (0,0) to the outer edge of the diffuser cone (0, 381.0 mm). The third region is referred to as the "overlap" region and it covers the portion not measured by either the "center region" nor the "near wall region"; and it also overlaps into each of these regions. The overlap region was selected to provide a redundant check on a portion of the measurement planes of the center and near wall regions. The overlap region is shown schematically in Figure 7.18.

The "shroud off" results of the 4-blade fan with the 7 degree diffuser cone are shown in Figure 7.19. As expected, this measurement location shows the transition from the higher speed flow of the near wall region to the low velocity of the center region. The location of the diffuser cone exit plane is again shown by the solid dark line that exists at z -= 0 mm. The subsequent results of the "low-pressure shroud" condition of ΔP_{shroud} = 496 Pa and the "high-pressure shroud" condition of ΔP_{shroud} = 998 Pa are shown in Figures 7.20

and 7.21, respectively. Again the general trends are the same, but the magnitude of the peak velocity component increases for each condition. This is the result of the high speed jet that is produced from the aerodynamic shroud.

7.1.3.4 Composite View of the Diffuser Cone Exit Plane (7 Degree Cone)

The composite view of each of the three measurement regions: i) center region, ii) near wall region, and iii) overlap region is shown for the "shroud off" case in Figure 7.22. This composite view provides a comprehensive look at the exit plane flow field of the diffuser cone. There is slight shift in the upper and lower limits of the z-component positioning of each of the three views, this is a result of having to re-position the camera for each of these measurement sets, which resulted in slight shifts in orientation and also slight changes in the field-of-view for each of these images. The location of each image plane was checked prior to each measurement set, so the resulting locations are accurate and reliable. The slight vertical shifts in the measurement planes of Figure 7.22 show the agreement between these independent measurement sets. This is particularly evident at the high velocity region that exists in the "near wall region" and the right hand side portion of the overlap region.

Figures 7.23 and 7.24 show the composite views for the two "shroud on" conditions of ΔP_{shroud} = 496 Pa and ΔP_{shroud} = 998 Pa, respectively. As was shown in the results of Figure 7.22, it is evident that there is good agreement between the overlapping portions. Also, the trend of increased flow in the larger radii (approximately from r = 250 mm to r = 360 mm) for the "shroud on" conditions can be seen. There also exists a slightly higher reversed flow for the "high-pressure shroud" condition than for the "low-pressure shroud" condition. A slightly higher reversed flow is also seen for the "low-pressure shroud" condition compared to the "shroud off" condition.

7.1.4 Exit Plane of the Diffuser Cone for the 4-Blade Fan with 11 Degree Cone

The effects of changing the diffuser cone were examined by replacing the 7 degree diffuser with the 11 degree diffuser and repeating the measurements of Section 7.1.3. Although the radius of the exit plane of the 11 degree diffuser (r = 423.0 mm) is considerably larger than that of the 7 degree diffuser (r = 381.0 mm), the entire span could still be measured by three measurement planes. Therefore, the same terminology will be used to describe the three measurement regions (center region, near wall region and overlap region). These approximately represent the same relative locations as those used in for the 7 degree diffuser.

7.1.4.1 Center Region of the Diffuser Cone Exit Plane (11 Degree Cone)

The center region of the 11 degree diffuser covered a region that was very similar to that of the 7 degree cone, and a visual description of this area can again be found in the schematic drawing of Figure 7.10. The field-of-view was very close, but not identical to, that of the center region measured for the 4-blade fan with the 7 degree diffuser. Figure 7.25 shows the results of the center region of the 4-blade fan with the 11 degree cone for the "shroud off" condition. This figure shows that there exists a strong region of reversed flow in the center of the cone. Whereas the velocity magnitudes in the reversed flow portions for the 7 degree cone were small (< 0.5m/s), this configuration has a much higher magnitude. The peak velocity in this region of reversed flow is nearly - 1.6 m/s, and this reversed flow region extends farther downstream than the reversed flow region of the 7 degree cone configuration. The left side of Figure 7.25 shows a region of positive velocity, with a peak velocity slightly greater than 2.0 m/s. Between this inner region of reversed flow and the outer region of positive velocity flow, there exists a large swirling region. This region spins in a clockwise direction and is driven by the two boundaries of opposite direction flow. The regions of reversed flow and the swirling region represent areas of the flow field that do not make positive contributions to the overall performance and efficiency of this fan system.

Figure 7.26 shows this same region in the "shroud on" condition, specifically for the case of ΔP_{shroud} = 498 Pa. These results show that with the aerodynamic shroud activated, the region of reversed flow has increased in size, extending out to a radial position of approximately r = 150 mm. The magnitude of this reversed flow has remained the same as that of the "shroud off" case. The large region of swirling flow in the center of the image is no longer present, and the region of positive direction flow has clearly shifted to a higher radius. This is most likely a result of the increased entrainment from the aerodynamic shroud wall jet in the cone wall region.

The results for the a higher "shroud on" condition, ΔP_{shroud} = 996 Pa, are shown in Figure 7.27. This figure shows that for this higher "shroud on" condition, the radial span of reversed flow has increased even farther beyond the reversed flow region that for the low-pressure shroud case (ΔP_{shroud} = 498 Pa). This region of reversed flow extends from the center of the cone (r = 0 mm) out to around r = 140 mm. Again, the large region of swirling flow in the center of the image does not exist and the positive direction flow has shifted outward to a higher radius. It appears that the effect of increased entrainment from the wall jet of the aerodynamic shroud is even more pronounced than the observed effect from the lower "shroud on" case (ΔP_{shroud} = 498 Pa).

7.1.4.2 Near Wall Region of the Diffuser Cone Exit Plane (11 Degree Cone)

The near wall region, as shown schematically in Figure 7.14, was measured for the same three shroud conditions: "shroud off", "low-pressure shroud" (ΔP_{shroud} = 498 Pa) and "high-pressure shroud" (ΔP_{shroud} = 996 Pa). Figure 7.28 shows the results for the "shroud off" condition. The edges of the diffuser cone sidewall and exit plane are marked in this figure by the solid black line. From this figure, there is a region of high speed flow (V > 6.0 m/s) that exists away from the wall of the diffuser cone, approximately between the radial positions of r = 280.0 mm and r = 370.0 mm. The outer edge of the cone is at r = 423.0 mm. In this figure, the region between r = 370.0 mm and r =423.0 mm has a much lower velocity.

Figure 7.29 contains the data for the same region in "low-pressure shroud" condition (ΔP_{shroud} = 498 Pa). Again, similar to the results of Figure 7.28, there exists a region of high speed fluid (V > 6.0 m/s) near the outer cone wall. However, for these results, the radial position of this region has shifted to a larger radial position; it now occupying the region between r = 315.0 mm and r = 395.0 mm. Since the percentage of total exit plane area represented by this region is much higher, this would represent an increase in total volume flow rate. The results for the "high-pressure shroud" condition (ΔP_{shroud} = 996 Pa) are shown in Figure 7.30. Similar to the results of "low-pressure shroud" condition, the region of high speed fluid (V > 6.0 m/s) has shifted towards the outer cone wall, and is occupying a region that is nominally identical to that of the "low-pressure shroud" condition. The primary difference at this condition is that the peak velocity within this region of high speed fluid has increased slightly, to a peak z-component of velocity of slightly higher than 7.0 m/s. This would most likely indicate a higher volume flow rate than both the "low-pressure shroud" and "shroud off" conditions, but not nearly as dramatic as the change from the "shroud off" to the "low-pressure shroud" case.

7.1.4.3 Overlap Region of the Diffuser Cone Exit Plane (11 Degree Cone)

The overlap region for the 4-blade fan with the 11 degree cone is again shown schematically in Figure 7.18. Given the large exit area of the 11 degree cone, there was slightly less redundant information between this region and the two adjacent regions (near wall region and center region). The results for this region with the "shroud off" condition are shown in Figure 7.31. This figure shows that there is no reversed flow (negative z-component of velocity) across the entire radial span, and also that the velocity increases with increased radius.

Figure 7.32 shows the same location for the "low-pressure shroud" condition (ΔP_{shroud} = 498 Pa). The surprising result here is that the low-pressure shroud condition shows a region of reversed flow (negative z-component of velocity) at the right edge of the figure. Additionally, the region of high speed fluid (V > 5.0 m/s) has shifted to a higher radial position. This appears to be the result of increased entrainment from the wall jet of the aerodynamic shroud. Referring to Figures 6.10 and 6.11, this condition was able to increase the volume flow rate, Q, but it was accompanied by a decrease in efficiency.

Figure 7.33 shows the results for the "high-pressure shroud" condition (ΔP_{shroud} = 996 Pa). These results are very similar to those of Figure 7.32, once again show that there is reversed flow that did not exist for the "shroud off" case and also the location of the high speed fluid (V>5.0 m/s) has shifted radially outward. The peak magnitude of this region of high speed fluid has also increased, which is most likely caused by the increased speed of the wall jet at this "high-pressure shroud" condition.

7.1.4.4 Composite View of the Diffuser Cone Exit Plane (11 Degree Cone)

By combining the three measurement regions: i) center region, ii) near wall region, and iii) overlap region, a composite view of the exit plane velocity was created. The three shroud conditions, "shroud off", "low-pressure shroud", and "high-pressure shroud" are shown in Figures 7.34, 7.35, and 7.36, respectively. These composite views clearly show the two key observations that were seen in the individual measurement regions, namely the outward shift in the high speed fluid (V > 5.0 m/s) for the two "shroud on" conditions and the subsequent increase in reversed flow at the center of the cone for the two "shroud on" conditions.

7.2 PIV Measurements on the 5-Blade Fan Configuration

The results of Section 6.4 on page 65 clearly showed that the 5-Blade fan, when tested with the aerodynamic shroud in the "shroud on" condition, could provide substantial increases in both volume flow rate, Q, and efficiency, η^*. While these gains were apparent, the mechanisms that caused this dramatic increase was not. Because of these improvements, there was considerable interest in using PIV at the exit plane of this diffuser cone. It was thought that information obtained from these measurements could provide an insight into the specific reasons why the aerodynamic shroud worked so well with this configuration, but not nearly as well with the previous configurations. Data collected in

Section 6.0 indicated that the optimal "shroud on" condition for this configuration was ΔP_{shroud} = 373 Pa. This was selected as optimal because it provide substantial increases in both the flow rate and the efficiency, 33.6% and 12.3% respectively, when examined at the operating condition of ΔP = 25 Pa. Because of these findings, only one "shroud on" condition of ΔP_{shroud} = 373 Pa was utilized for the following PIV data. Additionally, two operating points were examined for these data, to determine the effect of the system pressure rise on the fan exit plane in both the "shroud off" and "shroud on" conditions. These two operating points were ΔP = 25 Pa and ΔP = 50 Pa.

7.2.1 Exit Plane of the Diffuser Cone (11 Degree Cone)

Similar to the results of both Section 7.1.3 and Section 7.1.4, the exit plane of the 11 degree diffuser cone was measured in three separate regions: i) center region, ii) near wall region, and iii) overlap region. These regions are nominally identical to those used in Section 7.1.4 for the 4-blade fan with the 11 degree diffuser cone.

7.2.1.1 Center Region of the Diffuser Cone Exit Plane (11 Degree Cone)

The center region is defined schematically in Figure 7.10 for the 5-blade fan and the 11 degree cone. Figure 7.37 shows this region for the "shroud off" condition at a pressure rise of ΔP = 25 Pa. The exit plane of the diffuser cone is again indicated by the solid black line at the z = 0 mm position. This figure shows that the velocity near the exit plane at this operating point has a positive magnitude across the entire span; there is no area with a reversed flow (negative velocity) condition. Although there is no area showing reversed flow, the flow closest to the center of the cone has a very small magnitude. Specifically, the velocity magnitudes in the region from r = 0 mm out to r = 60 mm are less than 1.0 m/

s. However, when the pressure rise of the system is increased as shown in Figure 7.38, there is a region of reversed flow that forms near the centerline (0,0) of the exit plane.

Figure 7.39 displays the data for the center region when the "shroud on" condition (ΔP_{shroud} = 373 Pa) is applied. The operating point for this data set is ΔP = 25 Pa. Whereas Figure 7.37 showed that there was no reversed flow in this region, the "shroud on" condition shows that a region of reversed flow has appeared at the exit plane of the cone. These results are consistent with the findings of Section 7.1.4.1, which showed that the "shroud on" condition increased the region of reversed flow near the center of the 11 degree cone. It also interesting to note that the velocity gradient across this radial section is much smaller than for the "shroud off" case. The maximum velocity is approximately 2.66 m/s and the minimum velocity is - 0.42 m/s. The "shroud off" condition showed a much steeper gradient across this same section, with a peak velocity of 5.6 m/s and a minimum velocity of approximately 0.40 m/s. From these data, it is apparent that the wall jet from the aerodynamic shroud has made the velocity profile more uniform.

The "shroud on" condition was also evaluated at the higher back, ΔP = 50 Pa, for this region. The results of this test are shown in Figure 7.40. The results here are somewhat surprising because previous data had indicated that the higher operating point had a large region of reversed flow near the center of the cone. Yet when the "shroud on" condition was tested, this region disappeared, and only the exit velocity is positive across this entire radial span. It is also interesting to note that the exit velocity is once again much more uniform for the "shroud on" condition. Whereas the data in Figure 7.39 had a maximum velocity of nearly 2 m/s and a minimum of approximately -0.50 m/s at the exit plane, the data for the "shroud on" condition show a maximum velocity of approximately 0.70 m/s and a minimum velocity of approximately 0.10 m/s. It is apparent that the aerodynamic shroud is capable of creating a more uniform exit velocity profile for each of these operating points.

7.2.1.2 Near Wall Region of the Diffuser Cone Exit Plane (11 Degree Cone)

Data for the near wall region, as shown schematically in Figure 7.14, were measured for the same four conditions that were tested in Section 7.2.1.1. The results of the "shroud off" condition at an operating point of $\Delta P = 25$ Pa are shown in Figure 7.41. This figure shows that a region of high velocity fluid ($V > 5.0$ m/s) exists away from the wall, approximately from r = 250.0 mm out to r = 315.0 mm. A maximum velocity of about 6.8 m/s exists in this high velocity area, which steadily decreases to a minimum of approximately - 0.21 m/s. This minimum velocity occurs near the edge of the cone wall, where there is evidence of a very small reversed flow region.

Figure 7.42 shows the same near wall region in the "shroud off" condition for a higher operating point, $\Delta P = 50$ Pa. Again there exists a region of high speed fluid ($V > 5.0$ m/s) that exists adjacent to the wall, but for this operating condition the region is much larger and is situated closer to the wall, approximately between r = 250.0 mm and r = 400.0 mm. The peak velocity across this section is nearly 6.4 m/s and the minimum is near zero, but overall, the velocity profile is more uniform than that of the lower operating point.

The results of the "shroud on" condition for the lower operating point, $\Delta P = 25$ Pa, are shown in Figure 7.43. There exists a region of high speed fluid ($V > 5.0$ m/s) that is similar to that found in Figure 7.41, only with the aerodynamic shroud in the "shroud on" condition, this region has shifted outward, and now covers wider portion of this measurement region, spanning from r = 250.0 mm out to r = 350.0 mm. The results of Figure 7.41 indicated that there was a small region of reversed flow at the outer radial positions, but these appear to have vanished in the "shroud on" condition. Overall, the "shroud on" condition has caused the exit profile of this fan to be more uniform.

The "shroud on" condition was also measured for the operating point of $\Delta P = 50$ Pa. These results are shown in Figure 7.44. This figure shows a similar result to those found for the lower operating point; namely that the "shroud on" condition shows a more uniform velocity profile than that for the "shroud off" condition. There exists a large region of high speed fluid (V > 4.0 m/s) that extends across almost the entire radial span of this region, from approximately r = 250.0 mm to almost r = 420.0 mm.

7.2.1.3 Overlap Region of the Diffuser Cone Exit Plane (11 Degree Cone)

The overlap region for the 5-blade fan with the 11 degree diffuser cone is again shown schematically in Figure 7.18. The results for this region in the "shroud off" condition and at the lower operating point of $\Delta P = 25$ Pa are shown in Figure 7.45. This figure shows that unlike the previous cases for the 4-blade fan, the concentration of flow with the highest velocity occurs in this overlap region, as opposed to the near wall region. The central portion of this region, from approximately r = 170.0 mm to r = 250.0 mm has a z-component of velocity that is greater than 6.5 m/s. The velocity then begins to decrease for radial locations, r > 250.0 mm and r < 170.0 mm.

The "shroud off" data for the higher operating condition, $\Delta P = 50$ Pa, is shown in Figure 7.46. These data show that the velocity increases as the radial position increases.

Also, similar to the results for the lower operating point, the region of maximum velocity occurs in this region. Specifically, its location is approximately between r = 240.0 mm and r = 280.0 mm. The outer wall of the 11 degree diffuser is at approximately r = 423.0 mm; therefore this region of maximum velocity is significantly far away from the wall.

The results for the "shroud on" condition (ΔP_{shroud} = 373 Pa) when operated at the lower operating point of ΔP = 25 Pa are presented in Figure 7.47. These data show, somewhat surprisingly, that the addition of the aerodynamic shroud has actually reduced the velocity across the entire span of this region. The exit velocities along the z = 0 mm line range from approximately V = 0.5 m/s at the smallest radial position shown in this region to a maximum velocity of V = 5.2 m/s at the highest radial position shown. Figure 7.48 shows that this trend is consistent for the "shroud on" condition for the higher operating point. The exit velocities are also reduced at each radial position for this case when compared with those data for the "shroud off" condition.

7.2.1.4 Composite View of the Diffuser Cone Exit Plane (11 Degree Cone)

The composite view for each of the previous cases was created by combining the three measurement regions: i) center region, ii) near wall region, and iii) overlap region. Although specific details of each region can be more easily understood by looking at the figures presented in the previous sections, the composite results allow the reader to look at the entire radial span for a general comparison of the flow fields that exist for each operating point and shroud condition.

Figures 7.49 and 7.50 show the composite views for both the higher (ΔP = 50 Pa) and lower (ΔP = 25 Pa) back pressure operating points at the "shroud off" condition.

Figure 7.49 shows that the concentration of the highest velocity fluid is significantly farther away from the wall than the highest velocity fluid for the 4-blade fan with the 11 degree diffuser cone. Also there is very little reversed flow at any radial position, except for a small region at the outermost radial location. The innermost radial locations from around r = 0 mm to r = 60.0 mm have exit velocities that are small (V < 1.0 m/s), but are in the positive direction. For the higher back pressure operating point shown in Figure 7.50, this region of high velocity fluid occurs at a slightly larger radial position. This condition shows that reversed flow does exist at the inner most radial positions, from r = 0 mm to around r = 60.0 mm.

The composite views for the "shroud on" condition of both the lower and higher operating conditions are shown in Figures 7.51 and 7.52. These figures show that for each operating point, the "shroud on" condition shifted the location of the maximum velocity outward toward the wall of the diffuser, while simultaneously reducing the magnitude of the peak velocity region. This creates a more uniform exit profile for each of the two operating points.

7.3 Exit Plane Velocity Profiles and Mass Flow Rate Distributions

The previous sections that presented the results of the exit plane PIV for the 7 and 11 degree diffuser cones with both 4 and 5-blade fans have focused largely on the line along z = 0 mm. This line indicates the location of the downstream edge of the cone wall and represents the exit of the control volume that was originally presented in Section 2.0. Using the PIV data from Sections 7.1.3, 7.1.4, and 7.2.1, individual data points were extracted along the exit plane of the diffuser cone. These data are the z-components of velocity that exist along the z = 0 mm line. A total of 300 points were extracted from the line along z =

0 mm and these points were interpolated between the measured locations. These data are presented spatially in non-dimensional form by normalizing the radius, r, by the total radius, R. It should be noted that these velocity data can also be represented non-dimensionally by normalizing V_z by $\langle V_e \rangle$, where $\langle V_c \rangle = Q/A_e$. These data are not presented in this manner here since $\langle V_e \rangle$ is different for every combination of shroud condition and diffuser cone; therefore, normalizing the velocity data makes it difficult to make relative comparisons between the various shroud conditions.

Since the outer radial sections of the cone have the largest percentage of the total exit area, they make large contributions to the exit flow rate. This distribution is also presented in this section by plotting the mass flow rate, $\dot{m}$, as a function of r/R, as defined by:

$$\dot{m} = \rho 2\pi R^2 \langle V_e \rangle \int_0^1 \left(\frac{r}{R} \cdot \frac{V_z}{\langle V_e \rangle} \right) \frac{dr}{R} \tag{7.1}$$

7.3.1 Exit Plane Velocity Profiles: 4-Blade Fan with 7 Degree Diffuser Cone

The extracted velocity profiles for the 4-blade fan with the 7 degree cone are shown in Figure 7.53. This figure shows all three of the shroud conditions that were tested: "shroud off", the "low-pressure shroud" condition (ΔP_{shroud} = 498 Pa), and the "high-pressure shroud" condition (ΔP_{shroud} = 996 Pa). Focusing on the inner region of the cone, from r/R = 0 out to r/R = 0.50, it is apparent that the addition of the aerodynamic shroud had very little effect on the velocity profile. A small region of reversed flow exists from r/R = 0 out to approximately r/R = 0.24. The velocity increases monotonically in the positive direction from r/R = 0.24 out to r/R = 0.50.

For the region at the center of the exit plane, slight increases in velocity are observed for the two "shroud on" conditions when compared with the "shroud off" condition. This region is approximately from r/R = 0.50 out to r/R = 0.72. It should be noted that there appears to be a fluctuating aspect to the velocity in this region. This is actually “noise” caused by several interrogation regions that had low numbers of validated vectors. This was most likely caused by a small distortion on these portions of the lens of the CCD camera, which is possibly caused by condensed vapor droplets or small pieces of dirt. Evidence of these can be seen by referring back to Figs 7.19 - 7.21, which were described in detail in Section 7.1.3.3 on page 101. As shown in these figures, these small regions that had low validation numbers actually represent a small fraction of the total plot area. Despite this, they do lie on the line of z = 0 mm. By examining the regions that surround this area, it is apparent that the velocity in this region is increasing with increasing radius, but it is expected that this increase would be more monotonic.

In the outermost region of the 7 degree cone, from r/R = 0.72 out to r/R = 1.0, there exists a systematic increase in the z-component of velocity as the shroud pressure is increased. The velocity distribution in this region increases to a maximum value and then "flattens" until the velocity values decrease in the near wall region of the cone. That is, a relatively thick boundary layer is observed for these conditions. This increase in velocity occurs at the largest radial values of the diffuser, where the largest percentage of the exit area exists. It is evident that this velocity increase accounts for the enhanced volume flow rate for both the "low-pressure shroud" condition (ΔP_{shroud} = 498 Pa) and the "high-pressure shroud" condition (ΔP_{shroud} = 996 Pa) when compared with the "shroud off" condition.

7.3.2 Exit Plane Velocity Profiles: 4-Blade Fan with 11 Degree Diffuser Cone

The velocity profiles for the 4-blade fan with the 11 degree diffuser cone are shown in Figure 7.55. A similar set of three shroud conditions with one system pressure rise was measured for this configuration, and the results of all three are presented in this figure. This figure clearly shows that a region of reversed flow exists for the "shroud off" condition between the radial positions of r/R = 0 and approximately r/R = 0.26. The size of this reversed flow region increases substantially for both of the "shroud on" conditions. That is, $V_z < 0$ are observed for the radial positions from r/R = 0 to r/R = 0.37. The velocity profile shows that the velocity for each of the shroud conditions increases monotonically in the positive radial direction, reaching a maximum before it decreases in the boundary layer region. In this region of monotonic growth, the two "shroud on" conditions show velocity profiles that are lower than that of the "shroud off position". The maximum exit velocity increases with increasing shroud condition, with the "shroud off" position having a maximum velocity, V = 6.9 m/s and the "high-pressure shroud" condition (ΔP_{shroud} = 996 Pa) yielding a maximum velocity, V = 7.6 m/s.

7.3.3 Exit Plane Velocity Profiles: 5-Blade Fan with 11 Degree Diffuser Cone

The 5-blade fan was of particular interest since it was capable of substantially increasing the flow rate, while simultaneously increasing the efficiency. The previous results of the 4-blade fan with both the 7 and 11 degree diffuser cone showed that the aerodynamic shroud was able to increase the velocity profile in the outer regions of the exit plane of the diffuser. This increase in velocity accounts for the slight increases in volume flow rate; however, these increases in velocity were accompanied by a more non-uniform velocity profile that caused a decrease in the efficiency of the fan. These decreases were detailed in

Section 6.1.2 for the 4-blade fan with the 11 degree cone, where there was 14.0% increase in volume flow rate, Q, but a 26.5% decrease in system efficiency, η^*. Also, Section 6.3.1 showed a similar trend for the 4-blade fan with the 11 degree cone, where there was a 16.0% increase in volume flow rate, Q, accompanied by a 20.7% decrease in system efficiency, η^*.

Figure 7.57 shows the extracted exit velocity profile for the 5-blade fan with the 11 degree diffuser cone. Both of these tests were run at a system pressure rise, $\Delta P = 25$ Pa, which was the target operating point identified in the comparisons from Section 6.0. The data of Figure 7.57 show that in the interior region of the cone there exists no reversed flow for the "shroud off" condition, but instead a small positive velocity across the entire radial span. When the "shroud on" condition is evaluated ($\Delta P_{shroud} = 373$ Pa), a region of reverse flow appears in the central portion of the cone, from r/R = 0 out to approximately r/R = 0.18. The "shroud off" condition has a much higher exit velocity throughout the region spanning r/R = 0 to r/R = 0.70 and this condition reaches a maximum velocity, V = 7.0 m/s at a radial location, r/R = 0.51. The "shroud on" condition reaches a maximum exit velocity, V = 5.4 m/s at a radial position, r/R = 0.65. The "shroud on" condition has a consistently higher exit velocity in the outermost regions of the cone, from r/R = 0.70 mm out to the edge of the cone at r/R = 1.0. This shows that the 5-blade fan, when operated with the "shroud on" condition is able to provide a higher flow in the outer radial positions. These outer radial locations represent the largest percentage of the exit area and therefore the volume flow rate is higher. Referring back to Section 6.4.2, there was a 33.6% increase in volume flow rate, Q, when the "shroud off" condition is compared with the "shroud on" condition of $\Delta P_{shroud} = 373$ Pa. Additionally, the "shroud on" condition has a much more uniform exit profile than the "shroud off" condition, which accounts for the subsequent increase in efficiency. This was also shown in Section 6.4.2 to be an increase in η^* of 12.3%.

The effect of increasing the back pressure was also measured for the 5-blade fan with the 11 degree diffuser. These data were collected based on the observations from Figure 6.18 and Figure 6.19 which showed that the "shroud on" condition for 5-blade fan was also able to increase the Q and η^* for higher back pressure operating points. Previous results with the 4-blade fan had shown that even when improvements were made in the flow rate at lower operating points, the higher operating points showed very little, if at all, increases in flow rate. Similarly, the 4-blade fan typically showed reductions in efficiency at lower operating points, and a much greater reduction in the efficiency at the higher back pressure operating points. These PIV observations help to identify why the 5-blade fan was able to function more efficiently at these higher operating points.

The extracted velocity profiles for the higher operating point, $\Delta P = 50$ Pa, are shown in Figure 7.59. These data show that in the innermost region of the diffuser cone, from $r/R = 0$ out to $r/R = 0.25$, the "shroud on" condition exhibits a higher exit velocity. This exit velocity is much more uniform, as shown by the nearly flat profile. Also, in contrast with the situation for the low operating point, the "shroud on" condition has a region of reverse flow from $r/R = 0$ out to $r/R = 0.21$. The "shroud off" condition shows a higher exit velocity between the radial positions of $r/R = 0.25$ out to $r/R = 0.95$, with a maximum exit velocity of 6.75 m/s occurring at $r/R = 0.59$. The "shroud on" condition has a maximum exit velocity that is much lower, approximately 5.0 m/s, and it occurs at the same approximate radial location of $r/R = 0.59$. In the outermost region of the cone, from $r/R = 0.59$ out to $r/R = 1.0$, the "shroud on" condition has a larger exit velocity. This higher exit velocity in the outermost radial positions coupled with the absence of reverse flow accounts for the higher Q that was measured for this condition in Figure 6.18. Additionally, the more uniform profile of the "shroud on" condition accounts for the increased η^* that is shown in Figure 6.18.

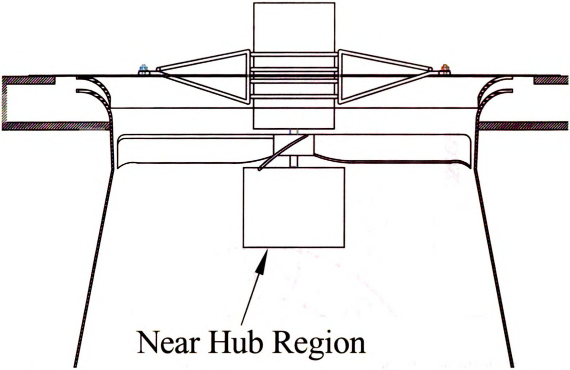

FIGURE 7.1 Schematic Defining the "Near Hub Region" PIV Measurement Plane

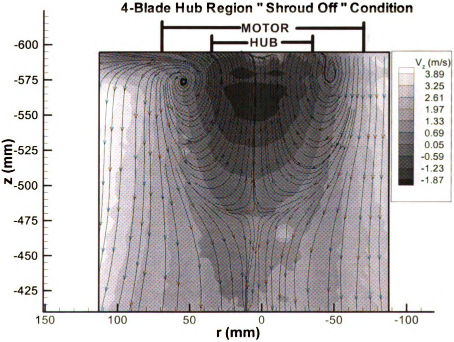

FIGURE 7.2 The 4-Blade Fan with 11 Deg. Cone - "Shroud Off" Condition - Near Hub Region

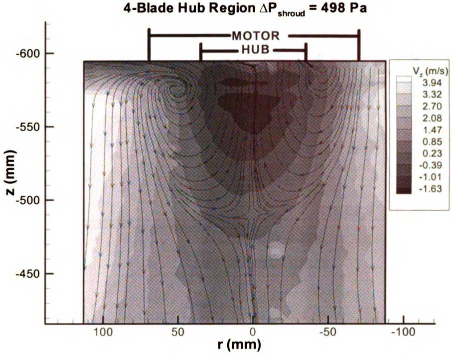

FIGURE 7.3 The 4-Blade Fan with 11 Deg. Cone - "Shroud On" Condition (ΔP_{shroud} = 498 Pa) Near Hub Region

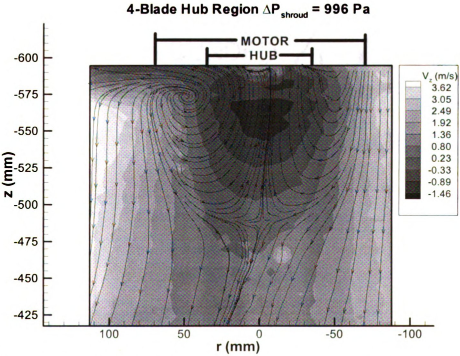

FIGURE 7.4 The 4-Blade Fan with 11 Deg. Cone - "Shroud On" Condition (ΔP_{shroud} = 996 Pa) Near Hub Region

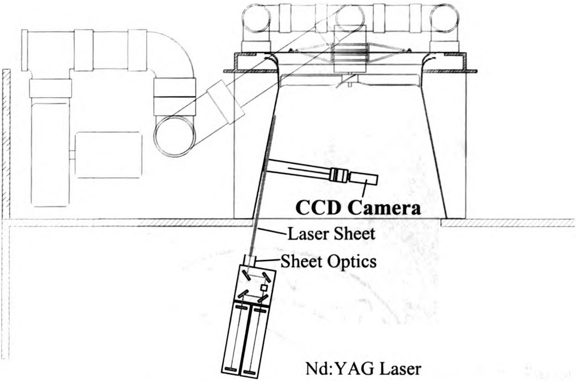

FIGURE 7.5 Setup for Interior Wall PIV Measurements

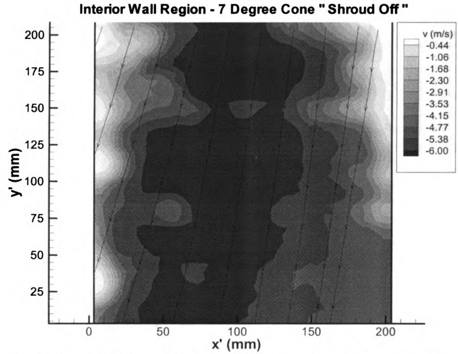

FIGURE 7.6 The 4-Blade Fan with 11 Degree Cone - "Shroud Off" Condition, Cone Wall Interior Region

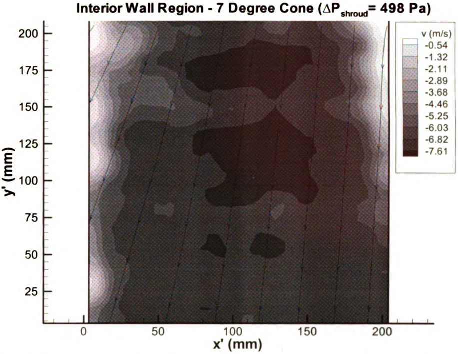

FIGURE 7.7 The 4-Blade Fan with 11 Degree Cone - "Shroud On" Condition (ΔP_{shroud} = 498 Pa), Cone Wall Interior Region

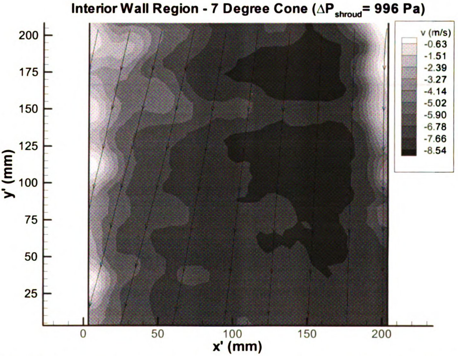

FIGURE 7.8 The 4-Blade Fan with 11 Degree Cone - "Shroud On" Condition (ΔP_{shroud} = 996 Pa), Cone Wall Interior Region

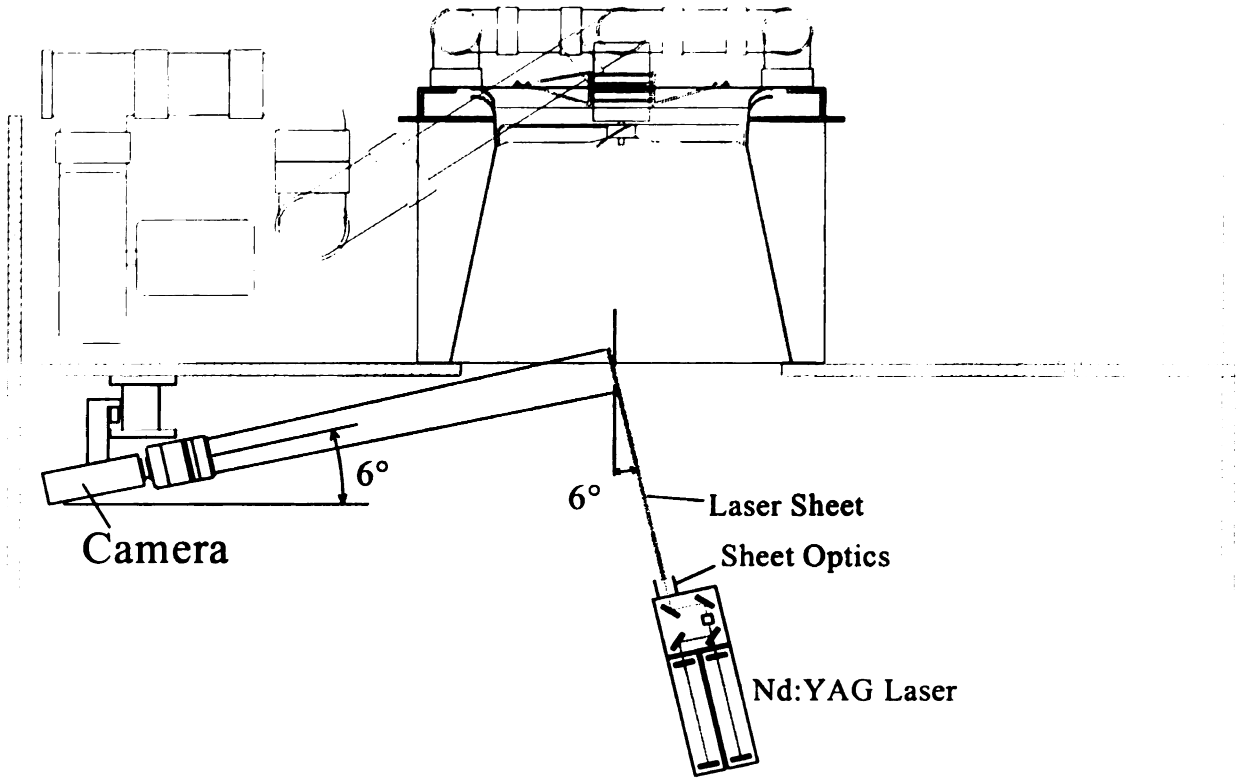

FIGURE 7.9 Setup for Exit Plane PIV Measurements

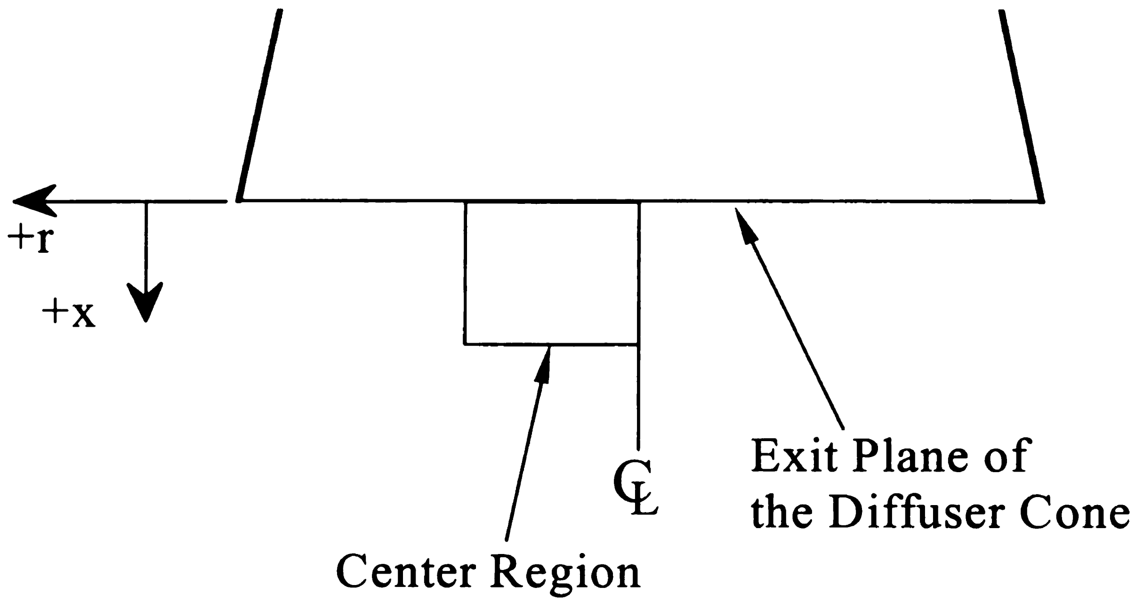

FIGURE 7.10 Schematic Defining the "Center Region" for the Exit Plane PIV

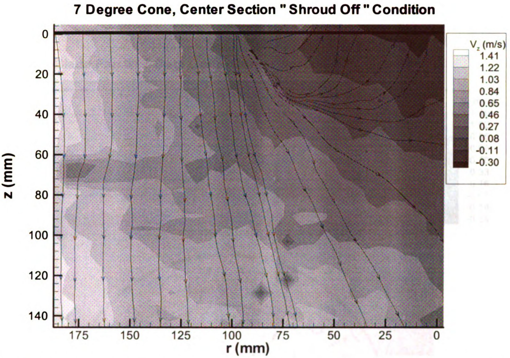

FIGURE 7.11 The 4-Blade Fan with 7 Deg. Cone - "Shroud Off" Condition Center Region

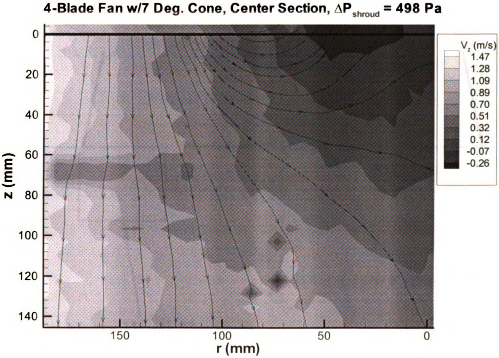

FIGURE 7.12 The 4-Blade Fan with 7 Deg. Cone - "Shroud On" Condition (ΔP_{shroud} = 498 Pa) Center Region

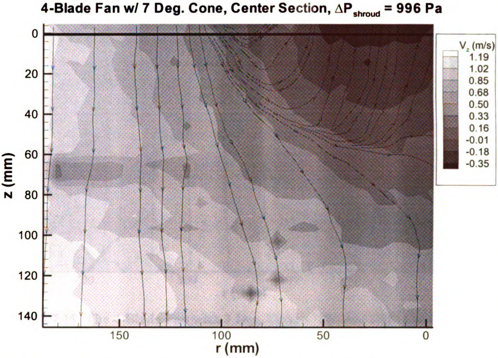

FIGURE 7.13 The 4-Blade Fan with 7 Deg. Cone - "Shroud On" Condition (ΔP_{shroud} = 996 Pa) Center Region

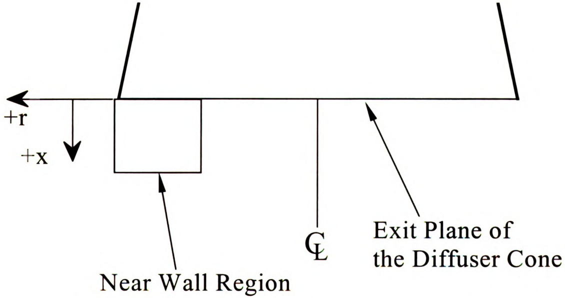

FIGURE 7.14 Schematic Defining the "Near Wall" for the Exit Plane PIV

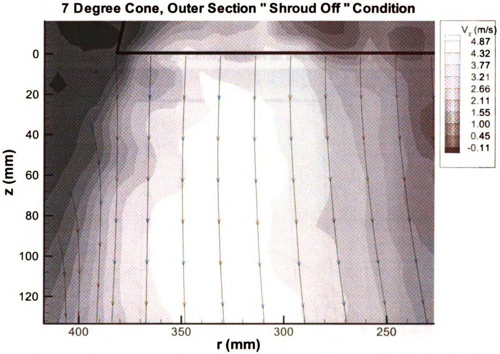

FIGURE 7.15 The 4-Blade Fan with 7 Deg. Cone - "Shroud Off" Condition Near Wall Region

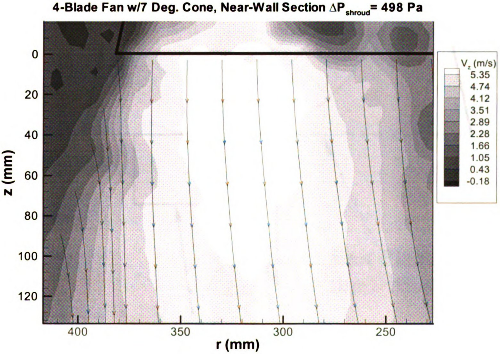

FIGURE 7.16 The 4-Blade Fan with 7 Deg. Cone - "Shroud On" Condition (ΔP_{shroud} = 498 Pa) Near Wall Region

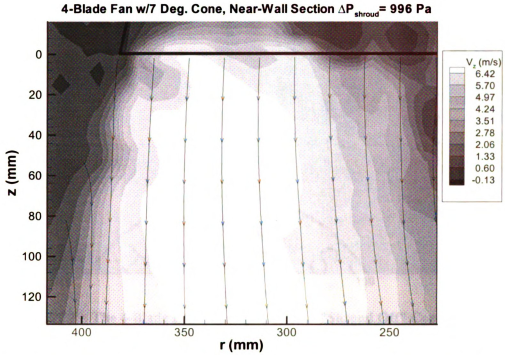

FIGURE 7.17 The 4-Blade Fan with 7 Deg. Cone - "Shroud On" Condition (ΔP_{shroud} = 996 Pa) Near Wall Region

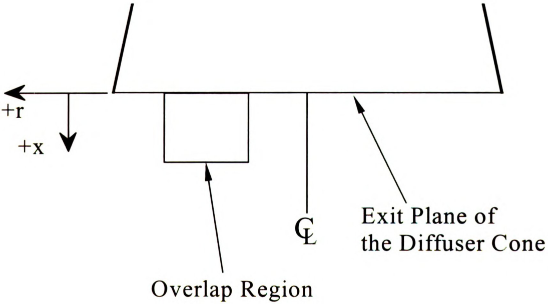

FIGURE 7.18 Schematic Defining the "Overlap" for the Exit Plane PIV

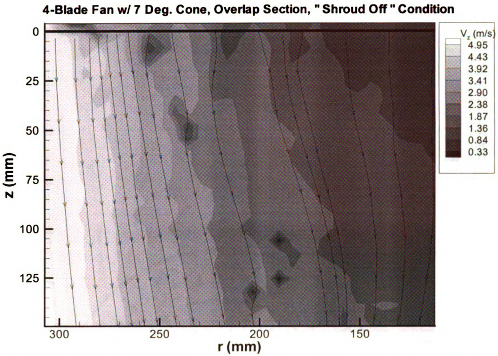

FIGURE 7.19 The 4-Blade Fan with 7 Deg. Cone - "Shroud Off" Condition Overlap Region

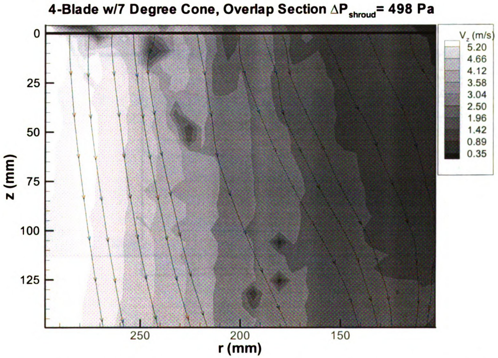

FIGURE 7.20 The 4-Blade Fan with 7 Deg. Cone - "Shroud On" Condition (ΔP_{shroud} = 498 Pa) Overlap Region

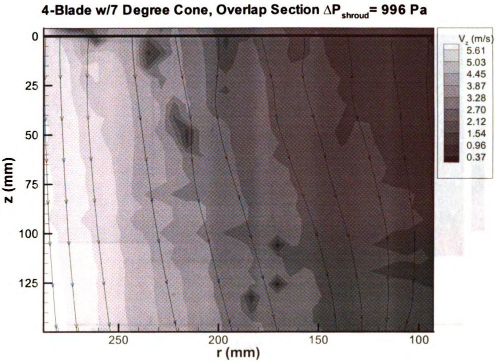

FIGURE 7.21 The 4-Blade Fan with 7 Deg. Cone - "Shroud On" Condition (ΔP_{shroud} = 996 Pa) Overlap Region

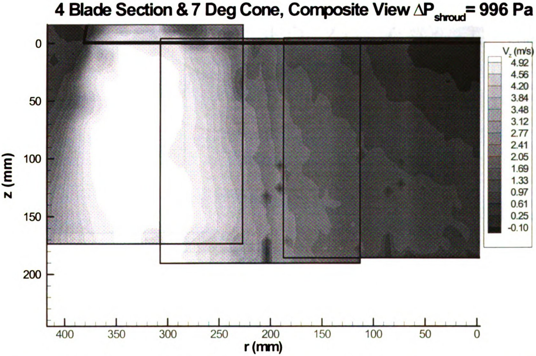

FIGURE 7.22 Composite View of the 4-Blade Fan with 7 Deg. Cone - "Shroud Off" Condition

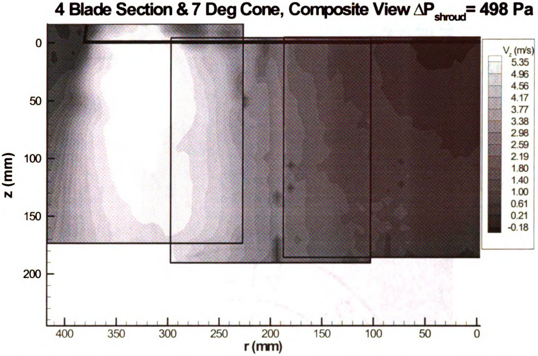

FIGURE 7.23 Composite View of the 4-Blade Fan with 7 Deg. Cone - "Shroud On" Condition (ΔP_{shroud} = 498 Pa)

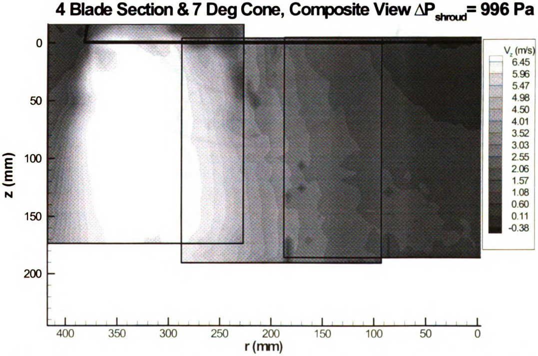

FIGURE 7.24 Composite View of the 4-Blade Fan with 7 Deg. Cone - "Shroud On" Condition (ΔP_{shroud} = 996 Pa)

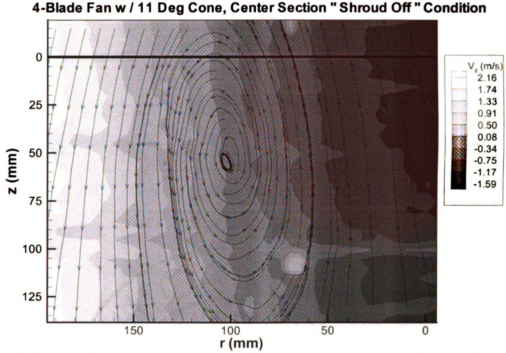

FIGURE 7.25 The 4-Blade Fan with 11 Deg. Cone - "Shroud Off" Condition Center Region

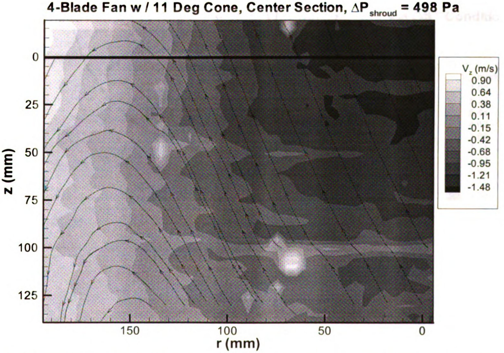

FIGURE 7.26 The 4-Blade Fan with 11 Deg. Cone - "Shroud On" Condition (ΔP_{shroud} = 498 Pa) Center Region

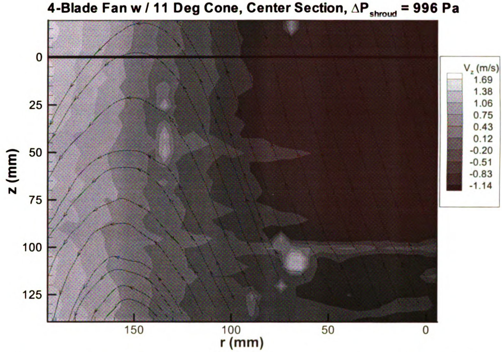

FIGURE 7.27 The 4-Blade Fan with 11 Deg. Cone - "Shroud On" Condition (ΔP_{shroud} = 996 Pa) Center Region

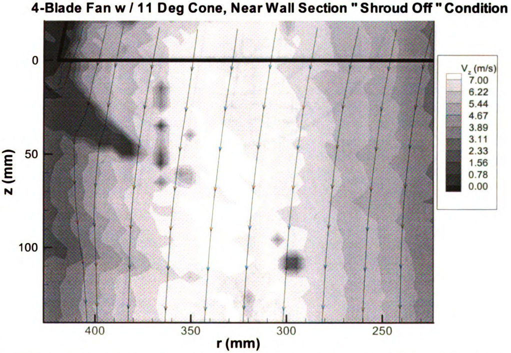

FIGURE 7.28 The 4-Blade Fan with 11 Deg. Cone - "Shroud Off" Condition Near Wall Region

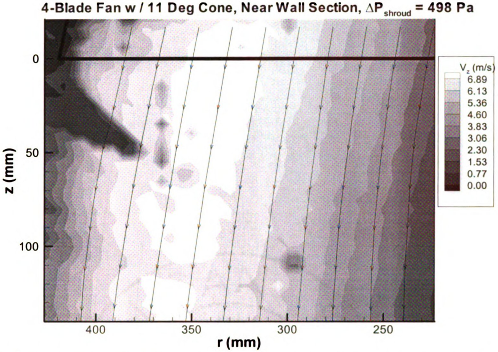

FIGURE 7.29 The 4-Blade Fan with 11 Deg. Cone - "Shroud On" Condition (ΔP_{shroud} = 498 Pa) Near Wall Region

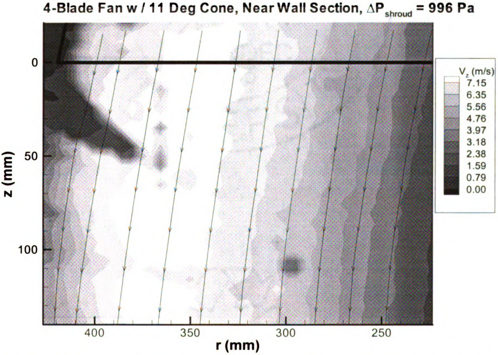

FIGURE 7.30 The 4-Blade Fan with 11 Deg. Cone - "Shroud On" Condition (ΔP_{shroud} = 996 Pa) Near Wall Region

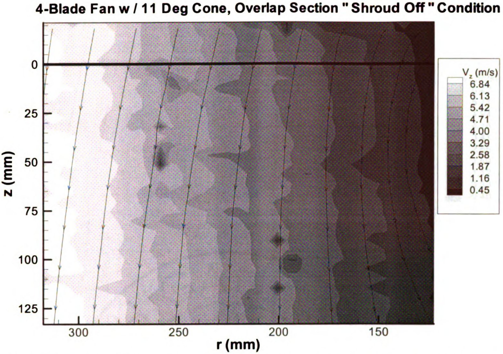

FIGURE 7.31 The 4-Blade Fan with 11 Deg. Cone - "Shroud Off" Condition Overlap Region

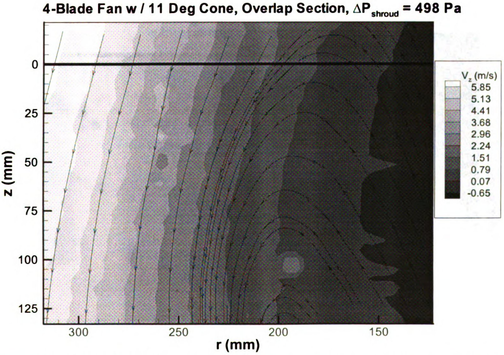

FIGURE 7.32 The 4-Blade Fan with 11 Deg. Cone - "Shroud On" Condition (ΔP_{shroud} = 498 Pa) Overlap Region

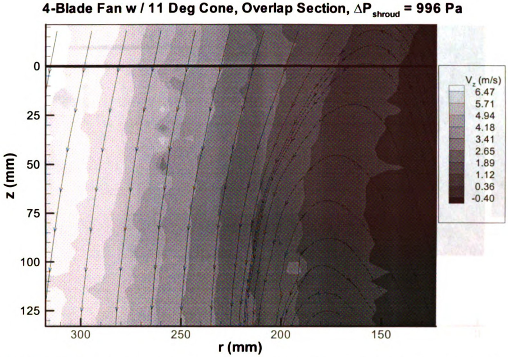

FIGURE 7.33 The 4-Blade Fan with 11 Deg. Cone - "Shroud On" Condition (ΔP_{shroud} = 996 Pa) Overlap Region

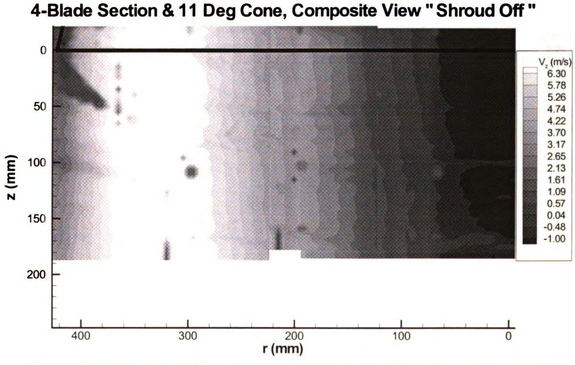

FIGURE 7.34 Composite View of the 4-Blade Fan with 11 Deg. Cone - "Shroud Off" Condition

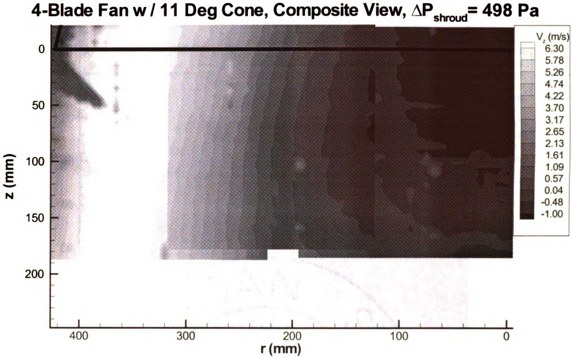

FIGURE 7.35 Composite View of the 4-Blade Fan with 11 Deg. Cone - "Shroud On" Condition ($\Delta P_{shroud} = 498$ Pa)

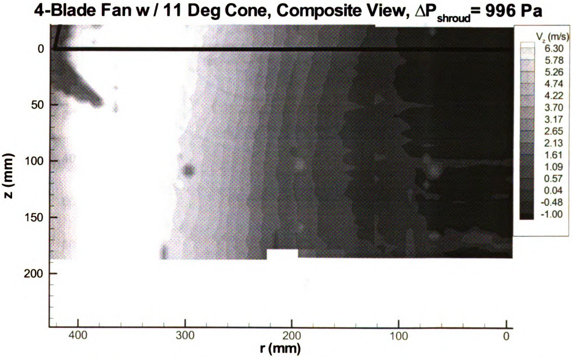

FIGURE 7.36 Composite View of the 4-Blade Fan with 11 Deg. Cone - "Shroud On" Condition ($\Delta P_{shroud} = 996$ Pa)

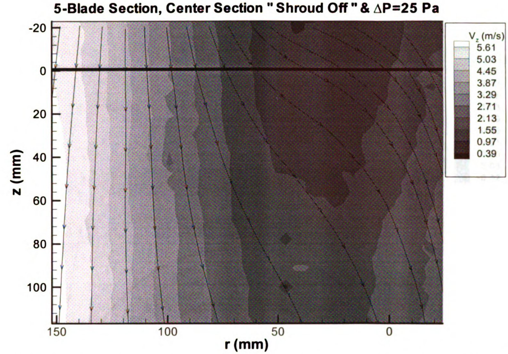

FIGURE 7.37 The 5-Blade Fan with 11 Degree Cone - "Shroud Off" Condition, $\Delta P = 25$ Pa - Center Region

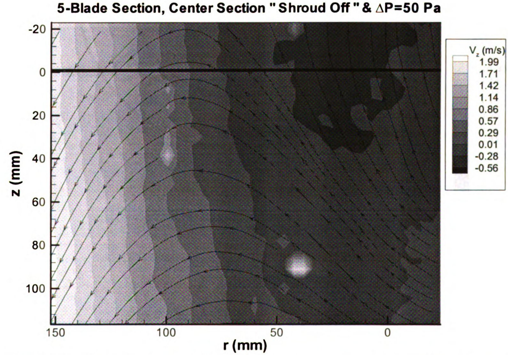

FIGURE 7.38 The 5-Blade Fan with 11 Degree Cone - "Shroud Off" Condition, $\Delta P = 50$ Pa - Center Region

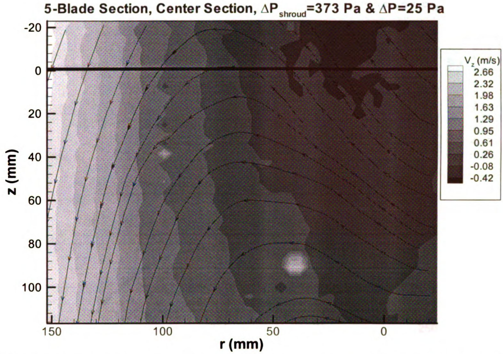

FIGURE 7.39 The 5-Blade Fan with 11 Degree Cone - "Shroud On" Condition (ΔP_{shroud} = 373 Pa), ΔP = 25 Pa - Center Region

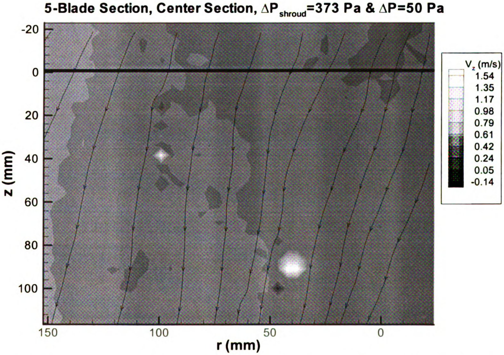

FIGURE 7.40 The 5-Blade Fan with 11 Degree Cone - "Shroud On" Condition (ΔP_{shroud} = 373 Pa), ΔP = 50 Pa - Center Region

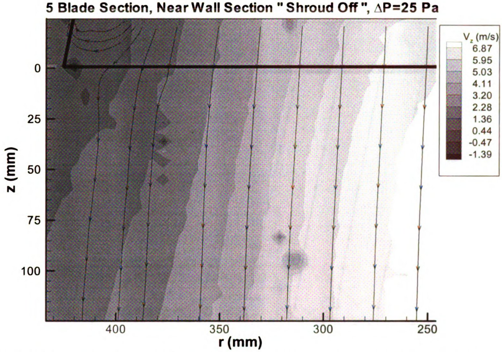

FIGURE 7.41 The 5-Blade Fan with 11 Degree Cone - "Shroud Off" Condition, ΔP = 25 Pa - Near Wall Region

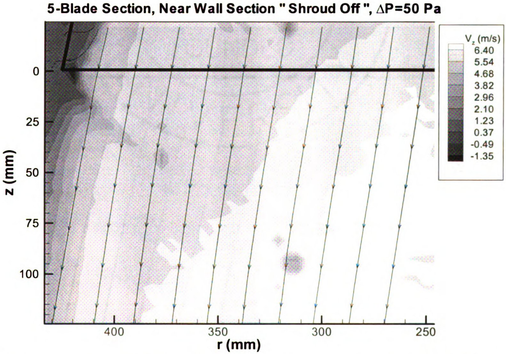

FIGURE 7.42 The 5-Blade Fan with 11 Degree Cone - "Shroud Off" Condition, ΔP = 50 Pa - Near Wall Region

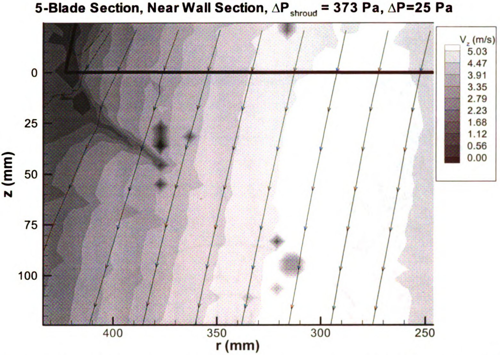

FIGURE 7.43 The 5-Blade Fan with 11 Degree Cone - "Shroud On" Condition (ΔP_{shroud} = 373 Pa), ΔP = 25 Pa - Near Wall Region

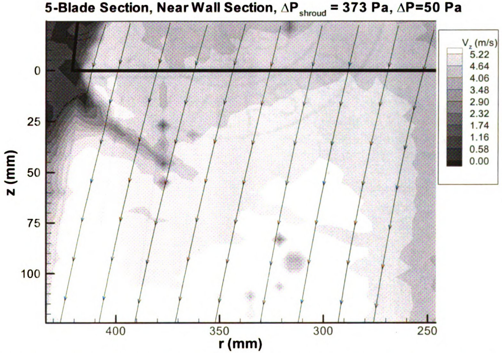

FIGURE 7.44 The 5-Blade Fan with 11 Degree Cone - "Shroud On" Condition (ΔP_{shroud} = 373 Pa), ΔP = 50 Pa - Near Wall Region

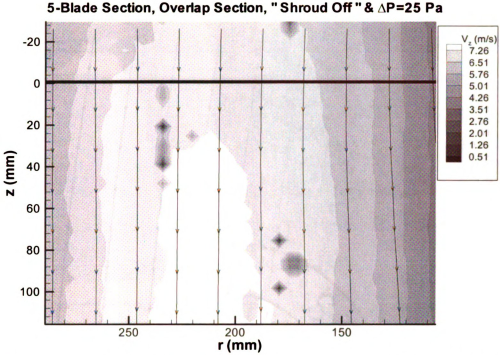

FIGURE 7.45 The 5-Blade Fan with 11 Degree Cone - "Shroud Off" Condition, ΔP = 25 Pa - Overlap Region

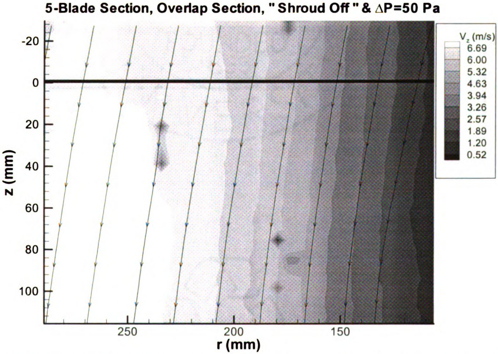

FIGURE 7.46 The 5-Blade Fan with 11 Degree Cone - "Shroud Off" Condition, ΔP = 50 Pa - Overlap Region

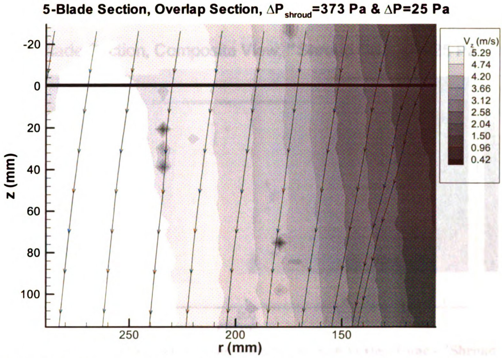

FIGURE 7.47 The 5-Blade Fan with 11 Degree Cone - "Shroud On" Condition (ΔP_{shroud} = 373 Pa), ΔP = 25 Pa - Overlap Region

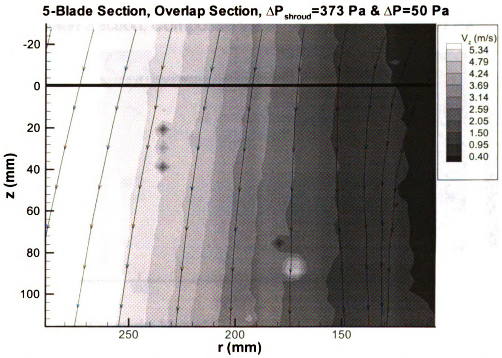

FIGURE 7.48 The 5-Blade Fan with 11 Degree Cone - "Shroud On" Condition (ΔP_{shroud} = 373 Pa), ΔP = 50 Pa - Overlap Region

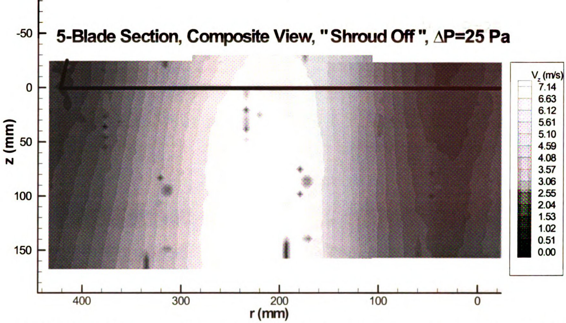

FIGURE 7.49 Composite View of the 4-Blade Fan with 11 Deg. Cone - "Shroud Off" Condition and ΔP = 25 Pa

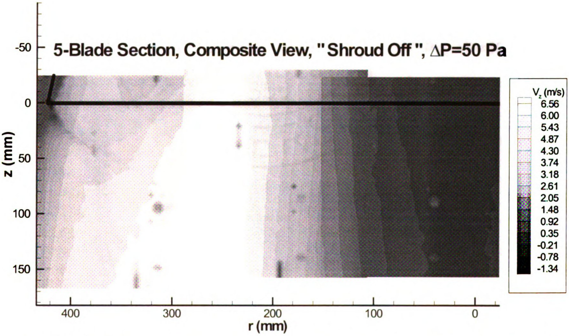

FIGURE 7.50 Composite View of the 4-Blade Fan with 11 Deg. Cone - "Shroud Off" Condition and ΔP = 50 Pa

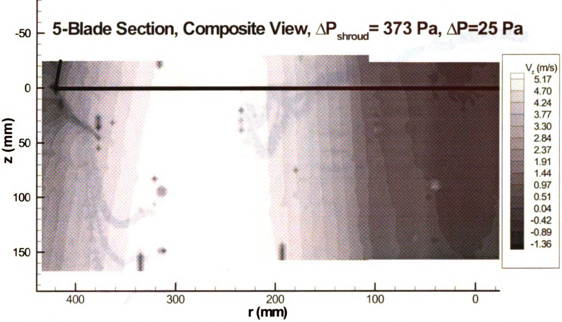

FIGURE 7.51 Composite View of the 4-Blade Fan with 11 Deg. Cone - "Shroud On" Condition (ΔP_{shroud} = 373 Pa) and ΔP = 25 Pa

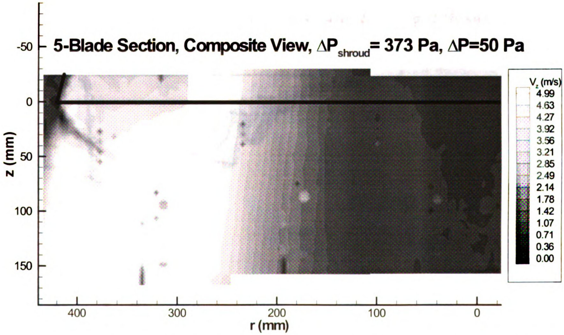

FIGURE 7.52 Composite View of the 4-Blade Fan with 11 Deg. Cone - "Shroud On" Condition (ΔP_{shroud} = 373 Pa) and ΔP = 50 Pa

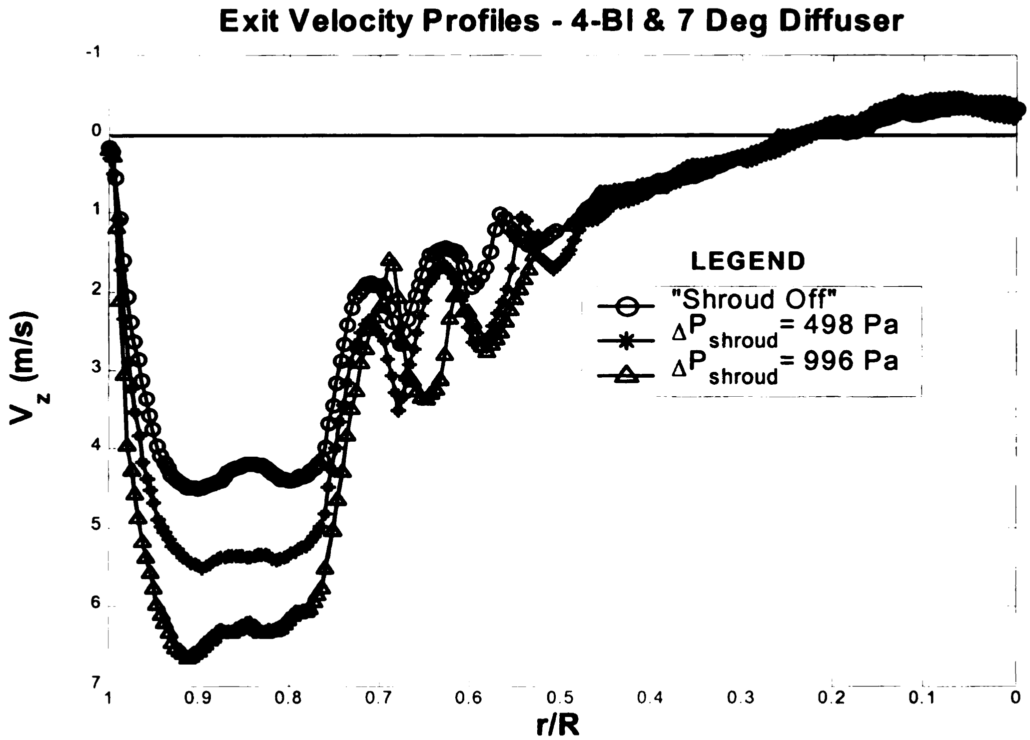

FIGURE 7.53 Exit Velocity Profiles: 4-Blade Fan with 7 Degree Cone, ΔP = 25 Pa

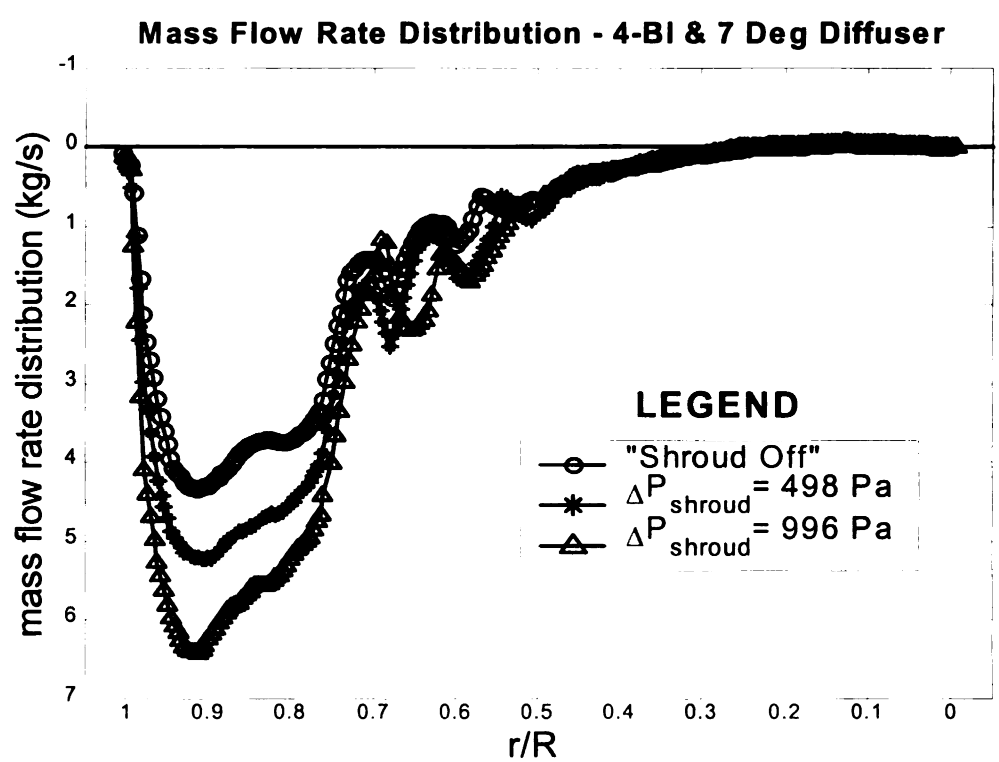

FIGURE 7.54 Mass Flow Rate Distribution: 4-Blade Fan with 7 Degree Cone, ΔP = 25 Pa

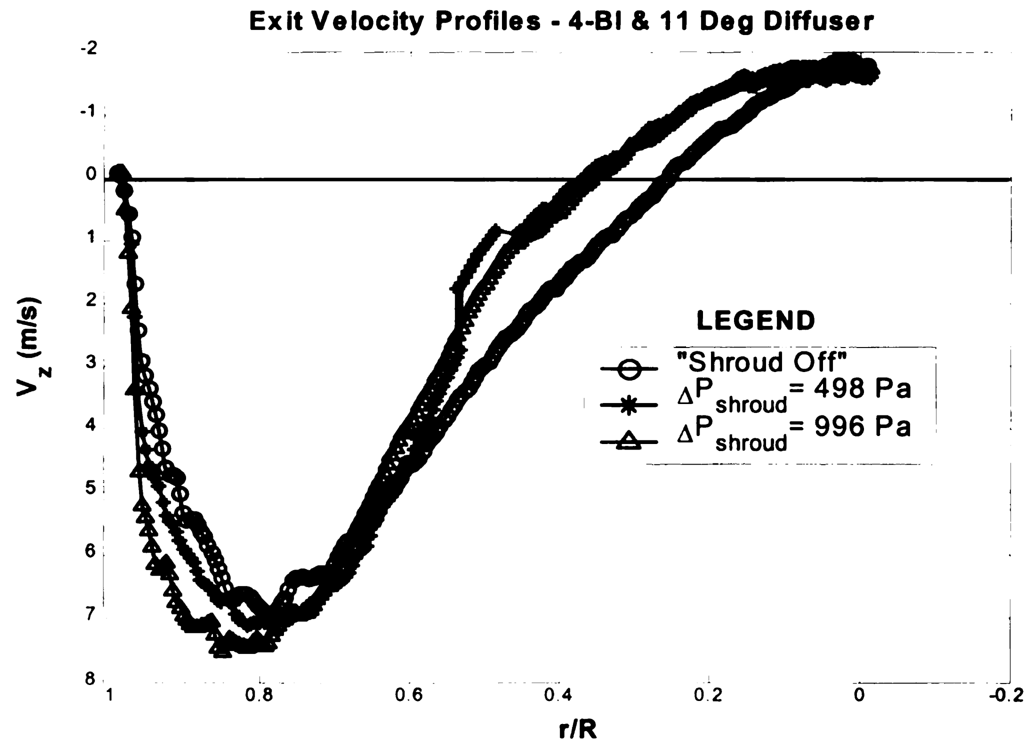

FIGURE 7.55 Exit Velocity Profiles: 4-Blade Fan with 11 Degree Cone, ΔP = 25 Pa

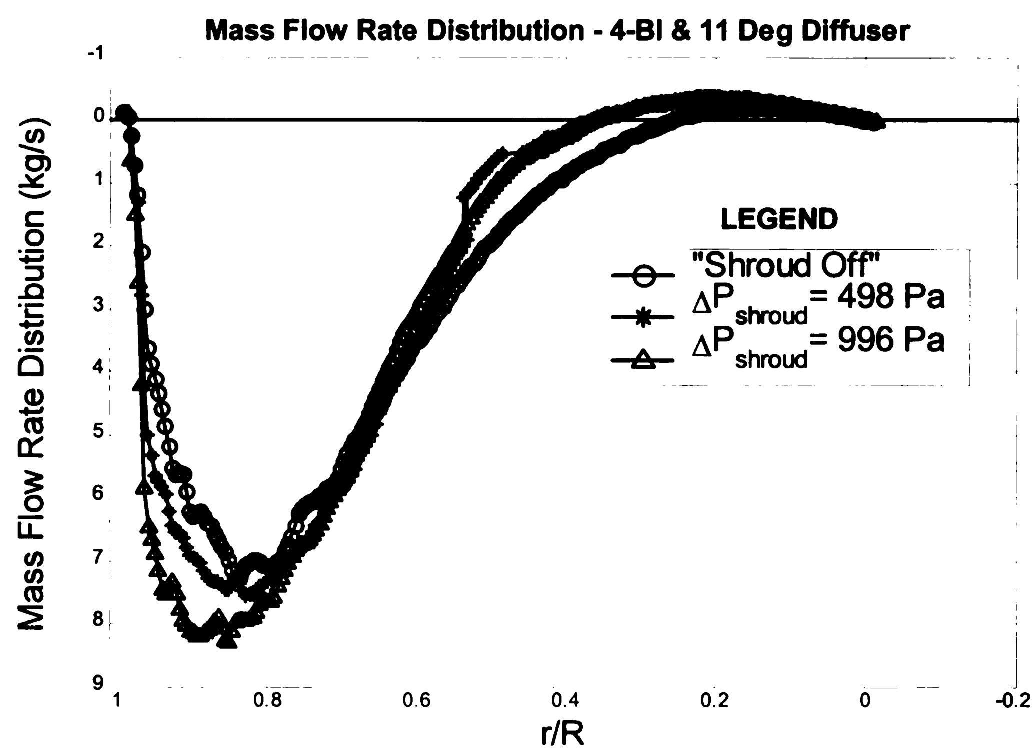

FIGURE 7.56 Mass Flow Rate Distribution: 4-Blade Fan with 11 Degree Cone, ΔP = 25 Pa

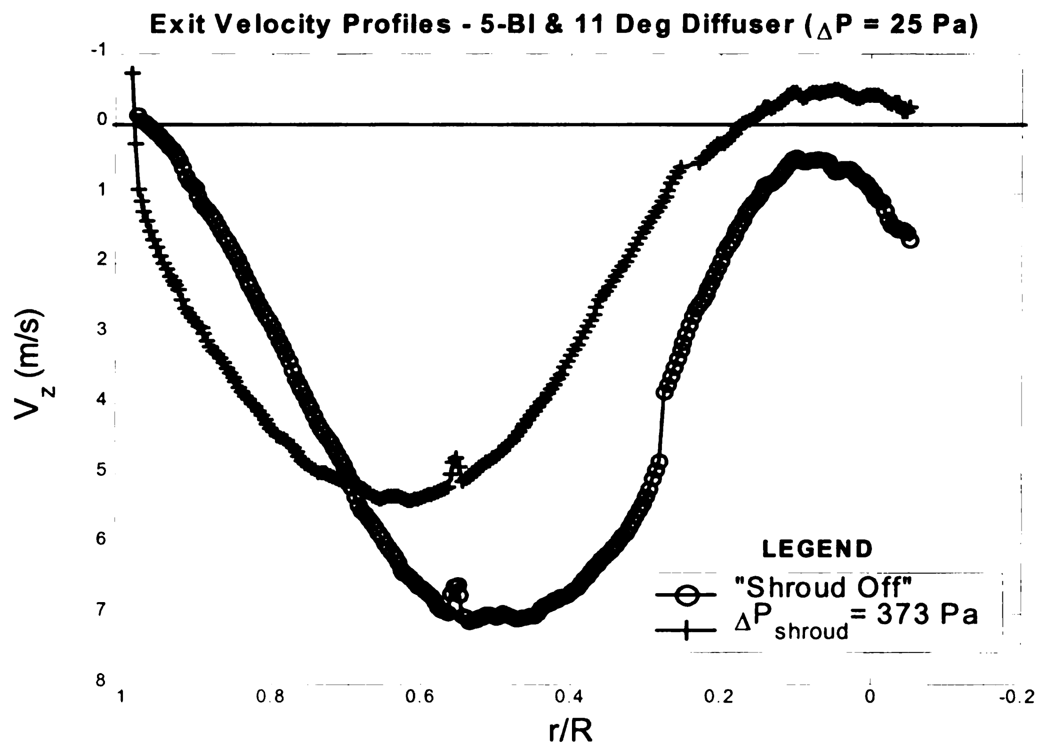

FIGURE 7.57 Exit Velocity Profiles: 5-Blade Fan with 11 Degree Cone, ΔP = 25 Pa

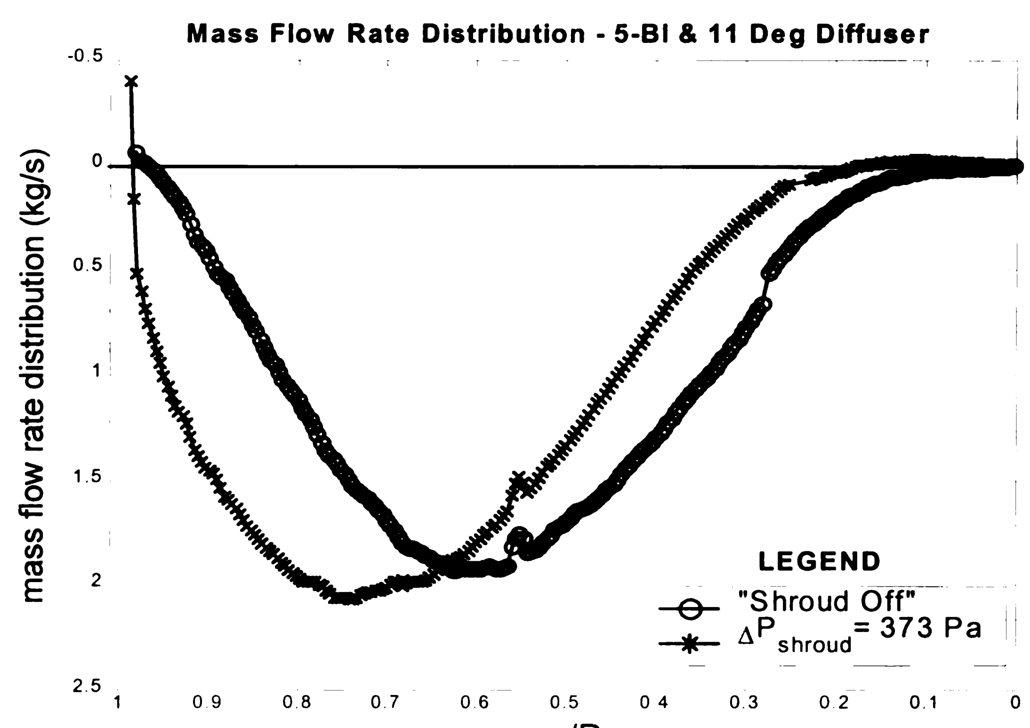

FIGURE 7.58 Mass Flow Rate Distribution: 5-Blade Fan with 11 Degree Cone, ΔP = 25 Pa

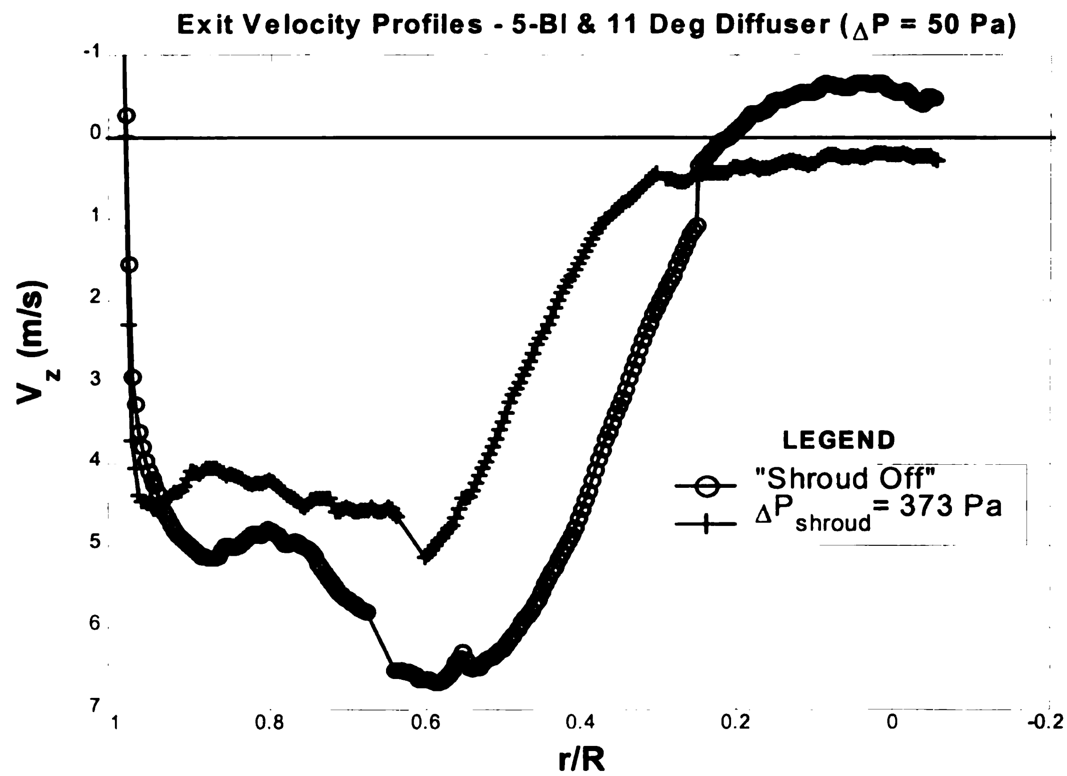

FIGURE 7.59 Exit Velocity Profiles: 5-Blade Fan with 11 Degree Cone, ΔP = 50 Pa

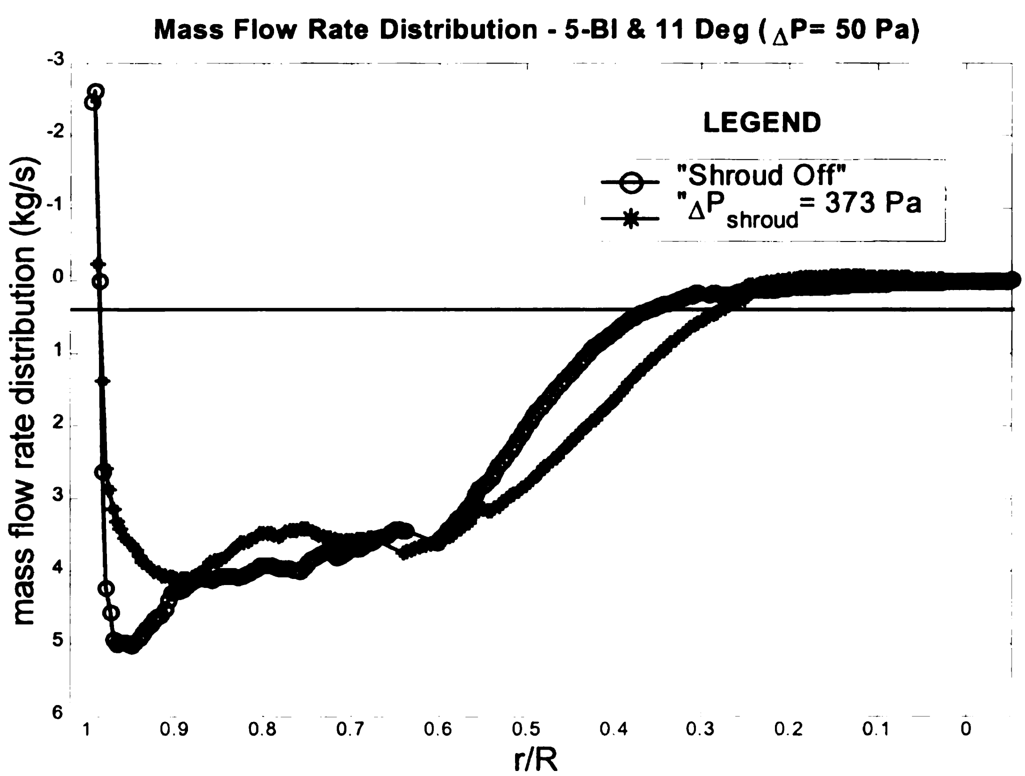

FIGURE 7.60 Mass Flow Rate Distributions: 5-Blade Fan with 11 Degree Cone, ΔP = 50 Pa

8.0 Conclusions, a Proposed New Fan System, and Future Work

8.1 Conclusions

The aerodynamic shroud has been applied to a new type of fan system, an agricultural building ventilation fan. This fan system is completely different from an automotive cooling fan system, which was the motivation problem for the application of the aerodynamic shroud, see Morris (1997). Although the aerodynamic shroud was originally intended for fan systems with large tip clearances and high back pressure operating conditions, it has now been successfully applied to a small tip clearance fan system that operates at very low pressure rise conditions. The results, as summarized below, show that the effectiveness of the aerodynamic shroud is highly dependent on the blade design that is used for the fan. Additionally, it has been shown that a blade design that is considered inferior when used without the aerodynamic shroud can be dramatically superior when used with the aerodynamic shroud. However, the proper choice of shroud operating conditions is required to realize the maximum gains (in both volumetric flow rate and efficiency).

Section 2.0 provides a control volume energy equation balance for the specific type of fan system that has been experimentally evaluated in the present investigation. This section also describes the loss mechanisms in detail and incorporates them into the energy balance for the fan system and aerodynamic shroud. The limitations of the popular definition of static efficiency (η) were demonstrated and a newer definition, η^*, was presented. This definition accounts for the kinetic energy that is created by a low pressure rise fan which, along with volumetric flow rate, Q, are argued to be useful outputs of the fan system. The conventionally used definition of $Q/\wp$ is also acknowledged here, but it is suggested that η^* is the preferred definition because it incorporates the kinetic energy and also because it is dimensionless. Finally, a formulation of η^* is derived which clearly shows the necessary terms that must be minimized in order to obtain a maximum efficiency for the fan system in question.

A comprehensive study of the integral quantities: i) system pressure rise, ΔP, vs. volumetric flow rate, Q, as well as the ii) system pressure rise, ΔP, vs. system efficiency, η^*, is presented in Section 6.0. These variables were presented in a manner described above because the pressure rise operating condition (nominally $\Delta P \approx 25$ Pa) is nearly constant for the majority of the life cycle of an agricultural building ventilation fan. Therefore, the benefits, or lack of benefits, for a particular combination of parameters can be quickly identified from the figures in Section 6.0. The uncertainty of the data measured in the AFRD facility was derived analytically and then evaluated by comparing them with published data. The reliability of the measurements was demonstrated by showing the small variation of several test results over several days.

There was a systematic increase in volumetric flow rate, Q, for the each of the 4-blade fan tests when the aerodynamic shroud in the "shroud on" condition. The magnitude of this increase increased as the shroud pressure, ΔP_{shroud}, was increased. The tests that used the 11 degree diffuser cone showed greater increases for a given shroud pressure than those that used the 7 degree diffuser cone. However, these gains were accompanied by significant decreases in system efficiency, η^*. The best results that involved the 4-blade propeller were those with the 11 degree cone and a shroud pressure, ΔP_{shroud}= 498 Pa. This configuration yielded an 11.5% gain in volumetric flow rate with a decrease in efficiency of 6.0%. The Particle Image Velocimetry results from these 4-blade tests confirm that the aerodynamic shroud does increase the velocity and mass flow rate in the outer regions of both of the diffuser cones. These increases result in higher exit velocities, V_e, and more non-uniform exit profile, represented by α_E. These PIV measurements also showed that there are strong secondary losses, k_{scc}, in the region directly downstream of the hub of the 4-blade fan.

A 5-blade propeller was obtained and utilized for a new set of measurements. This blade design did not provide significant increases in Q or η^*, with respect to those of the production 4-blade fan, when operating in the "shroud off" condition. However, when this propeller was operated in conjunction with the aerodynamic shroud, this combination showed substantial increases in both volumetric flow rate and system efficiency. Numerous combinations of shroud parameters were evaluated and a final optimal configuration was identified. This optimal configuration yielded an increase in volumetric flow rate, Q, of 33.6% and an increase in system efficiency of, η^*, of 12.3% when compared to the values for the 4-blade production fan system. The effects of increasing and decreasing the number of blades were examined, but the 5-blade was identified as the optimal propeller.

Particle Image Velocimetry measurements at the exit plane of 11 degree diffuser cone show that the 5-blade fan generates a velocity profile that reaches a maximum at a median radius ($r/R \approx 0.5$) of the exit plane. The aerodynamic shroud is able to shift this maximum velocity to a larger radius ($r/R \approx 0.65$) and also reduce the exit velocity across much of the exit plane. The resulting velocity profile is reduced over much of the exit plane, resulting in lower values of V_e, and it also more uniform, which would indicate a lower value for α_E. Both of these result in higher system efficiency values as was shown in equation 2.20.

Finally, a new device, termed the "centerbody" was added and its effects were measured. To the best of the author's knowledge, this type of device has not been used in an agricultural building ventilation fan, nor in any fan that used the aerodynamic shroud. This centerbody device, when used with the 5-blade fan and the 11 degree diffuser cone in the "shroud on" condition, provided even further improvements in Q and η^* when compared to those values for the 4-blade production fan system. The volumetric flow rate, Q, increased 35.7% and the system efficiency, η^*, increased 15.6%.

These data show that the effectiveness of the aerodynamic shroud is highly dependent on the design of the propeller that is used. The optimal blade design in this study provided lower flow rate and efficiency than the production design when operated in the "shroud off" condition, yet significant increases in both flow rate and efficiency when operated in an optimal "shroud on" condition. These data also suggest that higher diffuser angles than the widely regarded limit of 7-9 degrees are feasible when the aerodynamic shroud is operated in an optimal configuration.

8.2 Proposed New Fan System

The results, which were presented in Section 6.0 and Section 7.0 and then summarized above, have led to the identification of a new fan system. The features of this fan system are shown in Figure 8.1. It should be noted that these specific modifications are suggested for a 0.61 m agricultural ventilation building ventilation fan. However, these improvements could potentially apply to any fan which has a low pressure rise operating condition and a high volume flow rate. It is suggested that the aerodynamic shroud be implemented for this fan system. This feature can be integrated as shown in Figure 8.1 with a shroud gap of 5.0 mm and a shroud pressure of 373 Pa. The 5-blade propeller should be installed in this fan system and a cylindrical centerbody should be placed directly downstream of the propeller. This centerbody should have a diameter which matches the hub of the propeller. Since the centerbody is stationary and the propeller rotates, the spacing between these two devices should be minimal. The stationary centerbody can be supported by the downstream protective guard screens. A diffuser that is no smaller than 11 degrees should also be installed on this fan system. It is acknowledged that further improvements in flow rate and efficiency might be possible with larger-angled cones, but this has not been confirmed in this study.

8.3 Future Work

The present investigation represents a systematic study of several different blade designs and their effectiveness when used in conjunction with active control elements, such as the aerodynamic shroud, and passive elements such as a centerbody device. Although an optimum blade design was identified among those evaluated, it is anticipated that many design parameters exist that could be modified to improve upon the results presented here. Future work in this area could involve numerical computations and/or an optimization scheme to be used to identify a blade design that would best fit the assembly presented in Figure 8.1.

The usefulness of the centerbody device in this application, particularly when used with the aerodynamic shroud, has been demonstrated in the present study. The only centerbody shape that was evaluated was the cylindrical cone that is shown in Section 6.6. Additional shapes could possibly provide further improvements beyond those found here. Also, the use of small stator elements, which create pressure rise in a manner similar to diffusers, could be used on the surface of the centerbody.

The aerodynamic shroud has been shown to dramatically improve the performance of a fan that is completely different than that of the original application. Many other applications exists which have specific challenges different than those of this study and the previous study. The use of an aerodynamic shroud in turbomachinery applications of all type could have a profound effect on the design approaches and methodologies currently used to design fans.

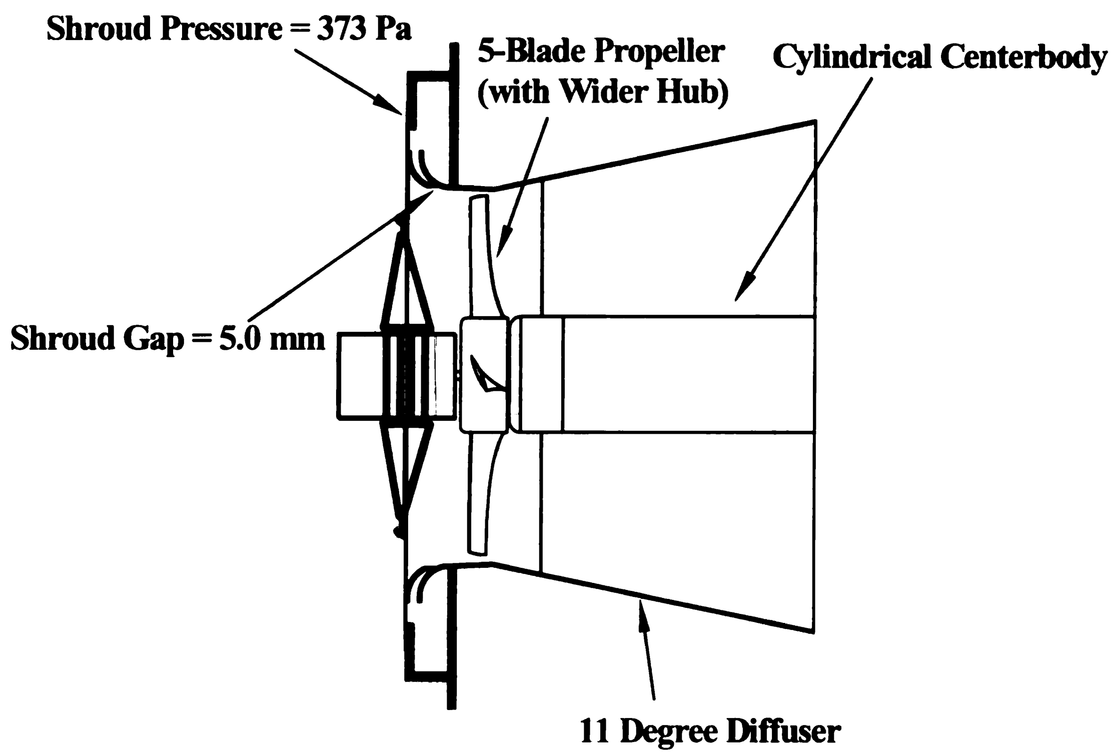

FIGURE 8.1 The Proposed New Fan Design

REFERENCES

1. AMCA *Directory of Agricultural Products with Certified Ratings* (2000), Air Movement and Control Association, Inc. Publication 262-00.
2. AMCA *Laboratory Methods of Testing Fans for Rating*, (1985), Air Movement and Control Association, Inc. Publication 210-85.
3. AMCA *Laboratory Certified Ratings Program Air Performance,* (1994), Air Movement and Control Association, Inc. Publication 211-94.
4. Bickert, W.G. (1988), "Full wall ventilation to improve warm weather environments in naturally ventilated livestock buildings," *Livestock Environment III,* Proc. of the Third Int'l. Livestock Envir. Symp. ASAE, 2950 Niles Rd., St. Joseph, MI. pp. 1-7.
5. Bleier, F. P. (1998), *Fan Handbook: Selection, Application and Design*, McGraw-Hill, New York.
6. Brody, S., Ragsdale, A.C., Thompson, H.J. and Worstell, D., (1954), "The effect of wind on milk production, feed and water consumption and body weight in dairy cattle," Mo. Agr. Exp. Sta. Res. Bull. 545. Univ. of Missouri, Columbia, MO.
7. Chastain, J.P. (1991), "Heat and mass transfer through the bovine hair coat during evaporative cooling," Unpublished PhD dissertation. University of Kentucky, Lexington, KY.
8. *FlowMap Installation and User's Guide*. (1997), Dantec Measurement Technology.
9. Ford, S.E., Christianson, L. L., Riskowski, G. L., Funk, T.L. (1999), *Agricultural Ventilation Fans, Performances and Efficiencies*, UILU ENG 99-7001.
10. Fuquay, J.W. (1981), "Heat stress as it affects animal production," *J. Animal Sci.* 52(10:164-174).
11. Hanan, J.J. (1998), *Greenhouses, Advanced Technology Protected Horticulture*, CRC Press, Boca Raton, FL.
12. *The Handbook of Fluid Dynamics,* edited by Johnson, Richard W., (1998), CRC Press.
13. Herz, S. A. (1998), "Centrifugal Blower Considerations for the Purpose of Aerodynamic Shroud Pressurization," ME 490 independent study final report, summer semester, Michigan State University College of Engineering.
14. Høst-Madsen, A. and McCluskey, D.R. (1994), "On the Accuracy and Reliablity of PIV measurements," *Proceedings of the Seventh International Symposium on Application of Laser Techniques to Flow Measurements*, Lisbon.
15. Johnson, H.D. (1965), "Environmental temperature and lactation," *Int'l J. Biometeor.* 9:103-116.
16. Keane, R.D. and Adrian, R.J. (1992), "Theory of cross-correlation analysis of PIV images," *Applied Scientific Research*, vol. 49, pp 191-215.
17. Lakshminarayana, B. (1996), *Fluid Dynamics and Heat Transfer of Turbomachinery*, Wiley and Sons, Inc., New York.

18. Mangold, D.W., Hazen, T.E. and Hays, V.W. (1967), "Effect of air temperature on performance of growing-finishing swine," *Trans. ASAE* 10(3):370-375, 377.

19. *Mass Airflow Test Stand (MAFS) Operator's Manual*, (1995), Engineered Systems, Inc., Project Nr. P93045A.

20. *Mass Airflow Test Stand Commercial Literature*, S.O. 2169, Model 11359 Testek, Inc., Livonia, MI.

21. Morris, S.C. (1997), M.S. Thesis, Department of Mechanical Engineering, Michigan State University.

22. Morris, S.C., Good, J.J., Foss, J.F. (1998), "Velocity Measurements in the Wake of an Automotive Cooling Fan," *Experimental Thermal and Fluid Science*, 17 pp 100-106.

23. Morris, S.C., Foss, J.F. and Pakkala, J.E. (1997), "The Automotive Cooling Fan Research and Development Facility," Society of Automotive Engineering Paper, No. 971784.

24. Morris, S.C. and Foss, J.F. (1997), "Performance Measurements and Detailed Flow Field Observations for a Light Truck Cooling Fan," Society of Automotive Engineering Paper, No. 971794.

25. Morris, S.C., Neal, D.R., Foss, J.F., Cloud, G.L. (2001, February), "A Unique Air Flow Measurement Device," *Measurement and Science Technology*, pp N9-N13.

26. Morris, S.C., Foss, J.F. (2001, June), "An Aerodynamic Shroud for Automotive Cooling Fans," *Journal of Fluids Engineering*, Vol. 123.

27. Neal, D.R. and Foss, J.F. (1999) "The Development of the Aerodynamic Shroud for Enhanced Ventilation in Livestock Buildings," USDA SBIR Phase I Final Report.

28. Neal, D.R. and Bardouwalla, A. (1998), "A Study of the Agricultural Livestock Ventilation Fan Market," Management of Technology and Innovation Final Report - MSC 890, Michigan State University College of Business.

29. Nienaber, J.A., Shanklin, M.D., Hahn, G.L. and Manak, R.C. (1985), "Performance of neonatal and newly-weaned pigs as affected by temperature and diet," *Trans. ASAE* 28(5):1626-1634.

30. Nienaber, J.A., Hahn, G.L. and Yen, J.T. (1987), "Thermal environmental effect on growing-finishing swine: Part I - Growth, feed intake and heat production," *Trans. ASAE* 30(6):1772-1775.

31. Overhults, D.G. and Gates, R.S. (1993), "Energy Use in Tunnel Ventilated Broiler Houses," Livestock Environment IV, Fourth Intl Symposium, Coventry, England, July 6-9, pp. 339-346.

32. Smith, R.H. and Wang, C-T. (1944), "Contracting Cones Giving Uniform Throat Speeds" *Jour. Aero. Sci.* pp 356-360.

33. Tillotson, R.J. and Bickert, W.G. (1994), "Dairy housing ventilation modification due to level of milk production," *Dairy Systems for the 21st Century*, Proc. of the Third Int'l Dairy Housing Conf. ASAE, 2950 Niles Rd., St. Joseph, MI. pp. 317-326.

34. Tyrrell, H.F., Brown, R.S., Reynolds, P.J., Haaland, G.C., Bauman, D.E., Peel, C.J. and Steinhour, W.D. (1988), "Effect of somatotropin on metabolism of lactating cows: energy and nitrogen utilization as determined by respiration calorimetry," *J. Nutr.* 118:1024-1030.

35. Osborne, W. C. (1966), *Fans*, Pergamon Press, Oxford.

36. Overhults, D.G. and Gates, R.S. (1997), "Energy requirements for operating tunnel ventilated broiler houses," *Proceedings of the Fifth International Livestock Environment Symposium*, Bloomington, MN, May 29-31, pp.859-865.

37. Patterson, G.N. (1938), *Modern Diffuser Design, Aircr. Engng.* 10, 267.

38. Potter, M.C. and Foss, J.F. (1982), *Fluid Mechanics,* Great Lakes Press, Okemos.

39. Squire, H.B. (1953), "Experiments on Conical Diffuser" R. and M. 2751 Aero. Res. Council.

40. Wallis, R. A., *Axial Flow Fans and Ducts,* Wiley and Sons, Inc., New York, 1983.

41. Wheeler, E. F. and Both, A. J. (2002), "Evaluating Greenhouse Mechanical Ventilation System Performance," Agricultural and Biological Engineering Fact Sheet I-42, The Pennsylvania State University, University Park PA. 4 pp.

42. Wheeler, E. F. and Both, A. J. (2002), "Evaluating Greenhouse Ventilation Fan Capacity," Agricultural and Biological Engineering Fact Sheet I-43, The Pennsylvania State University, University Park PA. 4 pp.

43. Wilcox, D.C. (1993), *Turbulence Modeling for CFD*, DCW Industries, La Canada, California.

44. Yousef, M.K. and Johnson, H.D. (1966), "Calorigenesis of dairy cattle as influenced by throxine and environmental temperature," *J. Animal Sci.* 25:150-155.